UNIVERSITÉ de Liège

Département MSM
1, chemin des Chevreuils
B 4000 Liège
Belgium

Anne.Habraken@ulg.ac.be

CONTRIBUTIONS TO CONSTITUTIVE LAWS OF METALS:

MICRO-MACRO AND DAMAGE MODELS

Parts C and D

Thèse présentée en vue de l'obtention du grade d'Agrégé de l'Enseignement Supérieur
par Anne-Marie HABRAKEN

Année académique 2000-2001

PART C

DAMAGE MODELS APPLIED TO METALS

Thèse présentée en vue de l'obtention du grade d'Agrégé de l'Enseignement Supérieur

par Anne Marie HABRAKEN

Année académique 2000-2001

Part C- Introduction

MSM research on damage began with Yongui Zhu's thesis, completed in December 1992. Supervised by Professor Serge Cescotto, this Ph.D. thesis proposes an isotropic elasto-plastic damage model, identified and validated on an aluminum alloy, and the theory of an anisotropic elasto-plastic damage model. As a member of the jury and a permanent member of the LAGAMINE team, I devoted much attention to this thesis and its programming work in order to be able to pursue research on this topic. By means of numerous research projects and with the help of several coworkers, Zhu's models have found new applications and new approaches have been developed. Here below are listed all the projects that I have supervised; their results are partially presented in part C of the thesis:

- *Numerical and Physical Study of Material Forming Processes, 1994-1996.* This scientific network groups 14 laboratories thanks to the Human Capital and Mobility Program of European Community. It enabled me to attend numerous meetings and to know other European teams working on Metal Forming Processes. This program supported Raphaël Estevez's 6-months post-doctoral stay with MSM.
- *Dynamic Forging Modeling, second phase, 1993-1996.* This project, which was financed by the Région Wallonne, concerned the improvement of our nonlinear finite element code (LAGAMINE) in order to model dynamic forging processes. I conducted this research with the help of Wang Xiao Chuan.
- *Integration of Micro-Macro Interactions in Metal Forming Finite Element Modeling, 1996-1998.* This Région Wallonne project involved a small part on damage, performed by Jean-François Charles.
- *Rupture Prediction, 1996-1997.* I supervised this graduation work by Anne-France Cambron for her degree in Physics Engineering.
- *Application of an Isotropic Elasto-Plastic Model coupled with Damage Theory to an Aluminum, 1997-1998.* This research comprised another student graduation work by Sylvie Castagne to obtain the degree in Physics Engineering.
- *Experimental and Numerical Approach of Metal Rupture thanks to Damage Theory, 1997-2001.* This research consists in Michaël Wauters's Ph.D. thesis, financed by FRIA (the Industry and Agriculture Research Training Fund of the Belgian French Community). I directed this thesis focused on metal sheet behavior.
- *Bodner's Model Coupled with Damage Theory, 1996-1999.* This research was performed by Zhang Li Hong thanks to the support of the University Research Council of Liège.

Chapters 1 to 5 summarize what is important to know before entering the ductile damage field; this review attempts to summarize the important concepts. Then Chapters 6 and 7 describe the models developed with my guidance. Chapter 8 concludes.

CONTENTS

Notations

Second order tensors are underlined once or noted with their 2 subscripts and fourth order tensor are identified by four subscripts or underlined twice. Capital Latin letters or Greek letters are used for these tensors. Einstein's summation on identical indices is always assumed unless otherwise specified.

The simple contracted tensor product is identified by ".".

$$\underline{C} = \underline{A}.\underline{B} \Leftrightarrow C_{ij} = A_{ik} B_{kj}$$

The tensorial product is :

$$\underline{\underline{C}} = \underline{A} \otimes \underline{B} \Leftrightarrow C_{ijkl} = A_{ij} B_{kl}$$

The double contracted tensor product is noted by ":"

$$s = \underline{A} : \underline{B} \Leftrightarrow s = A_{ij} B_{ij} \quad \underline{C} = \underline{\underline{S}} : \underline{B} \Leftrightarrow S_{ijkl} B_{kl}$$
$$s = \underline{A} : \underline{\underline{S}} : \underline{B} \Leftrightarrow s = A_{ij} S_{ijkl} B_{kl}$$

The tensorial norm is defined by :

$$\left|\underline{A}\right| = \sqrt{\underline{A} : \underline{A}}$$
$$\left|\underline{\underline{S}}\right| = \sqrt{S_{ijkl} S_{ijkl}}$$

The inverse operator is defined by the superscript -1 :

$$\underline{A}^{-1} \underline{A} = \underline{I} \Leftrightarrow A^{-1}_{ik} A_{kj} = \delta_{ij}$$

with $\underline{I}$ the unit second order tensor, δ_{ik} Kronecker symbol.

The transverse operator is defined by the subscript T :

$$(A^T)_{ij} = A_{ji}$$

Vectors are also underlined once, but small Latin letters are used. They can also be noted with one subscript. The vector operations are :

$$\underline{s} = \underline{v}.\underline{u} \Leftrightarrow s = v_i u_i$$

$$\underline{C} = \underline{v} \otimes \underline{u} \Leftrightarrow C_{ij} = v_i u_j$$

$$|\underline{v}| = \sqrt{\underline{v}.\underline{v}} = \sqrt{v_i v_i}$$

If $\underline{v}$ is a first order tensor and $\underline{\underline{A}}$ a second order one :

$$\underline{u} = \underline{\underline{A}}.\underline{v} \Leftrightarrow u_i = A_{ij} v_j$$

Scalars are not underlined.

The superscript * characterises unit vector :

$$\underline{u}^* \Rightarrow \left|\underline{u}^*\right| = 1$$

Abbreviations

FEM	Finite Element Method
BEM	Boundary Element Method
MSM	Mécanique des Structures et des Matériaux
MK	Marciniak and Kuczinsky's approach
SEM	Scanning Electron Microscope
TEM	Transmission Electron Microscope

Symbols

$\dot{(\,)} = \frac{d(\,)}{dt}$	derivative with respect to time
$\int (\,) d(\,)$	integration
x^e	variable associated with elasticity
x^p	variable associated with plasticity
$\overline{a}$	effective variable in damage model, value of one variable in the equivalent virgin state
$\underline{\hat{\alpha}}$	deviatoric tensor
$\underline{\overset{\nabla}{\alpha}}$	objective Jaumann time derivative
Δa	increment of variable a
$(\underline{A})_m$	mean value of tensor $\underline{A} = (1/3)\, A_{ii}$

Latin letters

a_1, a_2, a_3	scalar values in Bodner's damage model or Zhu's damage approach
A	material constant in numerous functions
A	set of equations in Boudeau-Gelin's approach
A_1, A_2	recovery coefficients of isotropic or directional hardening in damage Bodner's model
A_k	thermodynamic forces associated with internal variable α_k in the general thermodynamic formulation
A_d	damaged surface area taking into account area of micro-cracks, voids, microstress concentration iteraction between micro-cracks...
A_t	total cross sectional area of a unit cell cut by a plane
b	ratio between the diagonal of the smallest finite element and the notch radius in meshes dedicated to experiments on aluminum rods
$\underline{b}$	displacement discontinuity vector in Dragon's approach
B_0	initial damage strengthening threshold
B	increase of damage strengthening threshold force associated with scalar damage variable β in anisotropic damage model
B	hardening / softening variable of the loading damage surface in Fichant's model
c	ratio between maximal and minimal finite element edge in meshes dedicated to experiments on aluminum rods
c	square of the average internal length in Geer's model
$c^d\ c^p\ c^r$	material constants in Hayakawa & Murakami's model
$\underline{\underline{C}}^e$	tensor of elastic moduli
d	scalar deviatoric damage variable in Zhu's and Bodner's model
d	scalar variable defined in Fichant's model
d_n	damage variable in direction $\underline{n}$
D	unique damage scalar variable in isotropic damage model
D_0	assumed limit plastic-shear strain rate in Bodner's model
D_1	directional hardening coefficient in Bodner's model
$\underline{\underline{D}}$	second order damage tensor in anisotropic damage model, defined by its 3 principal values d_1, d_2, d_3 in principal axes
$\underline{D}^c$	rate of deformation, c means cinematic variable , not damage

e	specific internal energy
E	isotropic Young's modulus
E	void shape parameter in Rice & Tracey's model
E,F,G,H,L,M	material parameters in Hill's model
E_0	initial isotropic Young's modulus in damage model
$\overline{E}$	effective Young's modulus value
E_{eq}, E_m	hardening parameters respectively coming from equivalent and mean plastic macroscopic strain rate in Leblond's version of Gurson's model
E_t	tangent modulus of effective stress-plastic strain curve
f	microvoid volume fraction or porosity
f	loading surface in Fichant's model
f	axial force in Souza Neto's comparison of Gurson's and Lemaître's models
f^*	specific coalescence function in Gurson's model
f_0	initial microvoid volume fraction
f_c	microvoid volume fraction due to coalescence
f_{cr}	critical void volume fraction at onset of coalescence
f_F	porosity at final failure
f_g	microvoid growth volume fraction
f_n	nucleated microvoid volume fraction
f_N	potential nucleated microvoid volume fraction
f_u	ultimate value of f^* at rupture
f_v	volume fraction of inclusions
F	pseudo dissipation potential
F	triaxiality function in damage extension of Bodner's model
F_1	applied force in direction 1
F_d	damage dissipation potential
F_p	yield surface (equal to plastic dissipation potential in associate models)
F_T	triaxiality function to account for multiaxial stress state by a scalar indicator
F_1, F_2	functions defined by Leblond to improve Gurson's model
$\underline{\underline{F}}$	deformation gradient
g	function used to calibrate Bodner's model
g	function of Rousselier's model
$g(\underline{y})$	weighting function defining the intensity and the radius of the spatial non-local effect in Geer's model
G	energy released per unit extension of crack front per unit thickness in fracture mechanics
G	elastic shear modulus
G^d	damage Gibs' potential
G^e	elastic Gibs' potential

G^p	plastic Gibs' potential
$\overline{G}$	effective elastic shear modulus
G_0	initial elastic shear modulus in damage model
$Gibs$	themodynamic potential of Gibs
$\Delta G_{(max)}$	maximum activation enthalpy
H	height of the unit cell in Benzerga's approach
$\underline{\underline{H}}$	fourth order anisotropic Hill's tensor
i,j	orthotropy axes in Vacher's application of Marciniak and Kuczinsky's approach model
$\underline{I}$	second order unity tensor
$\underline{\underline{I}}$	fourth order unity tensor
J	well known parameter in fracture mechanics, rate of change of potential energy per unit cracked area
$\underline{J}$	damage characteristic tensor in anisotropic Zhu's model
J_2	second stress invariant = $\frac{1}{2}\hat{\underline{\sigma}} : \hat{\underline{\sigma}}$
K	isotropic part of the total scalar hardening variable in Bodner's model
K	material parameter in Swift's law
K_0	initial isotropic hardness in Bodner's model
K_I K_{II} K_{III}	stress intensity factor for crack opening modes *I, II, III* respectively
K_{IC}	critical value of the stress intensity factor, value at fracture
K_1	maximum or limiting isotropic hardness in Bodner's model
K_2	minimum or stable isotropic hardness in Bodner's model
l_c	material length scale for rupture
$l_{c(0)}$	(initial) intervoid length in a porous material
l_{10} l_{20} l_{30}	initial plate dimensions in directions 1 2 3 , superscripts *a* or *b* can define one zone of the plate
$l_1 l_2 l_3$	updated plate dimensions in directions 1 2 3
L	distance between the centers of 2 cavities in the transverse direction
$\underline{L}$	velocity gradient
$\underline{\underline{L}}$	fourth order damage tensor used to define the damage surface in Hayakawa & Murakami's model
m_1	hardening exponent of isotropic hardness in Bodner's model
m_2	hardening exponent of directional hardness in Bodner's model
M	point where instability occurs in Boudeau & Gelin's approach

$\underline{\underline{M}}$	fourth order damage tensor used to define the yield surface in Hayakawa & Murakami's model and Zhu's model
n	strain rate sensitivity coefficient in Bodner's model or classical strain hardening exponent in elastoplastic model
$\underline{n}$	unit normal direction to the defect in Marciniak & Kuczinsky's model or to the necking direction in Boudeau & Gelin's approach
$\underline{n}$	unit normal direction
o	origin of axes
p	plastic variable for general isotropic hardening model
p	parameter of the modified damage isotropic Zhu's model
$\underline{p}_i$	unit principal direction i
q, q_1, q_2, q_3	Tvergaard's parameters to improve Gurson's model
$\underline{q}$	heat flux
r	polar coordinate, distance from the crack tip in fracture mechanics
r	exponent of equivalent plastic strain rate in damage model
r	Lankford coefficient
r_H	Lankford coefficient computed with Hill's model
r_1	recovery exponent of isotropic hardness in Bodner's model
r_2	recovery exponent of directional hardness in Bodner's model
R	increase of plastic radius or plastic hardening threshold
R	spherical void radius
R_0	initial spherical void radius
$\dot{R}_k$	radius rate in principal strain direction k
R_1 R_2 R_3	ellipsoidal void radii, the subscript 0 also means initial value
s	stress function exponent in damage model
s	specific entropy
S	second Piola Kirchoff's uniaxial stress
S^k	micro-crack surface in Dragon's approach
S_N	Gaussian standard deviation of the normal distribution of inclusions
t	time
t	unit direction parallel to the defect in Marciniak Kuczinsky's model or to necking in Boudeau & Gelin's model
T	triaxiality ratio σ_m/σ_{eq}
T	temperature

$T_i = \sigma_{ij} n_j$	components of the normal stresses acting at the boundaries along an arbitrary contour for J-integral evaluation
u	axial displacement in Souza Neto's comparison of Gurson's and Lemaître's models
u_i	components of the displacement vector in J-integral evaluation
$\underline{u}$	direction of the stress tensor in Bodner's model
$\underline{u}$	vector of unknowns in Boudeau-Gelin's approach
$\underline{u}^0$	solution vector in Boudeau & Gelin's approach
$\delta\underline{u}$	perturbation of the solution vector in Boudeau & Gelin's approach
$\delta\underline{u}^0$	amplitude of the perturbation in in Boudeau & Gelin's approach
V	elementary representative volume
V_A	elementary apparent volume of the material (matrix +void)
V_M	elementary apparent volume of the matrix
$w = R_3/R_1 = R_3/R_2$	void shape factor ($w = 1$ sphere, $w = \infty$ cylinder, $w < 1$ oblate void)
W	strain energy density
W^p	plastic work
$\dot{W}^p$	plastic work rate or plastic power
W^t	total plastic and damage energy used in Chaouadi's approach
$\underline{x}, \underline{y}$	coordinates of a material point
$\underline{X}$	back stress due to kinematic hardening
Y or $\underline{Y}$	damage energy release rate in isotropic or anisotropic damage models
Z	total scalar hardening variable in Bodner's model
$x\,y\,z$	principal strain direction in Marciniak and Kuczinsky's model
xy	plane coordinates in fracture mechanics
$X\,Y\,Z$	principal stress directions in Marciniak and Kuczinsky's model
Z_D	directional part of the total scalar hardening variable in Bodner's model

Greek letters

α	triaxiality function parameter
α	material constant in Rice & Tracey's model
α	angle between a tensile test direction and the material Rolling Direction
α_k	internal variable in general thermodynamic formulation
$\underline{\alpha}$	internal variable related to kinematic hardening
α, β	material parameters of damage evolution law in Geer's model
β	strain ratio in Hora's criterion
β	scalar damage variable in anisotropic damage model
$\underline{\beta}$	directional hardening, symmetric tensor in Bodner's model
γ	scalar value derivative of the stress according to plastic work in Bodner's model
$\underline{\gamma}$	center of the plastic yield surface in Zhu's model
δ	volumetric damage variable in Zhu's and Bodner's model
$\varepsilon_1 \ \varepsilon_2 \ \varepsilon_3$	principal strains
$\varepsilon_{eq}\ (\varepsilon_{eq}^{p})$	von Mises equivalent (plastic) strain $\sqrt{\frac{2}{3}\varepsilon_{ij}\varepsilon_{ij}}$
$\dot{\varepsilon}_{eq}$	von Mises equivalent plastic strain rate
ε_{eq}^{d}	damage equivalent strain
$\dot{\varepsilon}_k^{p}$	plastic principal strain rate in direction k
ε_m	mean strain
ε_N	mean effective plastic strain of the matrix at incipient nucleation
ε_{ps}	prestrain strain applied in one direction before a second sollicitation
ε_f	equivalent fracture strain
ε_0	assumed initial strain in Swift's type law
$\underline{\varepsilon}$	strain tensor
$\underline{\dot{\varepsilon}}$	strain rate tensor
$\underline{\varepsilon}^{e(p)}$	elastic (plastic) strain tensor
$\underline{\tilde{\varepsilon}}(\theta)$	dimensionless function depending on polar coordinate θ in fracture mechanics
$\underline{\overline{\varepsilon}}$	effective strain tensor
$\underline{\hat{\varepsilon}}$	deviatoric strain tensor
η	time dependent part of the instability in Boudeau & Gelin's approach

θ	integration scalar in Bodner's integration scheme
θ	angle relative to the crack plane in fracture mechanics
κ	monotonically increasing deformation history parameter in Geer's model
$\dot{\kappa}$	rate of the deformation history parameter
$\lambda_{(o)}$	(initial) void distribution parameter in Benzerga's work
$\dot{\lambda}_p \quad \dot{\lambda}_d$	plastic and damage Lagrange multipliers
ν	Poisson's ratio
ξ	spatial part of the instability in Boudeau & Gelin's approach
ρ	specific mass
$\overline{\sigma}$	uniaxial reference effective yield stress of the fully dense matrix material
$\sigma_1 \sigma_2 \sigma_3$	principal stresses
σ_0	elastic stress limit
σ_D	damage threshold stress in Bodner's model
σ_{eq}	von Mises equivalent stress $= \sqrt{\frac{3}{2}\hat{\sigma}_{ij}\hat{\sigma}_{ij}}$
σ'_{eq}	equivalent stress affected by damage in Hayakawa and Murakami's model
σ_m	hydrostatic (mean) stress = $(1/3)\sigma_{ii}$
$\overline{\sigma}_{eq}$	equivalent effective stress, yield stress of the fully dense matrix
σ_F	updated plastic limit stress
σ_h	plastic stress computed by Hill's model
σ_s	global saturation stress
σ_y	initial yield stress
σ_{ls}	saturation stress of directional hardening in Bodner's model
$\underline{\sigma}$	Cauchy stress tensor
$\underline{\tilde{\sigma}}(\theta)$	dimensionless function depending on polar coordinate θ in fracture mechanics
$\underline{\tilde{\sigma}}$	stress divided by specific mass in Rousselier's model
$\underline{\overline{\sigma}}$	effective stress tensor
$\underline{\hat{\sigma}}$	deviatoric Cauchy stress tensor
$\overset{\nabla}{\underline{\hat{\sigma}}}$	Jaumann stress rate
$\Sigma_1 \quad \Sigma_2$	stresses that replace $\overline{\sigma}$ in Leblond's version of Gurson's model
τ	tensile effect coefficient (ratio between deviatoric and isotropic damage)

χ	bulk modulus
χ_0	initial value of the bulk modulus
$\underline{\Omega}$	antisymmetric part of the velocity gradient tensor or total spin
ψ	Helmholtz free energy per unit mass
$\psi^{(0)e}$	elastic free energy function (in the undamaged, virgin material)
ψ^{d}	damage contribution to free energy
ψ^{ed}	elastic damage contribution to free energy
$\psi^{(0)p}$	plastic contribution to free energy (in the undamaged, virgin material)

1. INTRODUCTION

For more than 20 years, there has been a tremendous amount of research work in the area of elasto-plastic and elasto-visco-plastic damage continuum theories (Gurson 1977, Tvergaard 1982, Lemaître 1985, Perzyna 1986, Gologanu *et al.* 1993, van der Giessen & Tvergaard 1994a). The goal of these studies is the prediction of fracture during forming processes or structural loading for materials like metals, concrete, polymers, rocks... Thanks to the numerous improvements of numerical methods (Finite Element Method -FEM-, or Boundary Element Method -BEM-, or new meshless methods...), scientists are now able to simulate processes as different as forging, extrusion, rolling, deep drawing, wire drawing, cutting... By means of parametric studies, numerical approaches allow optimizations of industrial processes and a deeper understanding of industrial problems. Such a numerical optimization process is often quicker and cheaper than the way of trials and errors. These advantages have progressively convinced the industrial world, and, in some fields like automotive industry or can production for instance, numerical simulations are routinely used. This success has increased the request for reliable constitutive models and rupture criteria in order to produce accurate results and to allow their interpretation with regard to defect prediction.

Zhu's Ph.D. thesis (Zhu 1992) presents a review of the two common approaches of rupture prediction: classical behavior laws coupled with calculation of rupture criteria and continuum damage theory producing constitutive laws coupled with damage. As he has demonstrated, the second approach is more attractive: it allows the prediction of different fracture types, the rupture zone is well identified and crack growth can be followed. According to Lemaître 1985, using uncoupled constitutive equations gives rise to small errors on stresses and strains if the loading is far from the rupture conditions, but the errors may be of the order of 10 to 50 % close to failure. So, MSM research team has concentrated its work on damage models. Even if this field still requires improvements (more sophisticated fracture criteria than threshold value of damage variable, general solution to avoid mesh dependence...) different formulations for the damage theory already exist. They have been developed in order to describe the behavior of materials submitted to high temperature creep, high cycle fatigue, creep-fatigue interaction, spalling and ductile fracture....

There are mainly four kinds of damages: brittle, ductile, creep and fatigue damages. Such a characterization of damage assumes that the material is not the only factor to be considered; in addition, for the same material, damage evolution may be triggered by very different physical mechanisms that fundamentally depend on loading type, loading rate, temperature, as well as environmental factors such as exposure to corrosive substances or nuclear radiation. Therefore, rather than the material alone, the material-process-environment triad must be considered in the study of internal damage.

For many metallic materials at low temperature, **brittle** damaging occurs mainly in the form of cleavage of crystallographic planes in presence of negligible inelastic deformations. At high temperature, brittle damage can also be observed in association with creep processes. In that case, the decohesion of interatomic bonds is concentrated at grain boundaries. At low stresses, this phenomenon is accompanied by relatively small strains.

Ductile damage, on the other hand, is normally associated with large plastic deformations in the neighborhood of crystal defects. The decohesion of interatomic bonds is initiated at the boundary interface between inclusions, precipitates and particles of alloying elements leading to the formation of microscopic cracks and cavities. Further evolution of local plastic deformations may cause the cavities to grow and eventually coalesce, resulting in final rupture. This mechanism is schematically illustrated in Figure 1-1.

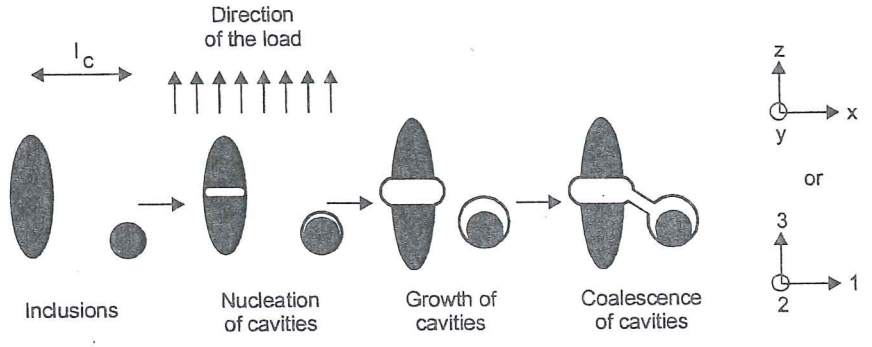

Figure 1-1 : Modeling of ductile fracture and definition of axis (adapted from Rousselier 1987).

The models developed in Liège and presented in Chapters 6 and 7 account for ductile fracture during forming processes; so the following review mainly deals with this specific topic.

Fatigue damage is normally observed in mechanical components subjected to a large number of load and/or temperature cycles. Although fatigue damage occurs at stress amplitudes below the plastic yield limit, the nucleation of micro-cracks is attributed to the accumulation of dislocations observed in connection with cyclic plastic deformation due to stress concentration near microscopic defects. A large number of complex interactive physical mechanisms take place from crack nucleation to complete failure. The understanding of fatigue degradation processes in metals remains a challenging issue in the field of material science. As roughly summarized by Lemaître 1985, the high-cycle fatigue loading, for which the number of cycles to failure is higher than 10^5, does not produce any significant macroscopic plastic strain. This damage is essentially due to transcristalline micro-cracking.

In order to represent the strain rate increase that characterizes tertiary **creep**, Kachanov 1958 replaced the observed uniaxial stress by an effective stress computed by means of a scalar damage internal variable. This was the first Continuum Damage Mechanics model. Later, Rabotnov 1963 proposed a physical significance for this damage variable: the reduction of the cross-section area due to micro-cracking. Then, Leckie & Onate 1981 used a sequence of even rank irreductible tensors to represent the void distribution on the grain boundaries in the context of creep-damage theories.

Another typical classification of damage models is deduced from their scales: the microscale, the mesoscale and the macroscale, as presented in Table 1-1 reproduced from Eckstein 1997.

Scale	Defects	Models
MICRO Atoms, molecule chains	 Vacancies and dislocations	Physics and material sciences
MESO Grains	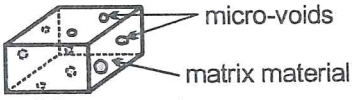 Micro-cracks, pores	Micromechanics
MACRO Test specimen structures	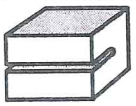 Macro-cracks, shear bands	Continuum theories

Table 1-1 Classification of damage models (from Eckstein *et al.* 1997).

The **microscale** description of damage characterizes the material at the atomic level. The simulation technique of molecular dynamics is based on the motion of a given number of atoms, governed by their mutual interactions described by means of continuous interatomic potentials. It requires the numerical integration of Hamilton's equation of motion. These models study samples of micron size on parallel computers and are therefore not appropriate for engineering applications. However, such approach significantly improves the understanding of the physical principles underlying the elementary processes involved in fracture. For instance, atomistic modeling explains why, depending on material, the dislocation nucleation models of Rice or Peierls are confirmed or not. In fact, the reason lies in different ratios of unstable stacking energy and surface energy (Gumbsch 1995). Another example is a better understanding of the transition between ductile and brittle rupture (Abraham 1995).

The **mesoscale** approach consists in evaluating the behavior of an elementary cell the scale of which lies between that of a subgrain (microscopic) and that of the specimen (macroscopic). For instance, finite element simulations predict the behavior of a

representative cell containing a simple cavity or an inclusion (Luo & Sthalberg 1998), embedded in an elasto-plastic or elasto-visco-plastic matrix, for all kinds of loading conditions, such as torsion, tension or various mechanical states with a constant triaxiality ratio. Figure 1-2 shows one example. Such an approach allows comparisons of void growth between mesoscopic analysis, experiments and macroscopic models like Gurson-Tvergaard's model or Gologanu's model, as presented by Brethenoux et *al.* 1997.

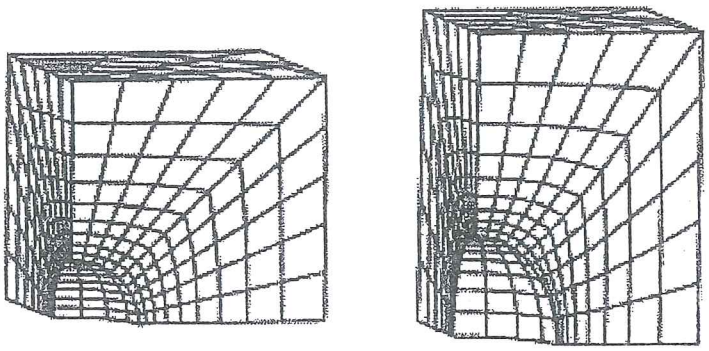

Figure 1-3 : Example of a mesoscopic mesh approach, evolution of a simple cavity; (from Brethenoux *et al.* 1997).

Boyer & Staub 1997 also use the mesoscopic approach to check void growth models such as Rice & Tracey's 1969 or Thomason's 1990. In Gologanu *et al.* 1993, mesoscopic finite element simulations, still limited to one cavity cell, suggest a slight modification of the damage model proposed by Gologanu. van der Giessen & Tvergaard 1994a, 1994b use the planar analysis of a unit cell containing many grains to study the effect of random variations in microstructure on failure events in a metal subjected to creep at high temperatures. Their model accounts for intergranular failure by cavity nucleation and growth to coalescence, or by grain boundary sliding.

As a researcher situated at the limit between two worlds, the metallurgical one and the mechanical one, and, within the latter, being more concerned by the particular sub-domain of numerical simulation, the mesoscale approach seems under-exploited. The advantages of this method are, for instance, to avoid restrictive assumptions usually used in analytical models (spherical or simple shape of void, matrix linear hardening ...) and to give a good account of ductile damage phenomena (nucleation, growth and coalescence) for all kinds of loading conditions. This last point is fundamental, when one is aware of the experimental difficulties to reproduce the mechanical states frequently applied to some metal pieces. It can be the only way to fit with accuracy the model parameters for shear state. It represents a very efficient tool for validating analytical models, for understanding the coalescence phenomena and for choosing adequate formulations. It can also be regarded as a rather easy way to reach some microscopic parameters like volume fraction of initial void when compared to SEM analysis or complete inverse modeling (Lauro *et al.* 1997). In conclusion, the

mesoscopic approach seems a promising way to increase the understanding of damage mechanism, to help with the development and validation of analytical models and hence to improve macroscopic modeling.

Finally the **macroscale** models are characterized by the homogenization of the material behavior. The presence of a large number of micro-defects is considered as smeared throughout the solid, leading to continuum damage theories. Evolution laws for damage variables can be defined by means of phenomenological models (Zhu 1992, Habraken *et al.* 1997) or deduced from micro-mechanical observations (Perez *et al.* Andrés 1997). These types of continuum damage models provide a computationally efficient investigation tool for large-scale structures and offer the advantage of being already implemented in commercial finite element codes, like for instance a Gurson's type law in ABAQUS (Picart *et al.* 1997). Numerous research teams prefer to work with their home made code, in which new or well-known damage models can be easily added. The damage laws implemented in the LAGAMINE code will be presented in Chapters 6 and 7 (Zhu *et al.* 1992, Zhu *et al.* 1995, Wang *et al.* 1996, Habraken *et al.* 1997, Zhang *et al.* 1998). Other examples are Gurson's type law implemented in the ASTRID code (Lazzaretto *et al.* 1996) or a mixed Gurson-Perzyna's law implemented in the METAFOR code (Stainier 1996). A historical review of the development of continuum damage mechanics is presented by de Souza Neto *et al.* 1998.

The book by Voyiadijs & Kattan 1999 about advances in damage mechanics in metal and metal matrix composites summarizes well the state of the art of this field. It offers the interest of presenting a connection between the models applied for metals and composites.

Nowadays, damage mechanics has become an efficient way to solve practical problems. For instance, Doghri 2000 includes a chapter on this topic in his recent introduction to the mechanics of deformable solids and structures.

The goal of next chapters is not to provide a complete overview of damage mechanics applied to metals. However, it has been tried to gather the information necessary to understand damage mechanics; it helps to seize the advantages and limitations of the models developed in Liège. Following this idea, Gurson's model and its further developments are presented in Chapter 2. This macroscopic model with its microscopic bases has met a great success, justified by its good performance as demonstrated by comparisons between simulation results and experimental fractures.
In Chapter 3, thermomechanical damage models are described. Because Lemaître's model is widely used and constitutes the basis of the work performed in MSM department, it is recalled in details.
Gurson and Lemaître's models represent examples of the model families respectively based on micromechanics and continuum thermodynamics. The constitutive models based on variational bounds, like the one of Ponte Castenada & Zaideman 1994 for instance, are not presented in details not for a lack of interest but because they are less

commonly used for metals. This approach is briefly summarized in section 2.2, which compares Gurson's and Hashin-Shtrikman's yield surfaces.

To take advantage of damage simulation results, one must be able to detect where and when fracture will happen. So Chapter 4 gathers interesting rupture criteria. However, this field still requires further research and it seems that no general unique criterion exists.

A well-known problem in FEM damage simulations is the mesh dependency of the results. This problem cannot be forgotten in any work dedicated to damage; so Chapter 5 briefly summarizes the research on this tropic.

Chapter 6 and 7 present the work performed by the MSM team under Habraken supervision. Each of them is dedicated to one specific application: respectively the study of aluminum rods in Chapter 6 and steel sheets in Chapter 7. The different models developed and applied in these cases are described as well as their results. The used models belong to the field of macroscopic continuum damage mechanics and present different characteristics:

- isotropic damage, isotropic elasto-plastic-law,
- isotropic damage, isotropic elasto-visco-plastic-law,
- anisotropic damage, anisotropic elasto-plastic-law.

Finally Chapter 8 gives some conclusions and perspectives.

References

Abraham F.F. (1996) Parallel molecular dynamics investigation fracture. *Computer simulation in materials science*, Kluwer Academic Publishers, 211-226.

Boyer, J.C., Staub, C., (1997) A ductile damage model including shear stress effects. *Advanced Methods in Materials Processing Defects*, Predeleanu, M., Gilormini, P., Eds., Elsevier, 13-22.

Brethenoux, G., Mazataud, P., Bourgain, E., Muzzi, M. & Giusti, J. (1997) A mesoscopic approach of ductile damage during col forming processes, *Advanced Methods in Materials Processing Defects*, Predeleanu, M., Gilormini, P., Eds., Elsevier, 23-32.

Doghri, I., (2000) Mechanics of Deformable Solids, Linear, Nonlinear, Analytical and Computational Aspects, Springer Ed.

Eckstein, A., Basar, Y. & Konke, C. (1997) Damage analysis of ductile metallic shells. *Computational plasticity – Fundamentals and Applications*, COMPLAS V, Owen, D.R.J, Onate, E., Huiton, E., Eds, CIMNE, Barcelona.

Gologanu, M., Leblond, J.B, Devaux, J., (1993) Approximate models for ductile metals containing non-spherical voids – case of axisymmetric prolate ellipsoïdal cavities, *J. Mech. Phys. Solids*, **41-11**, 1723-1754.

Gumbsch P., Atomistic modeling of failure mechanisms, *Computer simulation in materials science*, Kluwer Academic Publishers, 227-244.

Gurson, A.L. (1977) Continuum theory of ductile rupture by void nucleation and growth. *J. Engng. Materials Technology*, **99**, 2-15.

Habraken, A.M., Charles, J.F., Cescotto, S. (1997) Calibration and validation of an anisotropic elasto-plastic damage model for sheet metal forming, in *Damage Mechanics, in Engineering Materials*, Voyiadjis, G.Z., Ju, J.W., Chaboche, J.L., Eds., Elsevier, 401-420.

Kachanov, L.M. (1958) Time of the rupture process under creep condition, *Izv. Akad. Nauk SSSR, Otd. Tekhn. Nauk*, **8**, 26-31.

Krajcinovic, D., (2000) Damage mechanics : accomplishments, trends and needs, *International Journal of Solids and structures*, **37**, 267-277.

Lazzarotto, L., Picart, P. Oudin, J. (1996) Sensitivity of Material Parameters in the Finite Element Computation of Microvoid Nucleation and Growth, *Int. J. of Damage Mechanics*, **5**, 259.

Lauro, F., Barrière, T., Bennani, B., Drazetic, P., J. Oudin (1997) Damage framework for the prediction of material defects : identification of the damage material parameters by inverse technique, *Advanced Methods in Materials Processing Defects*, Predeleanu, M., Gilormini, P., Eds., Elsevier, 165-174.

Leckie, F.A., Onate, E.T. (1981) Tensorial nature of damage measuring internal variables, in Proceedings of the IUTAM *Symposium on physical nonlinearities in structures*, Springer, 140-155.

Lemaître, J. (1985) Coupled elastoplasticity and damage constitutive equations, *J. Comp. Meth. in Appl. Mech. and Eng.* **51**, 31-49.

Luo, C. , Stahlberg, U. (1998) FEM simulation of void formation close to an inclusion in a uniform matrix during plastic deformation, *NUMIFORM 98, Simulation of Materials Processing :Theory, Methods and Applications,* Huetink, J., Baaijens, F.P.T., Eds., Balkema, 379-384.

Peres Aparicio, J.L., de Andres, A., Ortiz, M. (1997) 3D interface element applied to the simulation of crack growth with plasticity. *Computational Plasticity – Fundamentals and Applications*, COMPLAS V, Owen, D.R.J, Onate, E., Huiton, E., Eds, CIMNE, Barcelona, 2011-2018.

Perzyna, P. (1986) Internal state variable description of dynamic fracture of ductile solids, *Int. J. Solids & Struct.*, **22**, 797-818.

Picart, P., Piechel, G. & Oudin, J. (1997) Damage influence in the finite element computations for large strains elastoplastic mechanical structures, *Advanced Methods in Materials Processing Defects*, Predeleanu, M., Gilormini, P., Eds., Elsevier, 175-184.

Ponte Castaneda, P., Zaidman, M. (1994) Constitutive models for porous materials with evolving microstructure, *J. Mech. Phys. Solids*, **42-9**, 1459-1497.

Rousselier, G. (1987) Ductile fracture models and their potential in local approach of fracture, *Nuclear Engineering and Design*, **105**, 97-111.

Rabotnov, Y.N., (1963) On the equations of state for creep. *Progress in Applied Mechanics*, Prager Anniversary Volume, New-York, Mac Millan, 307.

Rice, J.R., Tracey, D.M. (1969) On the ductile enlargement of voids in triaxial stress fields, *J. Mech. Phys. Solids*, **17**, 201-217.

de Souza Neto, E.A., Peric, D., Owen, D.R.J. (1998) Continuum modelling and numerical simulation of material damage at finite strains, *Archives of Computational Methods in Engineering*, **5-4**, 311-384.

Stainier, L. (1996) Modélisation numérique du comportement irréversible des métaux ductiles soumis à grandes déformations avec endommagement. Thèse de docteur en sciences appliquées, Université de Liège.

Thomason, P.F. (1990) Ductile fracture of metals, Pergamon Press.

Tvergaard, V. (1982) Material failure by void coalescence in localized shear bands, *Int. J. Solids & Struct.* **18**, 659-672.

Van der Giessen, E., Tvergaard, V. (1994a) Development of final creep failure in polycrystalline aggregates. *Acta Metall. mater.*, **42-3**, 959-973.

Van der Giessen, E., Tvergaard, V. (1994b) Effect of random variations in microstructure on the development of final creep failure in polycrystalline aggregates. *Modelling Simul. Mater. Sci. Eng.***2**, 721-738.

Voyiadijs, G.Z., Kattan, P.L., (1999) Advances in Damage Mechanics : Metals and Metal Matrix Composites, Elsevier.

Wang, X.C., Habraken, A.M. (1996) An elastic-visco-plastic damage model : from theory to application, *supplément au Journal de Physique*, **6**, 549-558.

Zhang, L.H., Habraken, A.M., Wang, X.C. (1998) Validation of an Elasto-Visco-Plastic Model of Bodner Type Coupled with Damage. *NUMIFORM 98, Simulation of Materials Processing : Theory, Methods and Applications*, Huetink, J., Baaijens, F.P.T., Eds., Balkema, 291-296.

Zhu, Y.Y. (1992) Contribution of the local approach of fracture in solid dynamics, Ph. D. Thesis, University of Liège, Department MSM.

Zhu, Y.Y., Cescotto, S. and Habraken, A.M. (1992) A fully coupled elastoplastic damage modeling and fracture criteria in metalforming processes, *J. of Mater. Processing Technology* **32**, 197-204.

Zhu, Y.Y., Cescotto, S., Habraken, A.M. (1995) Modelling of fracture initiation in metalforming processes, *Materials Processing Defects*, Gosh, S.K., Predeleanu, M., Eds, 155-170, Elsevier Science B.V.

2. GURSON'S MODEL

2.1. Description of Gurson's model and its further developments

Ductile fracture results from initiation, growth and coalescence of cavities as already summarized in Figure 1-1. In fact, Gurson has first derived his model from an approximate limit analysis of a hollow sphere made of rigid perfectly plastic material (representing a typical volume element in a porous medium) and subjected to some axisymmetric loading. Then, in a purely phenomenological and macroscopic way, he has extended his result to the case of a matrix exhibiting isotropic hardening. Finally, Gurson's yield function (Gurson 1977) improved by Tvergaard 1981 for ductile porous metals is defined by:

$$F_p = \frac{\sigma_{eq}^2}{\overline{\sigma}_{eq}^2} + 2q_1 f \cosh\left(\frac{3}{2} q_2 \frac{\sigma_m}{\overline{\sigma}_{eq}}\right) - (1 + q_3 f^2) = 0 \qquad (2\text{-}1)$$

with

σ_{eq} = macroscopic von Mises equivalent of Cauchy's stress, in the context of large strains,

$= \sqrt{\frac{3}{2} \underline{\hat{\sigma}} : \underline{\hat{\sigma}}}$ where $\underline{\hat{\sigma}}$ is the deviatoric stress tensor,

σ_m = macroscopic mean stress = 1/3 tr $\underline{\sigma}$,

f = microvoid volume fraction or porosity ,

$$f = (V_A - V_M)/V_A \qquad (2\text{-}2)$$

where V_A is the elementary apparent volume of the material,
V_M is the elementary volume of the matrix,

f_0 = initial microvoid volume fraction,

q_1, q_2, q_3 constant coefficients later introduced by Tvergaard (Tvergaard, 1981, 1982) but not used in the initial Gurson's law ($q_1=q_2=q_3=1$),

q_1 = parameter to account for interactions between voids,

q_2 = parameter to account for void shape,

q_3 = often defined as q_1^2, this parameter also takes into account void interaction,

$\overline{\sigma}_{eq}$ = yield stress of the fully dense matrix material.

The equivalence between the plastic power dissipated into the material and into the corresponding matrix enables to define the effective values:

$$(1-f)\overline{\sigma}_{eq}\dot{\overline{\varepsilon}}_{eq} = \underline{\sigma} : \underline{\dot{\varepsilon}}^p \qquad (2\text{-}3)$$

where $\dot{\bar{\varepsilon}}_{eq}$ is an average plastic strain rate in the fully dense matrix, also called effective plastic strain rate. $\bar{\sigma}_{eq}$, $\dot{\bar{\varepsilon}}_{eq}$ are scalar variables while $\underline{\sigma}$, $\underline{\dot{\varepsilon}}^{p}$ are Cauchy stress and plastic strain rate macroscopic tensors.

The additional parameters q_i ($q_1 \cong 1.5$; $q_2 \cong 1$; $q_3 \cong q_1^2$) were proposed by Tvergaard 1981 to bring predictions of shear band bifurcation based on Gurson's constitutive relation into closer agreement with corresponding results of a totally numerical analysis of a periodic array of voids. Perrin & Leblond 1990, using a self-consistent method and their improved version of Gurson's model, find q_1 between 1.35 and 1.38 and $q_2 = 1$. They also report that the experimental values q_1 of generally lie in the range from 1.5 to 2.0.

Note three properties of relation (2-1) :

- it reduces to the isotropic von Mises' yield criterion for $f=0$,
- the dependence on void volume fraction is simple when $\sigma_m = 0$ as in pure shear:

$$F_p = \frac{\sigma_{eq}^2}{\bar{\sigma}_{eq}^2} + 2q_1 f - 1 - q_3 f^2 = 0 \qquad (2\text{-}4)$$

- the dependence on stress triaxiality is exponential.

In Gurson's type models, damage is directly linked with the microvoid volume fraction f. Its evolution follows the three phases of void nucleation (f_n), growth (f_g), and coalescence (f_c). The final rate of microvoid volume fraction is given by additivity :

$$\dot{f} = \dot{f}_n + \dot{f}_g + \dot{f}_c \qquad (2\text{-}5)$$

- **The nucleation** of new microvoids is due for instance to decohesion of matrix - inclusion or matrix-second phase interfaces, or to hard particle fracture. Considering a Gaussian inclusion distribution, an assumption is that the microvoid nucleation rate is mainly controlled by the equivalent plastic strain and defined by the relationship proposed by Chu & Needleman 1980:

$$\dot{f}_n = \frac{f_N}{S_N\sqrt{2\pi}} \exp\left\{-\frac{1}{2}\left(\frac{\bar{\varepsilon}_{eq} - \varepsilon_N}{S_N}\right)^2\right\} \dot{\bar{\varepsilon}}_{eq} \qquad (2\text{-}6)$$

where

f_n = nucleated microvoid volume fraction,

f_N = potential nucleated microvoid volume fraction in relation, for instance, with the inclusion volume fraction,

ε_N = mean effective plastic strain of the matrix at incipient nucleation,

S_N = Gaussian standard deviation of the normal distribution of inclusions,

$\bar{\varepsilon}_{eq}$ = equivalent effective plastic strain in the matrix (see relation (2-3)).

For steel sheets, according Chu & Needleman 1980 or Lazzaretto *et al.* 1996, the possible values of the parameters are: $f_N = 0.04$; $0.01 \leq S_N \leq 0.2$; $0.3 \leq \varepsilon_N \leq 0.7$.

The interested reader can refer to the review paper by Montheillet & Moussy 1986 to have a description of the most common nucleation modes and models.

- **The growth of existing microvoids**: in Gurson's model, the growth rate equation comes from the apparent volume change, the mass conservation and the matrix plastic incompressibility. It is easily derived from relation (2-2):

$$\dot{f}_g = \frac{V_M \dot{V}_A}{V_A^2} = (1-f)\,tr\underline{\dot{\varepsilon}}^p \tag{2-7}$$

- **The coalescence of neighboring microvoids** yields to final material failure. As summarized in Pardoen's 1998 bibliographical review, numerous coalescence modes exist and experimental observations are difficult. This short presentation is limited to one possibility, proposed by Tvergaard & Needleman 1984, which is frequently used (Koplik & Needleman 1988, Brunet *et al.* 1997, Lauro *et al.* 1997). In this approach, f_c is not used as an additive part of the porosity but a specific coalescence function f^* replaces the porosity f in relation (2-1) .The aim of this parameter change is to model the complete vanishing of the carrying stress capacity due to void coalescence, at a realistic void volume fraction :

$$f^* = f \qquad if\, f < f_{cr}$$

$$f^* = f_{cr} + \frac{f_u - f_{cr}}{f_F - f_{cr}}(f - f_{cr}) \qquad if\, f > f_{cr} \tag{2-8}$$

where

f_u = the ultimate value of f^* at the occurrence of ductile rupture, also related to the material parameter q_1 introduced by Tvergaard ($f_u = 1/q_1$),

f_{cr} = the critical void volume fraction at coalescence onset, generally in the range [0.1-0.25] (Tvergaard 1982, Needleman & Tvergaard 1984),

f_F = the porosity at final failure.

As demonstrated by Koplik & Needleman 1988, this latter improvement f^* as well as the q_i coefficients of Tvergaard are necessary to enable Gurson's model to recover results from a mesoscopic approach (cell model of an array of voids loaded with different constant triaxiality ratios) near rupture. This article also shows a limit of Gurson's approach: a same initial void volume fraction f_0 can correspond to different cell geometries which are then characterized by different f_{cr} values (more details will be presented in section 4.1.).

As checked by Leblond, Perrin and Devaux 1995, Gurson's model is incompatible with the classical, exact solution of the problem of a hollow rigid hardenable sphere hydrostatically loaded. Another drawback of Gurson's model is the following one: for any loading path corresponding to a fixed triaxiality, it predicts that the "porosity-macroscopic equivalent plastic strain" curve depends only on the initial porosity f_o

and on the triaxiality T ($T = T_m / T_{eq}$) but not on the hardening exponent. This fact disagrees with both experiments and numerical simulations of the behavior of porous hardenable elementary cells (Leblond *et al.* 1995). These authors propose the following modified yield function :

$$F_p = \frac{\sigma_{eq}^2}{\Sigma_1^2} + 2qf\ cosh\left(\frac{3}{2}\frac{\sigma_m}{\Sigma_2}\right) - (1+qf^2) = 0 \qquad (2\text{-}9)$$

where the stresses $\Sigma_1 = F_1(f_0,E_{eq},E_m)$ and $\Sigma_2 = F_2(f_0,E_{eq},E_m)$ are directly determined from the analysis of a rigid hardenable hollow sphere subjected to an axisymmetric proportional prestraining. E_{eq}, E_m are two overall hardening parameters, respectively depending on the deviatoric and hydrostatic parts of the macroscopic plastic strain rate. Functions F_1 and F_2 are tabulated by integrating analytical expressions derived by Leblond *et al.* 1995. Two types of hardening are considered : isotropic, as in the original Gurson's model, and kinematic, as in Mear & Hutchinson's 1985 variant of Gurson's model. The adjustable factor q, introduced by Tvergaard 1981 to bring predictions into closer agreement with numerical analysis of a periodic array of voids is retained in Leblond & Perrin's model. This model helps to check that this parameter q depends only on the geometry of voids and not on the hardening exponent. Pardoen 1998 has performed an extended analysis of the behavior of a copper specimen. His numerous comparisons between experiments and simulations with Gurson's model (2-1) or Gurson-Leblond-Perrin's model (2-8) demonstrate the superiority of the latter model.

Gologanu *et al.* 1993 derive their model from the analysis of an ellipsoidal volume containing a co-focal ellipsoidal cavity. They propose another improvement of Gurson's approach. After some approximations, their theory can be reduced to a Gurson like criterion adapted to materials containing axisymmetric prolate ellipsoidal cavities with parallel orientations. The modifications of the classical Gurson-Tvergaard's criterion (2-1) are the following ones:

- a new internal parameter is introduced: the *void shape factor*, and its evolution rule;
- the hydrostatic stress is replaced by a stress taking into account the stress field anisotropy;
- a factor, function of porosity f, eccentricities e_1 and e_2 of the inner and outer ellipsoids, replaces q_2;
- the evolution of e_1 and e_2 depends *on the void shape factor*.

Since Zhu's model presented in Chapter 7 concerns anisotropy in both plastic and damage behavior, it is worth noticing the works of Doege *et al.* 1997a, 1997b or Brunet *et al.* 1997, Brunet *et al.* 2000. Both authors and co-workers use an anisotropic version of Gurson's model where the equivalent von Mises' stress in equation (2-1) is replaced by the equivalent value given by Hill's anisotropic model. This anisotropic Gurson's extension is empirical. However, Benzerga *et al.* 1997 propose an analysis of the problem of a hollow sphere made of a rigid perfectly

plastic material obeying Hill's criterion and deduce an anisotropic plastic potential quite similar to the one used by Doege and Brunet. Other descriptions of an anisotropic yield locus, such as Barlat & Lian 1989 have also been coupled with the modified Gurson-Tvergaard's model by Brunet *et al.* 1997.

Zhu's models (sections 6.3 and 7.2) and Bodner's damage model (section 6.2) take into account the decrease of elastic parameters due to damage, while the classic Gurson's approach neglects this phenomenon. So, it is interesting to note that Stainier 1996 has proposed a modification of Gurson's model to account for it. As in other well-known models like Perzyna 1986 or Eftis & Nemes 1991, he uses Mackenzie's 1959 relations to represent the degradation of elastic shear and bulk moduli with void growth. The law proposed by Stainier 1996 is a damage elasto-visco-plastic model since Perzyna potential is used with the plastic surface proposed by Gurson. Needleman & Tvergaard 1987 had already proposed such a viscous extension of Gurson's law.

An advantage of Gurson's model is the easy way to link it with microscopic fracture criteria. If spherical voids are assumed, their updated radius R is easily computed from porosity f and initial radius R_0 :

$$\frac{R}{R_0} = \left(\frac{f}{f_0}\right)^{1/3} \tag{2-10}$$

Following Pardoen's 1998 review about growth models (Rice & Tracey 1969, Worswick & Pick, 1990), the following equations, used as post-processor of the FEM analysis results, can approximate the updated ellipsoidal shape of the void:

$$\frac{dR}{R} = A\, exp\left(\frac{3\sigma_m}{2\sigma_{eq}}\right) d\varepsilon_{eq} \tag{2-11}$$

$$\frac{\dot{R}_k}{R} = \frac{\dot{R}}{R} + (1+E)\dot{\varepsilon}_k \tag{2-12}$$

where A is a material constant initially evaluated by Rice at 0.283 for a rigid plastic material, E is a void shape parameter and R_k is the void radius in the principal direction k.

2.2. Comparison between Gurson's and Hashin-Shtrikman's yield surfaces

As summarized in Ponte Castaneda & Zaidman 1994, an approach to account for void interactions can be associated with the effective properties of composites with random microstructures. Scientists in this field obtain bounds for the effective potentials of porous or rigidly reinforced materials with isotropic microstructures, using an extension of Hashin-Shtrikman's 1963 variational principles. For instance, this homogenization technique allows to recover Eshelby's 1957 estimates for a

material with dilute concentrations of aligned ellipsoidal inclusions dispersed in a matrix. So, using a lower bound of the effective potential of nonlinear composite materials, the particular case of a rigid-perfectly plastic matrix material with aligned ellipsoidal voids is expressed in terms of an upper bound effective yield function, hereafter called Hashin-Strickman's yield function (HS). The internal variables used in this HS function are the void volume fraction f and the ratios of the ellipsoidal pore radii: R_3/R_1 and R_2/R_1. The classical relation (2-6), deduced from matrix incompressibility, is used as evolution law for f. The rates of change of the void radii ratios are related to the strain rate within the voids, that can be estimated thanks to Hashin-Shtrikman's assumptions.

Figure 2-1 compares sections of the HS yield surface, computed with fixed values of porosity and void shape to sections of Gurson's yield surface, based on the assumption of spherical voids (GS) or cylindrical voids (GC). The void shape factor is defined by $w=R_3/R_1=R_3/R_2$; $w=1$ or $=\infty$ respectively means spherical or cylindrical voids, while values less (greater) than 1 characterize oblate (prolate) voids.

The axes are defined on Figure 1-1. For small values of porosity (Figure 2-1a. and b.) and highly triaxial loading ($T=\sigma_m/\sigma eq$), Gurson's yield surfaces for spherical (GS) and cylindrical (GC) voids are significantly smaller than the corresponding HS yield surface ($w=1$ and ∞ respectively). This indicates that the HS yield surface is not particularly useful for high triaxiality values. For relatively low values of the triaxiality variable, the yield surfaces GS, GC, HS $w=1$ or ∞ are in close agreement. Recalling that HS surfaces are upper bounds, the fact that the GS surface lies outside the HS yield surface for $w=0.1$ suggests that the GS model is not adequate for oblate voids. The HS model becomes a better option for the whole range of void shapes, from oblate to prolate, provided the triaxiality remains small ($|T|<4/3$).

For moderately large value of the porosity (Figure 2-1c. and d.), HS and Gurson's yield surfaces for both spherical and cylindrical voids are in fairly good agreement, even for high triaxiality. Again, Gurson's model provides rather poor estimates for the yield surfaces of porous materials with flat aligned voids.

Finally, comparing Figures 2-1a., b. and Figures 2-1c., d., one can observe that increasing porosity has a definite softening effect on the porous solid.

The HS surface can be computed simultaneously with the evolution of the void shape and porosity (Ponte Castaneda & Zaidman 1994). Such an approach has demonstrated that the effect of void shape can be as significant as porosity, especially in case of low triaxiality. It was also found that the predictions of shear localization are sensitive to the evolution of porosity, which acts as a hardening-softening mechanism in compression-tension. It is also sensitive to the anisotropy parameters, which typically act in opposite fashion.

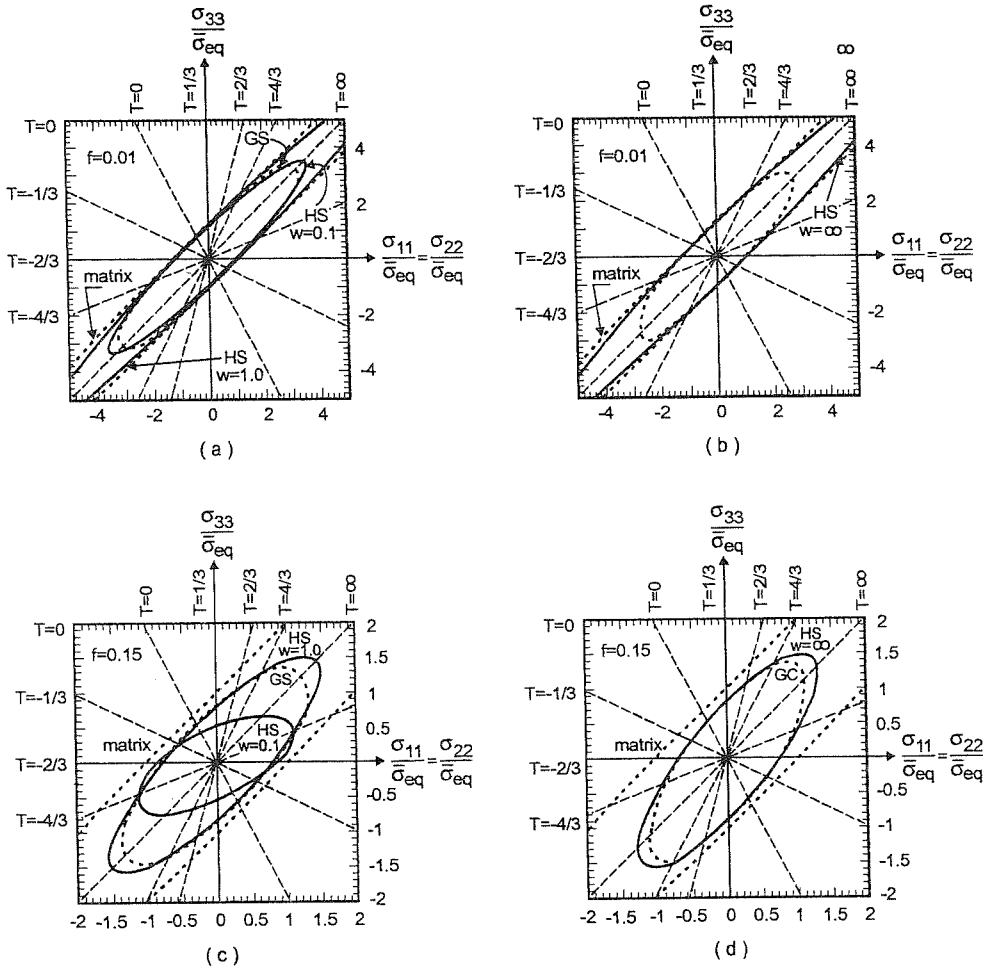

Figure 2-1 Comparison of cross sections of HS and Gurson's yield surfaces for porous materials with aligned spherical (w=1), cylindrical (w=∞) and oblate (w=0.1) voids (from Ponte Castenada & Zaidman 1994).

HS for w =1 and 0.1 versus Gurson with spherical voids (GS) at f=0.01
HS for w = ∞ versus Gurson with cylindrical voids (GC) at f=0.01
HS for w =1 and 0.1 versus Gurson with spherical voids (GS) at f=0.15
HS for w = ∞ versus Gurson with cylindrical voids (GC) at f=0.15

2.3. Conclusions about the use of Gurson's model

The microscopic physical bases of their development as well as their accuracy in fracture prediction explain the great success of Tvergaard-Gurson's model or its extensions. In practice, the model summarized by relations (2-1) to (2-7) requires 8 microscopic parameters:

- f_0 : initial void volume fraction,
- q_1,q_2, ($q_3=q_1^2$) : Tvergaard's material coefficients,
- nucleation parameters: ε_n, S_n, f_n,
- coalescence description: f_{cr}, f_F, ($f_u=1/q_1$).

One must add macroscopic parameters defining the hardening behavior of the matrix, to these 8 microscopic parameters. So, to retain the physical advantage of the model, the user should use optic and electronic microscopic analysis and accurate relative density measurements, obtained for instance by the double weight method, in order to reach the microscopic material parameters. Even with such an equipment, the deduction of f_0 is not always straightforward. A classical approximation is to choose it equal to the volume fraction of inclusions f_v. In some cases, this value can be estimated from the chemical composition of the material (Mudry 1982). However, due to the frequent high anisotropy of ductile fracture, different f_0 can be used depending on the direction of the main loading or the direction of the cracks to be examined. Mudry 1982 has observed that the formed cavities size basically depends on the dimensions d_x d_y of inclusions perpendicular to the load direction z (see Figure 1-1). He proposes to use:

$$f_0 = f_v \frac{(d_x d_y)^{1/2}}{d_z} \tag{2-13}$$

Some well-equipped researchers effectively define the parameters of Gurson's model by microscopic measurements (Rousselier *et al* 1989, Pardoen 1998, Benzerga *et al* 1999). However most mechanical engineers using Gurson's approach have no access to such techniques. So, they have to rely on bibliographical information like the one proposed by Chu & Needleman 1980 or Lazzaretto *et al.* 1996a, which does not always fit their materials. Note that, in his Ph. D. thesis, Wilsius 1999 proposes tables with Gurson-Tvergaard-Needleman parameters for a large set of materials.
This gives mechanical engineers an order of magnitude about values of the model microscopic parameters. In some cases, they try to fit microscopic parameters on macroscopic measurements from damage tests (notched tensile test or other ones) or, less convincingly, from a global tensile curve already used to find the macroscopic parameters of the model (apparent stress-strain curve function). In the latter case, an open question is: "Has their approach any advantage when compared to the use of phenomenological models like the one proposed by Lemaître 1985, in which, at least, the damage function is based on macroscopic measures of the decrease of apparent Young's modulus?" For Gurson's type law, some authors have studied the sensitivity of the microscopic material parameters in regard to the finite element simulation results. For Lazzarotto *et al.* 1996a and 1996b, the initial volume fraction f_0, the effective plastic strain at incipient nucleation ε_N and the potential nucleated microvoid volume fraction f_N are the most sensitive microscopic material parameters. For instance, in cold forging processes, modifications of the initial porosity induce significant variations of the required axial load and of the filling ratio in die cavities. However Picart *et al.* 1997 verify that an accurate characterization of f_0 is not

necessary for small values of the initial porosity. Both preceding studies use no coalescence description (parameters f_{cr}, f_F, f_u). Nevertheless, the work of Koplik & Needleman 1988 demonstrates the importance of f_{cr} to recover the sudden drop of macroscopic stress-strain curves, the parameter f_F being essential to obtain a good approximation of the curves of void volume fraction versus strain, for $f > f_{cr}$.

By means of the development of general inverse modeling techniques, mechanical engineers with no metallurgical microscopic equipment try to reach microscopic parameters with accuracy. It is well known that inverse techniques applied to non linear finite element simulations to identify constitutive law parameters are not straightforward. The unicity of the parameter set provided by such approach is not guaranteed. One must rely on of a set of experimental results sensitive to all the parameters. When strong differences exist between parameters sensitivities, the method convergence can be low. A good example is presented by Lauro *et al.* 1997 : they work on a notched tensile test and adopt the variation of the inner radius in function of the longitudinal elongation as macroscopic response. Their cost function, expressed in a least square sense, measures the difference between FEM simulations and experimental responses and they use a classical optimizer module to find the material parameters minimizing their cost function. They first take some bibliographic values for the microscopic parameters and fit the macroscopic parameters. Then, in a second run, the macroscopic parameters are fixed and they search for some microscopic ones (ε_N, f_N, q_1) related only to void nucleation and growth because their experiment is not able to produce reliable data on the coalescence process. This choice is also suggested by their sensitivity analysis. They report that the optimization of these 3 microscopic parameters has required 292 iterations, which means that the FEM modeling of their notch experiment must be CPU time efficient to avoid unacceptable CPU time.

Another example is available in Kleinermann's 2000 thesis; this scientist applies inverse analysis to identify all the microscopic parameters of Gurson's model except the initial porosity. The macroscopic parameters are known. The assumed experimental data also concern a notched tensile test. The tensile load, the contraction of the notch and the axial displacement of the notch boundary are recorded. These 3 functions of time are used in the cost function. The high number of parameters as well as the different sensitivity of the results provide a difficult problem for the inverse method. Kleinermann's 2000 computation has requested nearly 3 weeks of CPU time or the equivalent of 378 times the direct problem CPU time.

Considering the available mechanical equipment in MSM, the lack of metallurgical investigation technique (SEM, TEM) in this team and the heavy work to develop efficient inverse modeling, one can understand from the preceding paragraphs why phenomenological models of Lemaître's type have been preferred to Gurson's model.

Another element to explain this choice is the fact that the advantage of the microscopic foundation of Gurson's type models is restricted to specific loadings

such as uniaxial or multiaxial tensile states. The reality often deals with complex mechanical states with non-negligible shear components, where the superiority of Gurson's type law is not certified. Another disadvantage of Gurson's model compared to Lemaître's model is its lack of damage accumulation in cyclic loading, when compressive states decrease the porosity accumulated during tensile phases as shown in section 3.3. The last strong argument in favor of damage macroscopic models is their relatively easy identification on the basis of simple mechanical tests. This enables to find quickly and at low cost the parameters required to model a new material. In conclusion, the present thesis is limited to macroscopic damage models of the phenomenological type, identified without global inverse modeling tools.

References

Barlat, F., Lian, J. (1989) Plastic behaviour and stretchability of sheet metals. Part 1 : a yield function for orthotropic sheets under plane stress conditions, *Int. J. of Plasticity*, **5**, 51.

Benzerga, A., Besson, J., Pineau, A. (1997) Modèle couplé du comportement-endommagement ductile de tôles anisotropes. *3ème colloque national en calcul des structures*, 20-23 mai, Giens, France.

Benzerga, A., Besson, J., Pineau, A. (1999) Coalescence-controlled anisotropic ductile fracture. *J. Eng. Mat. Eng.* **121**, 221-229.

Brunet, M., Mguil-Touchal, S., Morestin, F. (1997) Numerical and experimental analysis of necking in 3D sheet forming processes using damage variable, *Advanced Methods in Materials Processing Defects*, Predeleanu, M. & Gilormini, P., 205-214.

Brunet, M., Morestin, F, Walter, H., Numerical Analysis of Failure in Sheet Metal Forming with Experimental Validation (2001), *Numerical Modelling in Damage Mechanics, Euromech 417,* University of Technology of Troyes, France, *Journal of Finite Elements to appear in Spring.*

Chu, C.C., Needleman,A. (1980), Void-nucleation affects in biaxially stretched sheets. *J. Eng. Mat. Techn.*, **102**, 1980, 249-256.

de Borst, R. (1991) Simulation of strain localization : a reappraisal of the Cosserat continuum, *Engineering Computations*, **8**, 317-332.

Doege, E., Bagaviev, A. & Dohrmann, H. (1997a) Application of an anisotropic extension of Gurson model to practical engineering problems, *Computational Plasticity – Fundamentals and Applications*, CIMNE, Barcelona, 1453-1458.

Doege, E., Bagaviev, A. & Dohrmann, H. (1997b) Formability analysis based on the anisotropically extended Gurson model, *Advanced Methods in Materials Processing Defects*, Predeleanu, M. & Gilormini, P., 281-288.

Eftis, J., Nemes, J.A. (1991) Evolution equation for the void volume growth rate in viscoplastic damage constitutive model. *Int. J. of Plasticity*, **7**, 275-293.

Eshelby, J.D. (1957) The determination of the elastic field of an ellipsoidal inclusion and related problems. *Proc. Roy. Soc. London*, **A241**, 376-396.

Gologanu, M., Leblond, J.B., J. Devaux (1993) Approximate models for ductile metals containing non-spherical voids – case of axisymmetric prolate ellipsoïdal cavities, *J. Mech. Phys. Solids*, **41-11**, 1723-1754.

Gurson, A.L. (1977) Continuum theory of ductile rupture by void nucleation and growth. *J. Engng. Materials Technology*, **99**, 2-15.

Hashin, Z., Shtrikman, S., (1963) A variational approach to the theory of the elastic behavior of multiphase materials. *J. Mech. Phys. Solids,* **11**, 127-140.

Kleinermann, J.P. (2000) Identification paramétrique et optimisation des procédés de mise à forme par problèmes inverses, Thèse de Doctorat, Université de Liège. .

Koplik, J. , Needleman, A. (1988) Void growth and coalescence in porous plastic solids. *Int. J. Solids Structures*, **24-8**, 835-853.

Lazzarotto, L., Picart, P. Oudin, J. (1996a) Sensitivity of Material Parameters in the Finite Element Computation of Microvoïd Nucleation and Growth, *Int. J. of Damage Mechanics*, **5**,259.

Lazzarotto, L., Picart, P. Oudin, J. (1996b) Benchmarks for finite element modeling of cold forging processes with elasto-plastic microvoided materials. *Computational Materials Science*, **5**, 167-176.

Lauro, F., Barrière, T., Bennani, B., Drazetic, P. and J. Oudin (1997) Damage framework for the prediction of material defects : identification of the damage material parameters by inverse technique, *Advanced Methods in Materials Processing Defects*, Predeleanu, M. & Gilormini, P., Eds. Elsevier 165-174.

Leblond, J.B., Perrin, G., Devaux, J. (1995) An improved Gurson-type model for hardenable ductile metals, *Eur. J. Mech. A/Solids*, **14**, 499-527.

Lemaître, J. (1985) Coupled elastoplasticity and damage constitutive equations, *J. Comp. Meth. in Appl. Mech. and Eng.* **51**, 31-49.

Mackenzie, J.K. (1959) The elastic constants of a solid containing spherical holes, *Proc. Phys. Soc.*, **63B**, 2-11.

Mear , H.E., Hutchison, J.W. (1985) Influence of yield surface curvature on flow localization in dilatant plasticity, *Mech. Mat.*, **4**, 395-407.

Montheillet, F., Moussy, F. (1986) Physique et mécanique de l'endommagement F. Montheillet and F. Moussy eds., GRECO, Editions de Physique, les Ulis, France.

Mudry, F. (1982) Etude de la rupture ductile et de la rupture par clivage d'aciers faiblement alliés, Thèse d'état, Université Technologique de Compiègne.

Needleman, A., Tvergaard, V. (1987) An anlysis of ductile rupture modes at a crack tip, *J. Mech. Phys. Solids*, **35-2**, 151-183.

Pardoen, T., (1998) Ductile fracture of cold-drawn copper bars : experimental investigation and micromechanical modelling, Doctorat en Sciences Appliquées, Université de Louvain-La-Neuve.

Perrin G., Leblond, J.B. (1990) Analytical study of a hollow sphere made of plastic porous material and subjected to hydrostatic tension-Application to some problems in ductile fracture of metals, *Int. J. of Plasticity*, **6**, 677-699.

Perzyna, P. (1986) Internal state variable description of dynamic fracture of ductile solids, *Int. J. Solids & Struct.*, **22**, 797-818.

Picart, P., Piechel, G. & Oudin, J. (1997) Damage influence in the finite element computations for large strains elastoplastic mechanical structures, *Advanced*

Methods in Materials Processing Defects, Predeleanu, M. & Gilormini, P., Eds. Elsevier, 175-184.

Ponte Castaneda, P., Zaidman, M. (1994) Constitutive models for porous materials with evolving microstructure, *J. Mech. Phys. Solids*, **42-9**, 1459-1497

Rice, J.R. , Tracey, D.M. (1969) On the ductile enlargement of voids in triaxial stress fields, *J. Mech. Phys. Solids*, **17**, 201-217.

Rousselier, G., Devaux, J.C., Mottet, G., Devesa, G. (1989) A methodology for ductile fracture analysis based on damage mechanics : an illustration of a local approach of fracture, *Nonlinear Fracture Mechanics : vol. II – Elastic-Plastic Fracture, ASTM STP 995*, J.D. Landes, A. Saxena, J.G. Merkle Eds, *American Society for Testing and Materials*, Philadelphia, 332-354.

Stainier, L. (1996) Modélisation numérique du comportement irréversible des métaux ductiles soumis à grandes déformations avec endommagement. Thèse de Docteur en Sciences Appliquées, Université de Liège.

Tvergaard, V. (1981) Influence of voids on shear band instabilities under plane strain conditions. *Int. J. Fract.*, **17**, 389-407.

Tvergaard, V. (1982) Material failure by void coalescence in localized shear bands, *Int. J. Solids & Struct.* **18**, 659-672.

Tvergaard, V., Needleman, A. (1984) Analysis of a cup and cone fracture in a round tensile bar. *Acta Metallica*, **32**, 157-169.

Wilsius, I., (1999) Etude expérimentale et numérique de la déchirure ductile basée sur des approches locales en mécanique de la rupture, Ph. D. Thesis Université des Sciences et Technologie de Lille.

Worswick, M.J. & Pick, R.J. (1990) Void growth and constitutive softening in a periodically voided solid. *J. Mech. Phys. Solids*, **38**, 601-625.

3. THERMODYNAMIC DAMAGE MODELS

In the present state of development of Continuum Damage Mechanics, it has been verified that, in general, the loss of microscopic information resulting from the phenomenological approach is compensated by the gain in analytical, experimental and computational tractability of such models.

The application field of coupled mechanical and damage constitutive equations is very large. For instance, Lemaître 1985 presents an elastic model coupled with damage for brittle failure of concrete or high-cycle fatigue of metals, an elasto-plastic model coupled with damage for ductile fracture or low-cycle fatigue, and an elasto-visco-plastic model coupled with creep and fatigue damages. As underlined by Desoyer 1995, one might apply Continuum Damage Mechanics (CDM) during quite a long time. According to material and loading type, first damage steps are induced by various mechanisms (void nucleation followed by growth for metallic alloys, or meso crack appearance followed by propagation in brittle rocks...) and require appropriate models. Then, the ultimate damage steps (void coalescence, strain localization...) are problems still open, calling for new bridges between Continuum Mechanics and Fracture Mechanics.

In this Chapter, the concepts of the thermodynamic approach to damage are summarized and some of the numerous models, that can be applied to ductile fracture of metallic alloys, are presented.

3.1. General thermodynamic formulation

An interesting summary of the well established rules in the continuum mechanics literature is proposed by de Souza Neto *et al.* 1998. Here, only the principles required for the model presentations of Chapters 6 and 7 are presented.
The basic concepts of thermodynamics of continuous media are:

- mass conservation;
- momentum balance;
- first principle = conservation of energy;
- second principle = irreversibility of entropy production.

Clausius-Duhem's inequality results from the combination of the first and the second principles :

$$\underline{\sigma} : \underline{\dot{\varepsilon}} - \rho(\dot{\psi} + s\dot{T}) - \frac{1}{T}\underline{grad}\, T.\underline{q} \geq 0 \qquad (3\text{-}1)$$

where $\underline{q}$ is the heat flux, ρ the specific mass, ψ the free energy per unit mass, also called Helmholtz' free energy, defined by :

$$\psi = e - Ts \qquad (3\text{-}2)$$

with e the specific internal energy, s the specific entropy, T the temperature.

The starting point of thermodynamics with internal variables is the hypothesis that, at any instant of a thermodynamic process, the thermodynamic state of a given material point can be completely determined by the knowledge of a finite number of state variables (kinematic variables such as the deformation gradient or the elastic strain $\underline{\varepsilon}^e$, the temperature T and its gradient), and internal variables α_k associated with dissipative mechanisms. Each α_k can be of scalar, vectorial or tensorial nature. One model is characterized by the choice of the variables. For instance, maintaining a general approach, the free energy is assumed to have the form:

$$\psi = \psi\ (\ \underline{\varepsilon}^e, T, \alpha_k\ ) \tag{3-3}$$

Consequently, its rate is given by:

$$\dot{\psi} = \frac{\partial \psi}{\partial \underline{\varepsilon}^e} : \dot{\underline{\varepsilon}}^e + \frac{\partial \psi}{\partial T}\dot{T} + \frac{\partial \psi}{\partial \alpha_k}\dot{\alpha}_k \tag{3-4}$$

Assuming additive decomposition of strain rate:

$$\dot{\underline{\varepsilon}} = \dot{\underline{\varepsilon}}^e + \dot{\underline{\varepsilon}}^p \tag{3-5}$$

the Clausius-Duhem inequality becomes:

$$(\underline{\sigma} - \rho\frac{\partial \psi}{\partial \underline{\varepsilon}^e}) : \dot{\underline{\varepsilon}} + \rho\frac{\partial \psi}{\partial \underline{\varepsilon}^e} : \dot{\varepsilon}^p - \rho(\frac{\partial \psi}{\partial T} + s)\dot{T} - \rho\frac{\partial \psi}{\partial \alpha_k}\ \dot{\alpha}_k - \frac{1}{T}\underline{grad\ T}.\underline{q} \geq 0 \tag{3-6}$$

Since this inequality must hold for any thermomechanical process and, among others, for arbitrary $\dot{\varepsilon}$, $\dot{T}$, the expressions between parentheses must be null. This yields the well-known expressions:

$$\underline{\sigma} = \rho\frac{\partial \psi}{\partial \underline{\varepsilon}^e} \qquad s = -\frac{\partial \psi}{\partial T} \tag{3-7}$$

The thermodynamic forces associated with each internal variable α_k are defined by:

$$A_k = \rho\frac{\partial \psi}{\partial \alpha_k} \tag{3-8}$$

For an isothermal process, Clausius-Duhem's inequality can be written:

$$\underline{\sigma} : \dot{\underline{\varepsilon}}^p - A_k\dot{\alpha}_k \geq 0 \tag{3-9}$$

In order to define a constitutive model, equations for $\dot{\alpha}_k$ must be derived. As the above inequality must be verified, this fact imposes some restrictions on the possible constitutive relations. An effective way of ensuring Clausius-Duhem's inequality consists in postulating the existence of a scalar pseudo dissipation potential, a convex function of all thermodynamical forces $\underline{\sigma}$, A_k, using the state variables $\underline{\varepsilon}^e, \underline{\varepsilon}^p, \alpha_k$ as parameters.

$$F = F(\underline{\sigma}, A_k ; \underline{\varepsilon}^e, \underline{\varepsilon}^p, \alpha_k) \tag{3-10}$$

A generalized normality rule is then applied :

$$\underline{\dot{\varepsilon}}^p = \frac{\partial F}{\partial \underline{\sigma}} \quad \dot{\alpha}_k = -\frac{\partial F}{\partial A_k} \tag{3-11}$$

For phenomena that do not explicitly depend on time, a multiplicator $\dot{\lambda}$ is added. For instance, for plasticity, F can be chosen equal to the yield surface F_p, and constitutive equations are written using a plasticity multiplicator λ_p calculated from the consistency condition $\dot{F}_p = 0$.

$$\underline{\dot{\varepsilon}}^p = \dot{\lambda}_p \frac{\partial F_p}{\partial \underline{\sigma}} \tag{3-12}$$

It should be noted that the constitutive description by means of convex potentials as explained above is not a consequence of thermodynamics but rather a tool for formulating constitutive equations without violating thermodynamics. Indeed, it is obvious that a constitutive model defined by (3-3), (3-7), (3-11) a priori satisfies the dissipation inequality.

The version of the above general principles taking into account the multiplicative split of the deformation gradient $\underline{F}$ can be found in Souza Neto *et al.* 1998. MSM hypoelastic formulation, that uses additive splitting of the strain rate and neglects the plastic spin, is historical. It assumes that elastic strains are small by comparison with plastic ones, which is acceptable in the metallic ductile rupture fields. Cauchy's stress and Jaumann's derivative are used with the assumption of neglecting the scale factor ($det\ \underline{F}^1$) that should affect Cauchy's stress. In 1987, these choices were classical for all codes taking into account large plastic strains as presented by Charlier 1987. The hyperelastic formulation, using multiplicative split of the deformation gradient (Weber & Anand 1990, Simo 1992), and Piola Kirchoff's stress or Cauchy's is now often used (Owen *et al.* 1995, MARC commercial code, EPIM3D code developed by Menezes 1994). However, even if this approach seems more elegant, it is not demonstrated that it simplifies the coding, provides robustness and yields such a better accuracy. So, as long as small elastic strains field are concerned, the traditional hypoelastic approach is applied in MSM.

Even if kinematic description and integration schemes are fundamental for any Finite Element Code, these topics are not treated here as the LAGAMINE choices have already been presented in several Ph.D. theses (Charlier 1987, Li 1995).

3.2. Thermodynamic damage models

3.2.1. Introduction

The material behavior is modeled by constitutive equations taking into account its progressive deterioration. The local loss of material integrity of a representative volume element is modeled by *continuous* (in space and time) variables defined at macro-scale and referred to as *the damage variables*. The notion of a continuous representation of -intrinsically discontinuous- material damage stems from the work of Kachanov 1958 on tertiary creep and was further developed by Rabotnov 1963. "Damage" can be defined as a collection of permanent microstructural changes concerning material thermomechanical properties (e.g. stiffness, strength, anisotropy, etc.) brought in a material by a set of irreversible physical microcracking processes resulting from the application of thermomechanical loadings (Talreja 1985).

Following this definition, the damage variable is not limited to a void volume fraction and to the well-known nucleation, growth and coalescence approach. For instance, it covers the decrease of stiffness cohesion between a matrix and an inclusion or the effect of micro-stress concentration. The word of micro-cracking process in Talreja's definition could even be replaced by internal micro-structural evolution if one looks at the effect of dislocation density modification and at the appearance of substructures. These changes modify the material response and result in softening behavior.

A large part of the experimental analysis of damage does not look at the microscopic level but measures the effect of damage on macroscopic variables such as stress and strain fields, optical wave reflection, acoustic wave transmission... A review of these techniques (photoelasticity, interferometry methods, acoustic emission, optical particle tracking, digital image processing...), applied to damage investigation, can be found in Geers 1997.

The classical technique, used in MSM research, to evaluate damage variables consists in measurements of Young's modulus decrease by means of accurate extensometers and/or electrical-resistance strain gages. Lemaître & Chaboche 1985 have already proposed such an approach to measure damage. It is interesting to note that Geoffroy *et al.* 1993 provide a microscopic explanation, without any connection to void growth assumption, to apparent Young's modulus decrease with strain hardening in steel sheets. In this article, four typical steels (interstitial free steel, aluminum killed deep drawing quality steel, high strength Niobium alloyed steel and rephosphorized steel for structural parts) have been studied by two different laboratories of the SOLLAC group. The first lab measures Young's modulus with an instrumented tensile test machine (strain gauge cell with 0.4N resolution and electronic extensometer with 5.10^{-2} micrometers resolution); the other one

ultrasonically, by measuring the resonant frequency of the material when a longitudinal wave is propagated through the specimen by a magneto-oscillator.

Their conclusion leads them to make a distinction between "Young's modulus" and "tangent elasticity modulus". Their "Young's modulus" is measured at very low magnitude of strains (10^{-6}) and high strain rates by the ultrasonic approach. Their "tangent elasticity modulus" results from the tensile test method. In this latter case, strains reach 2, 5 and 10 %; strain rates are not given but they report slow cross head speed of 2 mm/min, which corresponds to a rate 100 times slower than with ultrasonic approach.

The comparisons of their measurements on as-received samples and after 5 or 10 % pre-strain in tension allow to conclude that *"Young's modulus"* (as defined hereabove) *is a constant intrinsic mechanical property* and *"the tangent elasticity modulus" depends on deformation speed, strain and composition.* The four steels exhibit a strong decrease of "tangent elasticity modulus" when the applied stress increases. They propose the following explanation:

- in the ultrasonic approach, interstitial atoms cannot migrate and the measure is more intrinsic;
- in the tensile test on pre-strained steel, the material can be considered as a visco-elastic material described by a Kelvin-Voigt's rheological model (see Figure 3-1). The pure elastic behavior is represented by the spring E_2 submitted to strain ε_2; the visco-elastic behavior is represented by spring E_1 and damper η; the associated strain is ε_1 and the total material strain is $\varepsilon_1 + \varepsilon_2$.

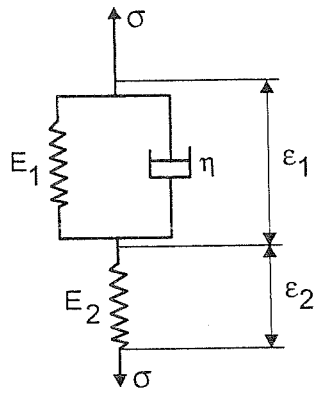

$$(1 + E_1 / E_2)\sigma + \eta / E_2 . \dot{\sigma} = E_1 . \varepsilon + \eta \dot{\varepsilon}$$

Figure 3-1 Kelvin-Voigt's rheological model (from Geoffroy *et al.* 1993).

Steel behavior is visco-elastic because the carbon and alloying elements act as pins for dislocations. As long as the applied stress remains at low level, the dislocations

cannot glide so they bend between atoms (see Figure 3-2a). If relaxed, dislocations return to their initial state. The residual strain is equal to zero but some energy has been dissipated. This phenomenon is observed at a stress level lower than real plastic stress when linear elasticity disappears before appearance of real permanent strain as shown on Figure 3-2b. This small quantity of energy is dissipated to bend the pinned dislocations.

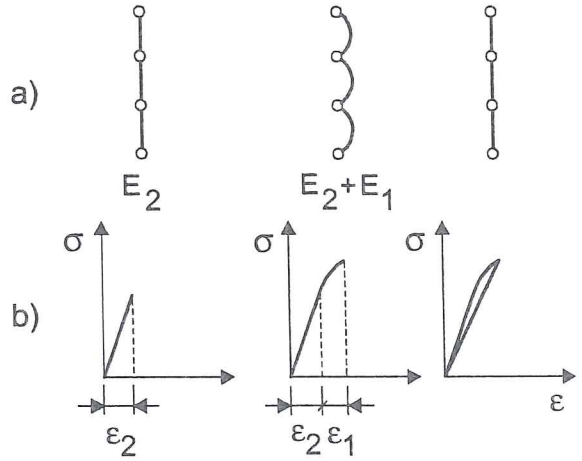

Figure 3-2 Pinned dislocations submitted to bending and unbending
a) visualisation of the phenomenon,
b) associated stress-strain curve (from Geoffroy *et al.* 1993).

Looking at the differential equation associated to Kelvin-Voigt's model, one can check that, at high strain rate, only the spring E_2 is activated and defines the tangent modulus. This fact recoups "Young's modulus" from ultrasonic measurements. At low strain rate, the material behavior results from both springs E_1 and E_2 and its stiffness is lower than "Young's modulus". When the steel sheet has been submitted to a pre-strain, dislocations multiply and this phenomenon is amplified. The "elastic tangent modulus" decreases sharply when "Young's modulus" remains the same as in as-received conditions.

In general, the literature makes no distinction between "Young's modulus" and "elastic tangent modulus". Scientists measuring "Young's modulus" decrease at different strain states by cyclic tensile tests determine in fact the "elastic tangent modulus". According to the above study, the macroscopic damage variable associated to this decrease is from a microscopic point of view an increased density of dislocations pinned on carbon and alloying elements. This explanation holds surely at incipient plasticity where a strong decrease of elastic tangent modulus is observed (see section 6.2.7). The continuous decrease after a few percents of plastic strains probably also results from additional phenomena such as void nucleation, growth and coalescence.

Hereafter, some traditional choices of damage variables are described. The damage variable d_n in the normal direction $\underline{n}$ defined by Lemaître & Chaboche 1985 is the following ratio:

$$d_n = \frac{A_d}{A_t} \tag{3-13}$$

A_t = total cross sectional area of a unit cell cut by a plane normal to direction $\underline{n}$,
A_d = damaged surface area taking into account the area of microcracks or/and voids, the microstress concentration and the interaction between microcracks.

If the phenomenon of damage is regarded as isotropic, it can be defined by a scalar D, which represents the same ratio as above but for any plane direction cutting the cell unit. In fact, the area which effectively resists the stress is $(1\text{-}D)A_t$.

A second-order damage tensor $\underline{D}$ has been proposed by Dragon 1985 :

$$\underline{D} = \frac{1}{2V}\sum_k \int_{S^k} (\underline{b} \otimes \underline{n} + \underline{n} \otimes \underline{b})^k dS^k \tag{3-14}$$

where $\underline{b}$ = displacement discontinuity vector,
$\underline{n}$ = unit normal vector across the k^{th} microcrack surface S^k,
V = representative volume.

As reported by Ju 1989, Krajcinovic has pointed out that such definition is thermodynamically incorrect, because it leads to energy dissipation during unloading. This tensor is nevertheless a good mean to add flexibility due to open microcracks.

Bruhns & Schiesse 1996 use a description of voids on grain boundaries with tensorial Fourier's series that they limit for practical purpose to second order tensors. Their final internal damage variables are a scalar one (the void volume fraction) and a tensorial one.

The second concept very often used in thermodynamic damage modeling is *the definition of effective values.* This concept was introduced by Kachanov in 1958 for the purpose of modeling fracture due to creep. He defines the effective stress by :

$$\overline{\underline{\sigma}} = \underline{\sigma} / (1 - D) \tag{3-15}$$

where D is the isotropic damage internal variable presented above, the value of which is 0 in the undamaged case. This effective stress is in fact the stress relative to the effective area $(1\text{-}D)A_t$. So, equilibrium imposes relation (3-15). The assumption of strain equivalence between a damaged material and a sound, equivalent virgin material is defined by:

$$\overline{\underline{\varepsilon}} = \underline{\varepsilon} \tag{3-16}$$

This assumption associated with the concept of effective stress leads to the fact that the constitutive relations of the damaged material are derived from those of the undamaged material by replacing $\underline{\sigma}$ by $\overline{\underline{\sigma}}$ and $\underline{\varepsilon}$ and by $\overline{\underline{\varepsilon}}$.
Remark that, without assuming the concept of effective stress, the model by Bruhns & Schiesse 1996 recovers relation (3-15) as their weighted Cauchy's stress tensor can finally be expressed by this relation. Rousselier *et al.* 1989 use $\underline{\sigma}/\rho$ in their plastic potential and not $\underline{\sigma}$ to take into account the variation of ρ, reflecting damage and elastic deformation.

As summarized by Zhu 1992, Simo & Ju 1987, who work with a stress-based formulation of elasto-plastic damage constitutive laws, propose an effective strain concept and an assumption of stress equivalence :

$$\overline{\underline{\varepsilon}} = (1-D)\underline{\varepsilon} \qquad \overline{\underline{\sigma}} = \underline{\sigma} \tag{3-17}$$

And finally, Cordebois & Sidoroff 1979 assume that the damaged material state can be replaced by a fictitious undamaged material state which is characterized by effective stresses and strains in the sense that the complementary elastic energy involved in the two states should be equal. This gives:

$$\overline{\underline{\varepsilon}} = (1-D)\underline{\varepsilon} \qquad \overline{\underline{\sigma}} = \underline{\sigma}/(1-D) \tag{3-18}$$

These equivalence principles help to define the expression of the free energy and the pseudo dissipation potential functions used in the models.

Different damage models are presented in the next sections. An unified notation has been adopted and is summarized in Table 3-1.

State variables		Associated thermodynamic forces	
ε^e	elastic strain	σ	Cauchy stress
p	isotropic hardening state variable, often equal to ε_{eq}	R	increase of the initial plastic threshold σ_y
$\underline{\alpha}$	kinematic hardening state variable	$\underline{X}$	back stress
D	isotropic scalar damage variable in isotropic damage model	Y	scalar damage energy release rate in isotropic damage model
$\underline{D}$	second order damage tensor in anisotropic damage model	$\underline{Y}$	damage energy release rate tensor in anisotropic damage model
β	isotropic scalar damage variable in anisotropic model.	B	increase of initial damage strengthening threshold B_0.

Table 3-1 Definition of state variables and associated thermodynamic forces.

3.2.2. Lemaître's model

This section presents the isotropic, isothermal version of Lemaître 1985 model. It assumes decoupling between elasticity and damage on one hand and plastic hardening on the other hand. The specific free energy is expressed by :

$$\psi = \psi^{ed}(\underline{\varepsilon}^e, D) + \psi^p(\underline{\alpha}, p) \tag{3-19}$$

where

$$\psi^{ed} = \frac{1}{2\rho}(1-D)\underline{\varepsilon}^e : \underline{\underline{C}}^e : \underline{\varepsilon} \tag{3-20}$$

- ψ^{ed} = elastic damage contribution to free energy, with $\underline{\underline{C}}^e$ the tensor of elastic moduli,
- ψ^p = plastic contribution to free energy,
- p = scalar, internal variable of isotropic hardening, associated with R, the increase of the radius of the yield surface,
- $\underline{\alpha}$ = an internal variable related to kinematic hardening; its dual associated force $\underline{X}$ is a kinematic tensorial variable, which represents the translation of the yield surface in stress space. It is a second order tensor.

According to (3-7), the elasticity law can be derived as:

$$\underline{\sigma} = \rho\frac{\partial\psi}{\partial\underline{\varepsilon}^e} = (1-D)\underline{\underline{C}}^e : \underline{\varepsilon}^e \tag{3-21}$$

One can verify that the effective stress $\underline{\overline{\sigma}}$, defined by (3-15), respects the classic elastic behavior. This relation (3-21) has very important experimental consequences. It justifies the experimental characterization of the damage state. Damage determination is reduced to the measurement of the degradation of the current effective elastic modulus with respect to the virgin state.

Using relation (3-8), the associated force of the damage variable, generally called Y is computed by:

$$Y = \rho\frac{\partial\psi}{\partial D} = -\frac{1}{2}\underline{\varepsilon}^e : \underline{\underline{C}}^e : \underline{\varepsilon}^e \tag{3-22}$$

which gives to $-Y$ the meaning of an elastic strain energy release rate associated with a unit damage growth. $-Y\dot{D}$ is the power dissipated in the creation of surfaces of separation. $-Y$ corresponds to the variation of internal energy density due to damage growth at constant stress; so it is commonly termed as the "damage energy released rate". As recalled by de Souza Neto *et al.* 1998, Rice 1968 considers $-Y$ as the continuum "damage" analogue of the J-integral used in linear fracture mechanics. Using (3-21) and (3-22), Lemaître's model yields :

$$-Y = \frac{\sigma_{eq}^2}{2(1-D)^2}\left[\frac{2}{3}(1+\nu)+3(1-2\nu)(\frac{\sigma_m}{\sigma_{eq}})^2\right] \tag{3-23}$$

According to the general thermodynamic formulation, one must now define a pseudo dissipation potential and apply normality rules to compute the rates of the state variables. Lemaître 1985 assumes that the pseudo dissipation potential is written as the sum of 2 functions, F_p and F_d, respectively related to plasticity and damage. As underlined by Hayakawa & Murakami 1998, such a choice can be justified by physics considerations. They assume that the dissipation associated with plastic deformation in polycrystalline materials is mainly produced by the dislocation motion under applied stress, while the damage dissipation is governed by the release of internal energy due to the development of microscopic cavities. This explains why these dissipation mechanisms are represented by two different potential functions. The presence of the damage internal variable in the equation of F_p is related to the fact that damage leads to a reduction of the load carrying area and induces stress concentrations around defects which finally result in the reduction of the yield surface.

$$F = F_p(\underline{\sigma}, \underline{X}, R; \underline{\varepsilon}^p, \underline{\alpha}, p, D) + F_d(Y; D) \tag{3-24}$$

The pseudo potential of plasticity is taken as the plasticity criterion function or, in other words, the associate flow rule is assumed. The von Mises' criterion is used to define the effective stress. Only isotropic hardening is taken into account for the sake of simplicity. So the coupling between plasticity and damage is introduced by :

$$F_p = \frac{\sigma_{eq} - R}{1-D} - \sigma_y \tag{3-25}$$

where σ_y is the initial yield stress of the material. Then, adding a multiplicator $\dot{\lambda}$ because damage elasto-plastic models do not explicitly depends on time, a generalized normality rule is applied.

$$\underline{\dot{\varepsilon}}^p = \dot{\lambda}\frac{\partial F_p}{\partial \sigma} = \frac{3}{2}\frac{\dot{\lambda}}{1-D}\frac{\underline{\hat{\sigma}}}{\sigma_{eq}} \qquad \dot{p} = -\dot{\lambda}\frac{\partial F_p}{\partial R} = \frac{\dot{\lambda}}{1-D} = (\frac{2}{3}\underline{\dot{\varepsilon}}^p : \underline{\dot{\varepsilon}}^p)^{1/2} \tag{3-26.a, b}$$

with the simple expression of the strain hardening curve:

$$R = \rho\frac{\partial \psi}{\partial p} = Kp^{1/M} \tag{3-27}$$

where K and M are material constants. The multiplicator $\dot{\lambda}$ is derived from the consistency condition $\dot{F}_p = 0$ (for details, see Lemaître 1985).

A general form of the damage pseudo potential, that can be used to represent brittle, fatigue, ductile or creep damage, is a power function of Y:

$$F_d = \frac{A}{(s+1)(1-D)}(\frac{-Y}{A})^{s+1} \tag{3-28}$$

This choice, the generalized normality rule and relation (3-26.b) leads to:

$$\dot{D} = \dot{\lambda}\,\frac{\partial F_d}{\partial Y} = \frac{\dot{\lambda}}{(1-D)}\left(\frac{-Y}{A}\right)^s = \left(\frac{-Y}{A}\right)^s \dot{p} \tag{3-29}$$

According to Lemaître, multidimensional experiments show that $s \equiv 1$, so the only material coefficient necessary for damage modeling is A. Thus the isotropic elastic-damage-plastic model proposed by Lemaître only requires 5 parameters : E, ν, K, M, A.

As already mentioned, this section purpose is not to describe the computational aspects such as time integration schemes or tangent modulus computation. Some information about these very important topics, for those who want to implement a damage model in a finite element code, can be found in Simo & Ju 1987, Doghri 1995, Doghri 2000, de Souza Neto *et al.* 1998.

3.2.3. Three choices of free energy function or its complementary Gibbs' function

As reported by Ju 1989, Lemaître's choice to uncouple plasticity and damage processes contradicts the fact that plastic variables also contribute to the initiation and growth of microcracks. So, he proposes another free energy function, which yields another expression of the thermodynamic force associated with the scalar damage variable D:

$$\psi = (1-D)\left[\psi^{0e}(\underline{\varepsilon}^e) + \psi^{0p}(p,\underline{\alpha})\right] \tag{3-30}$$

$$Y = \rho\frac{\partial \psi}{\partial D} = -\rho\left[\psi^{0e}(\underline{\varepsilon}^e) + \psi^{0p}(p,\underline{\alpha})\right] \tag{3-31}$$

where ψ^{0e}, ψ^{0p} respectively represent the elastic and plastic free energy functions of an undamaged (virgin) material. So, $-Y$ represents the damage energy release rate that controls the microcracks. It is related to the local debonding energy required to initiate and propagate these cracks. As underlined by Ju 1989, $(\psi^{0e} + \psi^{0p})$ is actually the local counterpart of the global J-integral fracture energy in nonlinear elasto-plastic fracture mechanics.

Rousselier 1987 applies the thermodynamic formulation and what he calls "the principle of simplicity" for choosing his functions. He proposes for the specific free energy :

$$\psi = \psi^e(\underline{\varepsilon}^e) + \psi^d(D) + \psi^p(p) \tag{3-32}$$

At this level, this choice seems to uncouple elasticity, damage and plasticity. However, as he works with a stress weighted by the specific weight: $\underline{\sigma}/\rho$, the coupling appears in both elastic and plastic descriptions.

When Helmholtz's free energy is used, the damage conjugate forces are expressed as functions of the elastic strain tensor. Thus, the examination of the validity of the theory requires experiments governed by the elastic strain. In the case of elastic-plastic-damage materials, such experiments are difficult as the elastic strain cannot be easily determined due to the change of elastic properties with damage development. So Hayakawa & Murakami's 1998 work with Gibbs' thermodynamic potential which is assumed to consist of 3 terms :

- the complementary energy due to elastic deformation $G^e(\sigma,\underline{D})$
- the lattice distortion energy related to dislocation structure $G^p(p)$
- the surface energy due to cavity nucleation $G^d(\beta)$

where $\underline{D}$ is a damage second order tensor and β is a scalar variable related to damage development. The need for a tensorial damage state variable is linked to the anisotropy of the cases studied by these authors. As Lemaître does, they assume a strong coupling of the elastic complementary energy with damage but a small influence on the other terms. So damage coupling only appears in the first term.

3.2.4. Three choices of the pseudo potential function

Murakami *et al.* 1998 and Hayakawa & Murakami 1998 report a research on spheroidized graphite cast iron FCD400. Their experiments were concerned with verification of the existence of the damage surface and with validation of the assumption of associated flow rule and normality rule of damage evolution, i.e. the existence of the damage potential. The experimental results show that the shape of the damage and yield surfaces does not always remain similar but may depend on the current damage state. Furthermore, the development of damage is also dependent on plastic deformation. Thus, the proposed damage potential F_d is not only a function of the damage internal variable but also of the internal state variable controlling isotropic hardening.

Hayakawa & Murakami's model describes the material state by 3 variables: a second rank symmetric damage tensor $\underline{D}$, a scalar isotropic hardening variable p and a scalar β, which controls the further development of damage. Their conjugate forces are respectively $\underline{Y}$, R and B. The yield surface is defined as:

$$F_p(\underline{\sigma},R;\underline{D},p)=\sigma_{eq}^I-(\sigma_y+R)=0 \tag{3-33}$$

with

$$\sigma_{eq}^I=\sqrt{\frac{3}{2}\underline{\hat{\sigma}}:\underline{\underline{M}}(\underline{D}):\underline{\hat{\sigma}}} \tag{3-34}$$

where $\underline{\hat{\sigma}}$ is the deviatoric stress tensor and $\underline{\underline{M}}$ is defined by :

$$\left[\underline{\underline{M}}(\underline{D})\right]_{ijkl}=\frac{1}{2}(\delta_{ik}\delta_{jl}+\delta_{il}\delta_{jk})+\frac{1}{2}c^p(\delta_{ik}D_{jl}+D_{il}\delta_{jk}+\delta_{il}D_{jk}+D_{il}\delta_{jk}) \tag{3-35}$$

It is a fourth rank symmetric tensor with the damage tensor $\underline{D}$ as an argument and c^p a material constant. The above linear function postulates moderate effects of $\underline{D}$ on plastic deformation.

The yield function derivatives multiplied by a plastic multiplicator $\dot{\lambda}_p$ give the plastic strain rate $\underline{\dot{\varepsilon}}^p$ and the rate of the isotropic hardening variable $\dot{p}$. This plastic multiplicator $\dot{\lambda}_p$ is determined from the consistency condition $\dot{F}_p = 0$. The loading/unloading conditions are defined by Kuhn-Trucker's relations :

$$\dot{\lambda}_p \geq 0, \quad F_p \leq 0, \quad \dot{\lambda}_p F_p = 0 \tag{3-36}$$

Hayakawa & Murakami tensile and torsion tests consolidate the assumptions of a damage potential and corresponding normality rule. The proposed damage surface is found identical to the damage potential :

$$F_d\ (\underline{Y}, B; \underline{D}, \beta\ ) = Y_{eq} + c^r\, p\, tr\underline{D}\, tr\underline{Y} - (B_0 + B) = 0 \tag{3-37}$$

$$Y_{eq} = \sqrt{\frac{1}{2}\underline{Y} : \underline{\underline{L}}(\underline{D}) : \underline{Y}} \tag{3-38}$$

$$\left[\underline{\underline{L}}(\underline{D})\right]_{ijkl} = \frac{1}{2}(\delta_{ik}\delta_{jl} + \delta_{il}\delta_{jk}) + \frac{1}{2}c^d\,(\delta_{ik}D_{jl} + D_{il}\delta_{jk} + \delta_{il}D_{jk} + D_{il}\delta_{jk}) \tag{3-39}$$

where c^r, c^d are material constants, as well as B_0 which specifies the size of the initial damage surface. The choice of $\underline{L}$, linear function of damage tensor $\underline{D}$, was justified because, from experimental results, the material damage in the studied elastic-plastic material was not so significant. As in plasticity, the evolution equations of the damage variables $\dot{\underline{D}}$, $\dot{\beta}$ are given by the derivatives of the damage function multiplied by a damage multiplicator $\dot{\lambda}_d$. Again the latter is computed thanks to the consistency condition $\dot{F}_d = 0$ and the loading/unloading conditions for the damage evolution are specified by Kuhn-Tucker's conditions :

$$\dot{\lambda}_d \geq 0, \quad F_d \leq 0, \quad \dot{\lambda}_d F_d = 0 \tag{3-40}$$

This model is very interesting. To the 5 material constants c^r, c^d, c^p, B_o, σ_y presented here, 10 other constants are required to define the complementary energy used to derive $\underline{\dot{\varepsilon}}^e$, $\underline{Y}$, R, B. This Gibbs thermodynamic potential has been briefly described at the end of preceding section 3.2.3. So, finally, this model is defined by 15 variables. It is quite general as the yield surface and the damage surface shape and size are affected by damage. Damage anisotropy is taken into account by a second rank symmetric damage tensor $\underline{D}$. For instance, Figure 3-3 presents the damage surface in the space of tensile stress σ and shear stress τ.

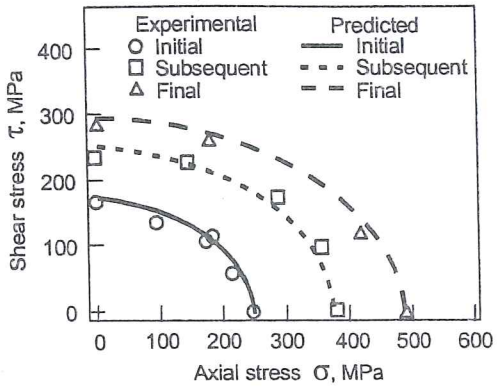

Figure 3-3 Damage surfaces in a combined stress space for a spheroidized graphite cast iron (from Hayakawa & Murakami 1998).

The aspect ratio σ/τ of the initial damage surface is 1.46, in contrast to the ellipse of the initial yield surface of von Mises type the aspect ratio of which is $\sqrt{3}$. This difference may be explained as follows: while plastic yielding is governed by deviatoric stresses, the influence of hydrostatic stresses cannot be neglected for damage development due to the nucleation and growth of microcracks. On the other hand, the aspect ratio of the updated damage surface is 1.62, closer to the aspect ratio of von Mises' yield surface. This can be explained by the fact that the increasing plastic deformation of the ferrite matrix gradually governs the damage process. The aspect ratio of the final damage surface is very close to $\sqrt{3}$. This provides information to define the elastic–damage complementary energy the derivative of which allows to compute the damage conjugate force $\underline{Y}$.

Rousselier 1987 proposes a pseudo dissipation potential divided into two terms:

$$F = F_1(\tilde{\sigma}_{eq}, R) + F_2(\tilde{\sigma}_m, Y) \tag{3-41}$$

where $\underline{\tilde{\sigma}} = \underline{\sigma}/\rho$ is used. R and Y follow above definitions. The functions F_1, F_2 are respectively related to plasticity (von Mises' criterion) and damage:

$$F_1 = \tilde{\sigma}_{eq} + R(p) \tag{3-42}$$

$$F_2 = Y(D)\, g(\tilde{\sigma}_m) \tag{3-43}$$

The choice of F_2 is as simple of possible. Taking into account mass conservation and neglecting elastic volume change yields :

$$\dot{\rho} + 3\rho\dot{\varepsilon}^p_m = 0 \tag{3-44}$$

Then, assuming that, in first approximation, $\rho=\rho(D)$ and applying the normality rule :

$$\underline{\dot{\varepsilon}}^p = \dot{\lambda}\,\partial F / \partial(\underline{\tilde{\sigma}}) \quad \text{and} \quad \dot{D} = \dot{\lambda}\,\partial F / \partial Y \tag{3-45}$$

one gets :

$$\frac{\partial g / \partial \tilde{\sigma}_m}{g} = -\frac{\partial \rho / \partial D}{Y\rho} \tag{3-46}$$

The two members of the latter equation being functions of different variables $\underline{\tilde{\sigma}}$ and D, the only possibility is that they are equal constants, which produces after integration:

$$F = \frac{\sigma_{eq}}{\rho} - R(p) + Y(D)\ c^d\ exp(\frac{\sigma_m}{\rho\sigma_1}) \tag{3-47}$$

If one assumes $Y(D) = \sigma_1 f$, where f is the microvoid volume fraction the growth of which can be linked to Rice and Tracey's relation (2-10), this pseudo potential is very close to Gurson's criterion (2-1). This model is interesting as it contains only 7 parameters: E, ν, K, M (if relation 3-27 is assumed), σ_1, c^d, f_0, and proves that phenomenological models based on thermodynamics can recover Gurson's model. An extension of this model, adapted to large strains, has been used by Eckstein *et al.* 1997, Eckstein & Basar 2000. Rousselier's model is quite popular, it is used for instance by Baaser & Gross 2000 or Besson *et al.* 2000.

Gelin & Danescu 1992 work with a symmetric second order tensor $\underline{D}$ in order to describe anisotropic damage. They propose to decompose the stress tensor into a part $\underline{\sigma}^D$, normal to $\underline{D}$, and a part parallel to $\underline{D}$:

$$\underline{\sigma} = \underline{\sigma}^D + \frac{\underline{\sigma} : \underline{D}}{\underline{D} : \underline{D}} \underline{D} \tag{3-48}$$

They use a generalized von Mises' yield condition:

$$F_p(\underline{\sigma}, \underline{D}, R) = \underline{\sigma} : \underline{\sigma} + c^d\ \underline{\sigma}^D : \underline{\sigma}^D - \frac{(\sigma_y + R)^2}{\underline{D} : \underline{D}} \tag{3-49}$$

Finally, their damage evolution equation, defining the objective damage derivative, is:

$$\overset{\nabla}{\underline{D}} = \dot{\lambda} \left[-\frac{\underline{\sigma} : \underline{D}}{\underline{D} : \underline{D}} \underline{\sigma}^D + \left(\frac{\sigma_y + R}{\underline{D} : \underline{D}} \right)^2 \underline{D} \right] \tag{3-50}$$

The consequences of their choices are :

- the damage norm is increased by the part of the stress that may produce the plastic flow,
- supposing that the stress tensor has a fixed orientation, the damage tensor tends to achieve an orientation normal to the stress,
- plastic anisotropy and softening are induced due to the damage tensor,
- the symmetry of the elastic response is not changed qualitatively in the presence of damage.

3.2.5. The strain decomposition

Ju 1989 uses a split of the total strain tensor into "elastic-damage (reversible)" and "plastic-damage (irreversible)" parts. However he does not try to express separately the reversible and irreversible damage strains from the elastic and plastic strains. So he finally uses simple additive relation (3-5) as Lemaître.

Further steps are proposed by Bruhns & Schiess 1996, who propose three strains: elastic, plastic and damage strains. Voyiadjis & Park 1998 go even further as they split the strain into four terms: ε^e elastic, ε^p plastic, $\varepsilon^{d'}$ recoverable damage and $\varepsilon^{d''}$ irreversible damage strains. Their approach is represented by Figure 3-4 for a uniaxial stress-strain curve. The microscopic events supporting damage strain splitting are the following ones:

- $\varepsilon^{d'}$ "recoverable" damage strain due to the reduction of elastic stiffness tensor,
- $\varepsilon^{d''}$ "irreversible" damage strain tensor due to the lack of closure of microcracks and microvoids during unloading.

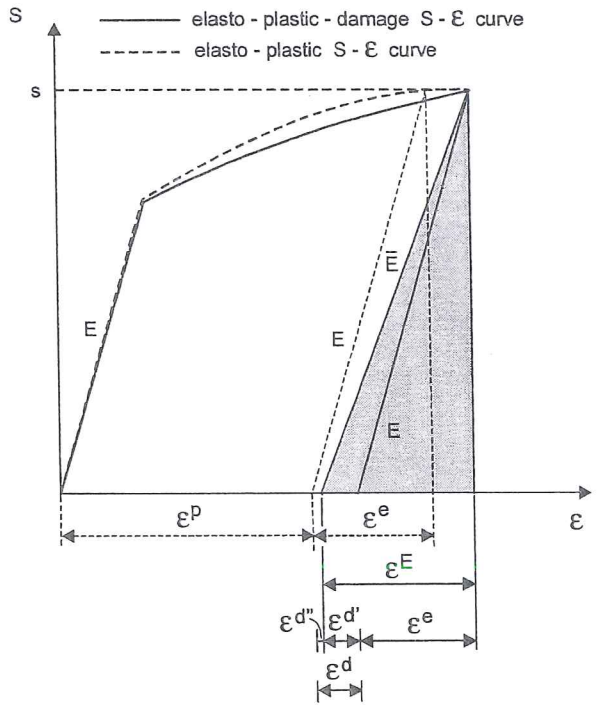

Figure 3-4 Schematic representation of elasto-plastic damage strain increments in the case of a uniaxial stress-strain curve with second Piola Kirchhoff stress S and the Lagrangian strain ε (from Voyiadjis & Park 1998).

Voyiadjis & Park 1998 propose a kinematics of damage for elasto-plastic behavior with finite strains. The multiplicative decomposition of the deformation gradient and the additive decomposition of the Lagrangian strain tensor are used to deduce separately each strain.

3.2.6. Microcrack opening and closing

This state of the art cannot forget the very useful concept, introduced by Ortiz 1985 and Ju 1989, to consider different mechanisms under tensile and compressive states. They use the spectral decomposition of tensors and retain the positive spectral projection to define functions such as, for instance, the elastic free energy. For a second order tensor $\underline{A}$, with principal values a_i and unit principal directions $\underline{p}$, Ju defines the positive spectral projection $\underline{A}^+$ as :

$$\underline{A}^+ = \sum_{i=1}^{3} H(a_i)\, \underline{p} \otimes \underline{p} \tag{3-51}$$

where H is the Heaviside step function. In their respective damage models, several authors replace tensors such as strain $\underline{\varepsilon}$ (Ju 1989), stress $\underline{\sigma}$ (Zhu 1992), damage associated force $\underline{Y}$ (Gallerneau 1995) by their positive projections.

3.2.7. Crack induced anisotropy

The present literature review is not dedicated to quasi-brittle materials. However, it is interesting to note that brittle approach can be quite close to ductile one. For instance, in the model proposed by Fichant *et al.* 1996 or 1998, the concepts of effective stress and damage surface are also applied. Their model is based on the approximation of the relationship between the effective stress in the damage material and the macroscopic stress. Given a vector normal to a microplane in the material, the microplane stress is proportional to the effective stress. The coefficient of proportionality is expressed as a function of the damage in the direction defined by the vector normal to the microplane. The macroscopic stress-strain relationship is obtained according to the principle of virtual work, with a kinematic constraint. The micro-strain on each plane is equal to the macroscopic strain. So the microplane strains represent the projections of the macroscopic strain tensor but the microplane stresses are not equal to the resolved components of the macroscopic stress tensor. The constitutive relation can be viewed as a simplified micro-plane type model (Bazant & Ozbolt 1990) where the behavior of the damaged material is discretised in a finite set of directions.

The damage surface and its evolution are summarized here because the approach of Fichant *et al.* 1996, 1998 could be extended to ductile materials. The simplest approximation, which does not yield to isotropy, corresponds to an ellipsoidal damage surface characterized by three principal directions and the values of three damage scalars along these directions. Initially, the damage surface is reduced to a point:

$$d(\underline{n})=0 \tag{3-52}$$

where d is a scalar quantity which introduces the effect of damage in the relation between the effective stress tensor and the macroscopic stress. It is known for a finite set of directions $\underline{n}$. The evolution of damage is controlled by a loading surface f:

$$f(\underline{n}) = \underline{n}.\underline{\varepsilon}.\underline{n} - \varepsilon_d - B(\underline{n}) \tag{3-53}$$

with B a hardening/softening variable which is interpolated in the same fashion as the damage surface and ε_d is a damage threshold strain value. The evolution of the damage surface is defined by:

$$\text{if } f(\underline{n}^*) = 0 \text{ and } \underline{n}^*.\dot{\underline{\varepsilon}}.\underline{n}^* > 0 \text{ then}$$

$$\dot{d}(\underline{n}^*) = \left[\frac{\varepsilon_d(1 + a(\underline{n}^*.\underline{\varepsilon}.\underline{n}^*)}{(\underline{n}^*.\underline{\varepsilon}.\underline{n}^*)^2} exp(-a(\underline{n}^*.\underline{\varepsilon}.\underline{n}^*) - \varepsilon_d \right] (\underline{n}^*.\dot{\underline{\varepsilon}}.\underline{n}^*) \tag{3-54a, b}$$

$$\dot{B}(\underline{n}^*) = \underline{n}^* \dot{\underline{\varepsilon}} \underline{n}^* \tag{3-54c, d}$$

$$\text{else } \dot{d}(\underline{n}^*)=0 \quad \dot{B}(\underline{n}^*)=0$$

Note that the vectors $\underline{n}^*$ are the three principal directions of the incremental strain whenever damage grows. The parameters of this damage model are the initial value of $B(\underline{n})$, which is assumed to be initially isotropic since the undamaged material is isotropic, and the parameter a. The first parameter can be related to the tensile strength of the material, if one assumes that damage in uniaxial tension occurs at the peak stress, and the second one will be related to the fracture energy of the material. The new damage surface is the combination of two ellipsoidal surfaces: one surface corresponding to the initial damage, and the other one corresponding to the incremental growth of damage.

These two surfaces do not have the same principal axes and the resulting surface has not the same principal directions as the total strain tensor, except when the principal directions of strains and damage do not rotate during the strain increment. So principal directions of strains and stresses are not necessarily the same. This approach, initially coupled only with elastic behavior (Fichant *et al.* 1996) has been adapted to an elasto-plastic case (Fichant *et al.* 1998). Applied to concrete, this model allows structural analysis of bending of beams, compression, shear and tension-shear of concrete panels.

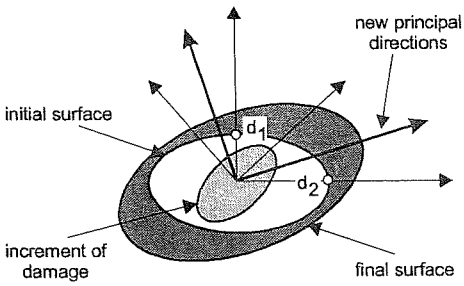

Figure 3-5 Evolution of the damage surface in plane 12 (from Fichant *et al.* 1998).

3.3. Comparison of models

Gelin & Danescu 1992 summarize quite well the main differences between micro-macro damage models, as the one proposed by Gurson or Ponte Castenada, and phenomenological approaches with internal variables. They point out that to build a Gurson's type approach generally involves five different steps:

1. Definitions of strain and stress at macroscale.
2. The choice of a particular geometry for the cell and the void. Very often one adds as much symmetry as possible to allow analytical study.
3. A lower bound result. This is a point in which different approaches give different results.
4. A particular velocity field used to describe the void growth.
5. An optimization procedure. Since the lower bound result only gives a lower bound, it is expected that the real form of the macroscopic potential is found, or at least approximated, by maximizing this lower bound.

These steps are required to find the macroscopic yield function. In fact, the crucial role played by the choice of the velocity field and the geometry of the cell in Gurson's type models is the counterpart of the evolution equations of the internal damage variable or the pseudo potential function choice in phenomenological model. For such approaches, these functions are deduced according to thermodynamics limitations and experimental observations.

In contrast to Gurson's model, the evolution of the damage variables of Lemaître's type damage model is associated with a dissipative mechanism. The simple problem of a uniaxially stressed bar subjected to cyclic loading (Figure 3-6) has been simulated by FEM codes using Lemaître's and Gurson's damage models by de Souza Neto *et al.* 1998.

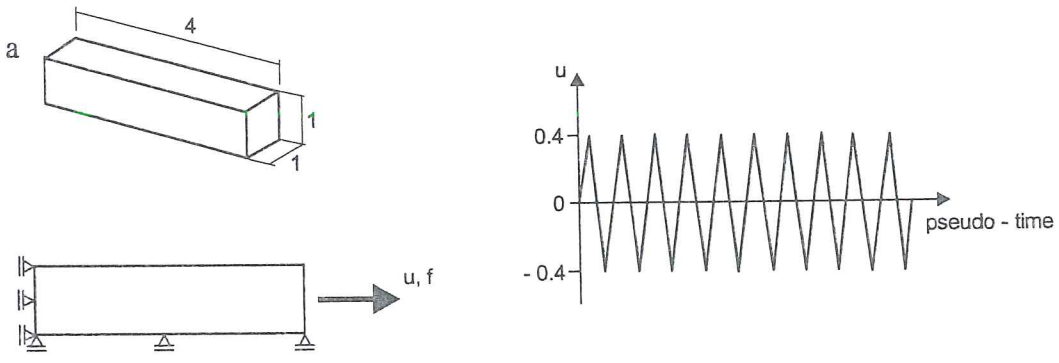

Figure 3-6 Bar geometry and loading (from de Souza Neto *et al.* 1998).

Figure 3-7 presents the axial reaction force f obtained in the simulations versus the imposed displacement u. With Lemaître's model simulation, the reaction force is progressively decreasing over the cycles. This is a direct result of damage

accumulation and consequent material softening. The elastic unloading after the end of the last cycle also proves the degradation of the elastic modulus. In contrast, the reaction forces obtained with Gurson's model are practically constant over the cycles. Indeed for this model, damage growth resulting from the extension of the bar is compensated by damage healing that occurs during compression. In this case, no cumulative damage occurs and the damage variable returns to its initial value after each cycle. This does not correspond to the experimental observation of progressive damaging in cyclic tests with ductile materials.

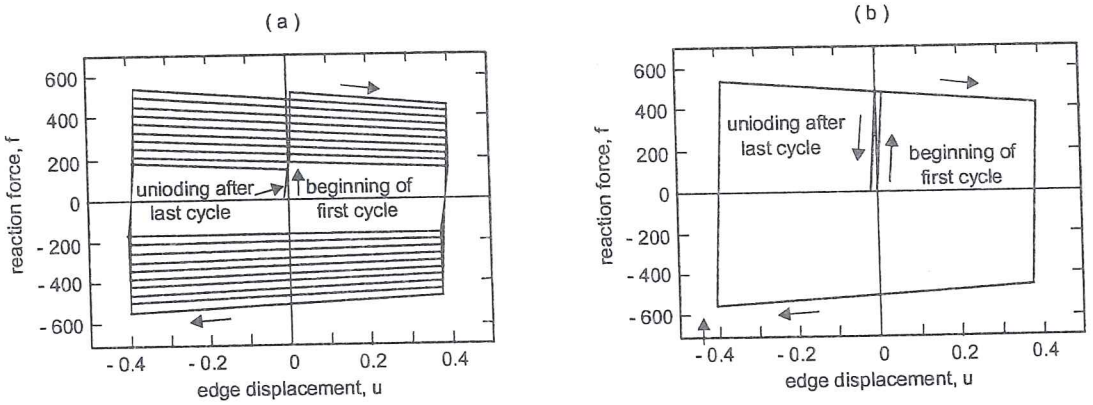

Figure 3-7 Bar cyclic extension/compression without hardening, force-displacement curves obtained with: (a) Lemaitre's model; (b) Gurson's model (from Souza Neto *et al.* 1998).

3.4. Summary

Chapter 3 describes thermodynamics damage models. It does not expand over their integration scheme or their link with physical metallurgy but provides examples of choices such as internal variables and pseudo potential functions.

As this thesis is focused on ductile rupture, very few references are dedicated to brittle models, nothing is devoted to fatigue. However, it is important to note that thermodynamics damage models also predict fracture appearance in such cases.

The « French school » of damage models is presented by means of Lemaître & Chaboche 1985. However, it is worth to underline that this approach is now applied all over the world : see for instance Bruhns & Schiesse 1996 in Germany, Geers 1997 in the Netherlands, Ju 1989 in United States, Hayakawa & Murakami 1998 in Japan.

The principles presented here help the reader to understand the context of the models used in Chapters 6 and 7.

References

Baaser, H., Gross, D., (2000) 3D simulation of ductile crack growth, a numerical realisation, Euromech 417, *Numerical Modelling in Damage Mechanics*, University of Technology of Troyes, France, 27-29.

Bazant, Z.P., Ozbolt J. (1990) Nonlocal microplane model for fracture, Damage and size effect in structures, ASCE, *J. of Eng. Mech.*, **116**, 2485-2505.

Besson, J., Brocks, W., Chabanet, O., Steglich, D., (2000) Ductile rupture of aluminium sheet materials, Euromech 417, *Numerical Modelling in Damage Mechanics*, University of Technology of Troyes, France, 30-31.

Bruhns, O.T., Schiesse, P. (1996) A continuum model of elastic-plastic materials with anisotropic damage by oriented microvoids. *Eur. J. Mech. A/Solids*, **15-3**, 367-396.

Charlier, R. (1987) Approche unifiée de quelques problèmes non linéaires de mécaniques des milieux continus par la méthode des éléments finis (grandes déformations des métaux et des sols), contact unilatéral de solides, conduction thermique et écoulements en milieux poreux. Université de Liège, thèse de doctorat en sciences appliquées.

Cordebois, J.P., Sidoroff, F. (1979) Damage induced elastic anisotropy, *Euromech*, **115**, Villars de Lans, France.

Desoyer, T. (1995) Contribution à la modélisation de l'endommagement diffus et localisé, Mémoire pour l'obtention de l'habilitation à diriger les recherches, Université de Poitiers.

Doghri, I., (1995) Numerical implementation and analysis of a class of metal plasticity models coupled with ductile damage, *Int. J. Num. Meth. Engin.*, **38**, 3403-3431.

Doghri, I. (2000), Mechanics of Deformable Solids, Springer.

Dragon, A., (1985) Plasticity and ductile fracture damage : study of void growth in metals, *Eng. Fract. Mech.*, **21**, 875-885.

Eckstein, A., Basar, Y. & Konke, C. (1997) Damage analysis of ductile metallic shells. *Computational plasticity – Fundamentals and Applications,* Owen, D.R.J, Onate, E. Hinton, E., editors, CIMNE, Barcelona.

Eckstein, A., Basar, Y. (2000) Ductile damage analysis of elasto-plastic shells at large inelastic strains, *Int. J. Num. Meth. Engin.*, **47**, 1663-1667.

Fichant, S., Pijaudier-Cabot G., La Borderie, C. (1996) Continuum damage modelling with crack induced anisotropy, *Numerical Methods in Engineering,* John Wiley & Sons

Fichant, S., La Borderie, C., Pijaudier-Cabot G. (1998) A comparative study of isotropic and anisotropic descriptions of damage in concrete structures, *Damage mechanics in engineering materials*, Voyiadjis, G.S., Ju, J.W., Chaboche, J.L. Eds, Elsevier 259-274.

Gallerneau, F. (1995) Etude et modélisation de l'endommagement d'un superalliage monocristallin revêtu pour aube de turbine, Thèse Docteur en sciences et génie des matériaux, Ecole Nationale Supérieure des Mines de Paris.

Geers, M.G.D., (1997) Experimental Analysis and Computational Modelling of Damage and Fracture, Ph. D. thesis, Technische Universiteit Eindhoven.

Gelin, J.C., Danescu, A., (1992) Constitutive model and computational strategies for finite-strain elasto-plasticity with isotropic or anisotropic ductile damage, *Proc. of the third Int. Conf. Computational plasticity*, D.R.S. Owen *et al.* editors, Pineridge Press, 1413-1424.

Geoffroy, J.L., Cambien, I., Mareuse, D., (1993) Assessment of intrinsic elastic constants by mean of both tensile test and resonance frequency measurements, *IDDRG 93: Working group Nr.3.*

Hayakawa, K., Murakami, S. (1998) Space of damage conjugate force and damage potential of elastic-plastic-damage materials, *Damage Mechanics in Engineering Materials*, Voyiadjis, G.S., Ju, J.W., Chaboche, J.L. Eds, Elsevier, 27-44.

Ju, J.W. (1989) On energy-based coupled elastoplastic damage theories : constitutive modelling and computational aspects, *Int. J. Solids & Structures*, **25-7**, 803-833.

Kachanov, L.M. (1958) Time of the rupture process under creep condition, *Izv. Akad. Nauk SSSR, Otd. Tekhn. Nauk*, **8**, 26-31.

Lemaître, J. (1985) Coupled elastoplasticity and damage constitutive equations, *J. Comp. Meth. in Appl. Mech. and Eng.*, **51**, 31-49.

Lemaître, J., Chaboche, J.L. (1985) Mécanique des matériaux solides, Dunod, Paris.

Li, K. (1995) Contribution to the finitie element simulation of three-dimensional sheet metal forming, Université de Liège, thèse de doctorat en sciences appliqués.

Martins Meneze, K.F., (1994) Modélisation tridimensionnelle et simulation numérique des processus de mise en forme, Application à l'Emboutissage des Tôles Métalliques, version française, Faculdade de ciências e tecnologia da Universidade de Coimbra Departamento de engenharia mecânica.

Murakami, S., Hayakawa, K., Liu, Y. (1998) Damage evolution and damage surface of elastic-plastic-damage materials under multiaxial loading, *Int. J. of Damage Mechanics*, **7**, 103.

Ortiz, M. (1985) A constitutive theory for the inelastic behaviour of concrete. *Mech. Mater.*, **4**, 67-93.

Owen, D.R.J., Peric, D., de Souza Neto, E.A., Jianguo, Y., Dutko, M., Crook, A.J.L. (1995) Advanced computational strategies for 3-D large scale metal forming simulations, *NUMIFORM 95, Simulation of materials processing: theory, methods and applications*, Shen & Dawson Eds, Balkema Press, Rotterdam.

Rabotnov, Y.N., (1963) On the equations of state for creep. *Progress in Applied Mechanics*, Prager Anniversary Volume, New-York, Mac Millan, 307.

Rice, J.R. (1968) A path independent integral and the approximate analysis of strain concentration by notches and cracks, *J. Appl. Mech.*, **35**, 379-386.

Rousselier, G. (1987) Ductile fracture models and their potential in local approach of fracture, *Nuclear Engineering and Design*, **105**, 97-111.

Rousselier, G., Devaux, J.C., Mottet, G., Devesa, G. (1989) A methodology for ductile fracture analysis based on damage mechanics : an illustration of a local approach of fracture, *Nonlinear Fracture Mechanics : vol. II – Elastic-Plastic Fracture, ASTM STP 995,* J.D. Landes, A. Saxena, J.G. Merkle Eds, American Society for Testing and Materials, Philadelphia, 332-354.

Simo, J.C., Ju, J.W. (1987) Strain – and stress – based continuum damage models. I. Formulation, *Int. J. Solids & Structures*, **23-7**, 821-840.

Simo, J.C. (1992) Algorithms for static and dynamic multiplicative plasticity that preserve the classical return mapping schemes of the infinitesimal theory, *Comp. Method. in Appl. Mech. & Eng.*, **99**, 61-112.

de Souza Neto, E.A., Peric, D., Owen, D.R.J. (1998) Continuum modelling and numerical simulation of material damage at finite strains, *Archives of Computational Methods in Engineering*, **5-4**, 311-384.

Taljera (1985) A continuum mechanics characterization of damage in composite materials. *Proc. R. Soc. Lond. Ser. A*, **399**, 195-216.

Voyiadijs, G.Z., Park, T., (1998) Kinematics of Large Elastoplastic Damage Deformation, *Damage Mechanics engineering Materials*, Eds. Voyiadijs, G.Z., Ju, J-W.W., Chaboche, J.L., Elsevier.

Weber, G., Anand, L. (1990) Finite deformation constitutive equations and a time integration procedure for isotropic, Hyper elastic-viscoplastic solids, *Comp. Meth. In Appl. Mech. & Eng.*, **79**, 173-202.

Zhu, Y.Y. (1992) Contribution to the local approach of fracture in solid dynamics, Ph. D. thesis, University of Liège, MSM Department .

4. RUPTURE CRITERIA USED WITH CONTINUUM DAMAGE MODELS

To write a compilation of all failure criteria is an impossible task due to the incredible amount of work in this field. The present review is limited to criteria applied to **ductile fracture** and compatible with finite elements using continuum damage models. As final rupture quickly follows void coalescence, this study includes coalescence criteria. Fracture criteria can be divided into four families:

- simple damage criteria;
- criteria deduced from stress and strain fields;
- complex criteria issued from microscopic observations or mesoscopic approach and taking into account the microscopic phenomena;
- criteria attempting to bridge classical fracture mechanics and damage continuum mechanics.

For each family, a few criteria are proposed together with their advantages and weaknesses as well as their suitability for use in macroscopic damage models.

4.1. Simple damage criteria

For isotropic damage models with only one scalar variable, it seems straightforward to define its threshold value thanks to one experiment conducted until rupture. The fracture criterion is then fulfilled when the damage variable reaches this level :

- Gurson's type model : $f = f_{cr}$ if coalescence is not modeled,
  $f = f_F$ if coalescence is modeled.
- Lemaître's type model : $D = D_{rupture}$

Such easy fracture criteria are very current and have been used successfully by, among others, Picart *et al.* 1997, Doege *et al.* 1997, Lemaître 1985, Zhu 1992, Tvergaard 1982, Rousselier *et al.* 1989, Brocks *et al.* 1995, Eckstein *et al. 1997*. The advantage of such an approach is its simplicity. Its drawback is a poor accuracy as different rupture types are detected by the same threshold value. To detect chevron crack in drawing, Komori 1998 uses critical void volume fraction coupled with critical axial stress.

The mesoscopic approach allows an interesting verification of such limit values. For instance, assume that the internal damage variable is the void volume fraction or porosity like in classical Gurson's model. The FEM discretization of an elementary cell with one void can be submitted to different loadings (torsion, triaxial loading deduced from notched tensile test,...). Such FEM simulations will produce porosity-equivalent strain curves, showing for each loading a vertical branch clearly localizing the porosity and equivalent strain at the rupture onset. This validates the use of a critical value of the void volume fraction as a criterion of final material failure.

Brethenoux *et al.* 1996 present experimental fracture strains close to the ones computed by means of their mesoscopic models. For their studied materials (steel grade 22MnCrB5, 27CrMo4, 42CrMo4), very low values of critical porosity are deduced (0.01 to 0.06).

Koplik & Needleman 1988 present numerical computations of the behavior of a cell model and also the corresponding predictions based on improved Gurson's model (version with Tvergaard coefficients and function f^*). Their cell model simulates a three-dimensional periodic array of spherical voids in an isotropically hardening elastic-viscoplastic matrix. This cell model is submitted to both axial and radial stresses ($T = \sigma_m / \sigma_{eq}$ = 1, 2 or 3). The cell model calculations show a shift from a general axisymmetric deformation state to a mode of uniaxial straining of the ligament between neighboring voids. The plastic deformation localizes on this ligament and this event is associated with the accelerated void growth accompanying coalescence. Figure 4-1 illustrates that the same void volume fraction can characterize various geometries and Figure 4-2 shows the macroscopic stress-strain curves deduced from the cell model with b_0/R_0= 8 or 1. The exact cell material properties and the definitions of macroscopic effective stress and strain are given in Koplik & Needleman 1988.

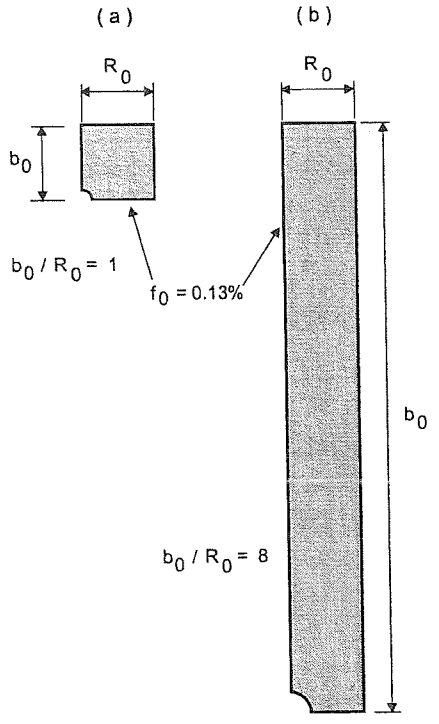

Figure 4-1 Two cell geometries with identical initial void volume fraction (adapted from Koplik & Needleman 1988).

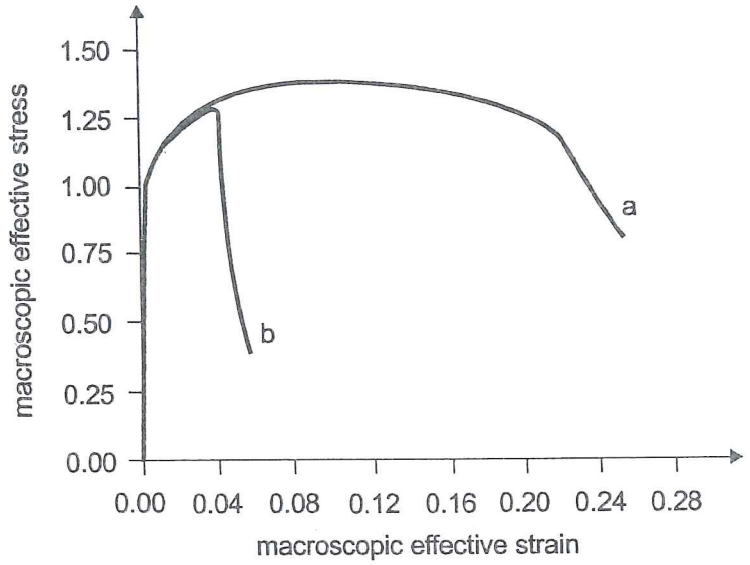

Figure 4-2 Macroscopic effective stress-strain curves according to cell geometry defined by Figure 4-1 (from Koplik & Needleman 1988).

Before the stress drop, the stress-strain response is identical. However the maximum stress reached and the shift to a uniaxial straining mode is sensitive to the void distribution. For a square cell, the authors show good agreements between Gurson's and cell models (Figure 4-3). They also verify that f_{cr} value, at which the onset of coalescence appears, varies slowly with the stress triaxiality and the matrix strain hardening, but depends strongly on the initial void volume fraction. Brocks *et al.* 1995's researches confirm that the void volume fraction at void coalescence f_{cr} does not significantly depend on the triaxiality if the initial volume fraction of primary voids is small and if there are no secondary voids. The strain rate does not affect f_{cr} either.

In conclusion, the simple threshold value of void volume fraction in Gurson's model appears to be valid if the whole parameter set is accurately fitted. As actual materials are non periodic, the definition of f_{cr} is even more difficult. Section 4.4 summarizes recent information on the dependence of f_{cr}.

Results of cell calculations performed by Brocks *et al.* 1995 indicate that a single internal variable, as the void volume fraction, is not sufficient to characterize the fracture processes in materials containing two different size scales of void nucleating particles.

In case of multiple scalar damage variables, threshold values can be applied on each damage variable as performed by Zhu 1992. However, the existence of interactions between these variables is an open question. For tensor damage variables, one could use a tensor norm to define one scalar threshold value (Zhu 1992). Experimental verification is however still lacking.

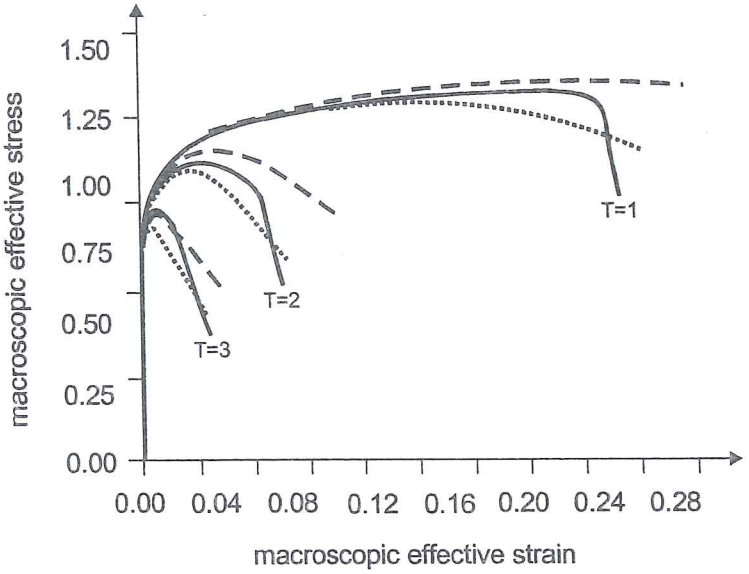

Figure 4-3 Comparison of macroscopic stress-strain curves:
cell model response, (——),
initial Gurson's model (- - - -),
modified Gurson's model with q_1, q_2 & f^* (.....)
(from Koplik & Needleman 1988).

4.2. Criteria based on stress or strain field analysis

Using improved Gurson's law (with Tvergaard coefficient q_1 and function f^*) to simulate ductile rupture in notched bars, Needleman & Tvergaard 1984 correctly identify the experimental failure strain when the computed porosity reaches a constant value of $f_{cr}=0.15$.

They find that, as long as deviations from a constant triaxiality history are not too big, the onset of failure can also be represented by a curve relating effective strain with stress triaxiality. Later, the research performed by Chiou 1996, using an extension of Gurson's model, seems to prove that the critical porosity value is not a constant. However, Chiou proposes, like Needleman & Tvergaard 1984, to use a fracture strain related to the triaxiality ratio. The fracture criterion is :

$$\varepsilon_{eq} \leq \varepsilon_{rupture} = A \quad exp(-B\frac{\sigma_m}{\sigma_{eq}}) \tag{4-1}$$

Table 4-1 compiles the review performed by Zhu 1992 and Esche *et al.* 1996.

Criterion name	Formula	Origin, Physical assumptions
Gosh 1976 version of Zhu, Cescotto, Habraken 1992	$(\sigma_1+\sigma_2+\sigma_3)(\sigma_1-\sigma_3)=C$	This criterion is based on the statistical process of shear joining of voids.
Freudenthal 1950	$\int_o^{\varepsilon_f}\sigma_{eq}d\varepsilon_{eq}=C$	The absorbed energy per unit volume characterizes the critical fracture state.
Cockroft & Latham 1968	$\int_o^{\varepsilon_f}\sigma_1 d\varepsilon_{eq}=C$	This maximum tensile work criterion assumes that the maximum principal tensile stress rather than the effective stress causes fracture initiation.
Brozzo, de Luca, Rendina 1972	$\int_o^{\varepsilon_f}\frac{2\sigma_1}{3(\sigma_1-\sigma_m)}d\varepsilon_{eq}=C$	This criterion improves the preceding one by including the effect of hydrostatic stress.
MC Clintock 1968 Version of Oh, Chen, Kobayashi 1979	$\int_o^{\varepsilon_f}\left\{\frac{2}{\sqrt{3}(-n)}sinh\left[\frac{\sqrt{3}(1-n)}{2}\frac{\sigma_3-\sigma_1}{\bar{\sigma}_{eq}}\right]+\frac{\sigma_3-\sigma_1}{\bar{\sigma}_{eq}}\right\}$	This criterion is based on the analysis of the expansion of cylindrical cavities in a plastic material under a triaxial state of stress of fixed orientation.
Rice & Tracey 1969	$\int_o^{\varepsilon_f}B\,exp\left(\frac{A\sigma_m}{\sigma_{eq}}\right)d\varepsilon_{eq}=C$	Spherical voids in a plastic material are assumed to grow exponentially with the triaxiality. This criterion is widely used.
Oyane 1972	$\int_o^{\varepsilon_f}\left(1+\frac{\sigma_m}{A\sigma}\right)\varepsilon_{eq}^B d\varepsilon_{eq}=C$	This criterion is derived from the equation of plasticity theory for porous material.

Norris, Reaugh, Moran, Quinones 1978 Version of Atkins1981	$\int_o^{\varepsilon_f} \left(\frac{1+\frac{d\varepsilon_1}{d\varepsilon_2}\cdot\frac{1}{2}}{1-A\sigma_m} \right) d\varepsilon_{eq} = C$	Empirical criterion which considers the effect of principal strain ratio and hydrostatic stress.

Table 4-1 Some fracture criteria, where:

C	is the critical value of the scalar damage value, computed as a function of the stress and strain deformation history,
A	is a material constant,
σ_m	is the hydrostatic stress,
σ_{eq}	is the von Mises' stress,
$\sigma_1\ \sigma_2\ \sigma$	are the principal stresses,
$\varepsilon_1\ \varepsilon_2$	are the principal strains,
ε_f	is the effective equivalent fracture strain,
n	is the material hardening exponent,

(adapted from Zhu 1992 and Esche *et al.* 1996).

As concluded in both reviews, the drawbacks of the above criteria are their accuracy dependency on the mode in which failure takes place and the difficulty to find accurate material constants. In fact, the critical damage values are not purely material constants but rather depend to some degree on the type of boundary conditions. Their advantage is an easy implementation in the Finite Element code. A more complete review can be found in Wilsius 1999.

4.3. Criteria based on stress or strain fields dedicated to sheet metal forming

This section is specifically dedicated to sheet metal forming. Different approaches were considered to detect the localized necks that are quickly followed by rupture:

1. experimental work to define the material limits (Forming Limit Diagram FLD);
2. analytical work based on Marciniak & Kuczynski's 1967 approach (MK), which requires the assumption of an initial defect and allows to predict FLD;
3. analytical plastic instability criteria which require no additional data or defect assumption and allow to predict necking in any conditions.

4.3.1. Forming Limit Diagram (FLD)

A forming limit diagram (FLD) divides the plane of major principal strain versus minor principal strain into a safe zone and a failure zone. Commonly, such diagram is experimentally determined by means of proportional loadings, which keep a constant ratio between the major and minor principal strains throughout the deformation process (depending on the authors, such a loading is called a radial, linear or direct strain path). Figure 4-4, relative to an isotropic material, presents the restrained, stretched, failure and safe zones. For anisotropic material, the relation between the stress and strain ratios differs, FLD diagram keeps classical directions defined by the train increment ratio.

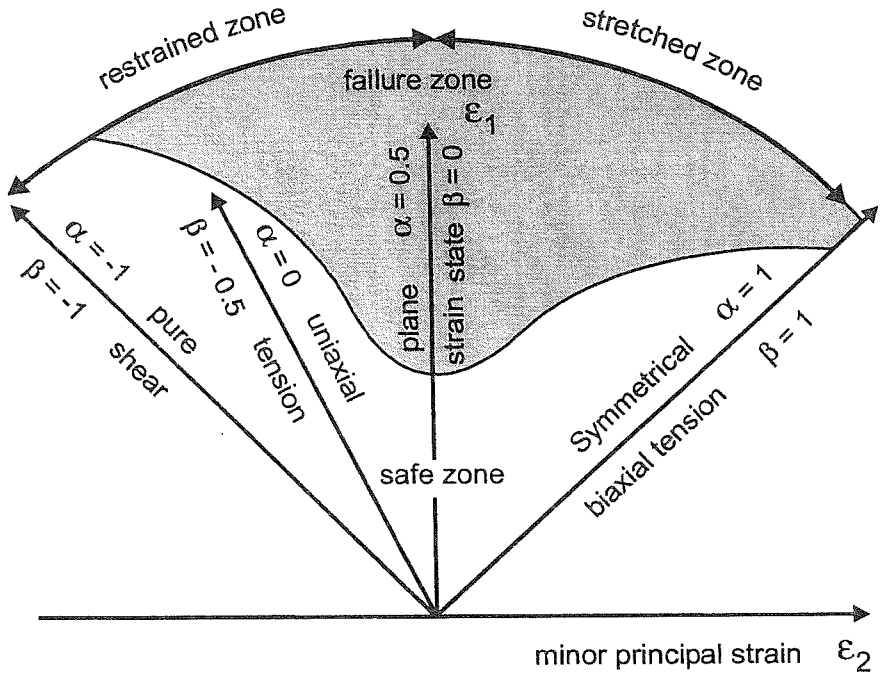

Figure 4-4 Forming Limit Diagram, where α is the stress ratio ($\alpha = \sigma_2/\sigma_1$) and β is the strain increment ratio ($\beta = d\varepsilon_2 / d\varepsilon_1$), isotropic material, (adapted from Barata da Rocha 1985).

A short historical survey of FLD is proposed by Esche *et al.* 1996.

FLD deduced from direct strain paths cannot be used in all cases, because they are not overlaid by FLD obtained by means of broken strain paths (stretching or large tensile tests followed by radial strain paths...). However, they can still serve for comparing different materials or determining the best orientation of the sheet to optimize a deep drawing operation. Arrieux 1990, Vacher *et al.* 1988 propose to employ a Stress Forming Limit Diagram, which seems to be a better intrinsic material property. The Stress FLD deduced from broken or direct strain paths are very close to each other and the one deduced from linear strains is almost always located slightly below the others. So, the current practice in deep drawing is to

implement experimentally measured Stress or Strain Forming Limit Diagrams in FEM codes. Then, the computed principal stresses or strains are compared to these limit curves which allows to detect fracture. Such an approach can be used with a law which is coupled or not with damage. Note that the intrinsic property of Stress FLD can be very dependent on the quality of the stress calculation procedure (Boudeau 1995).

Vacher *et al.* 1988 introduce in fact a Forming Limit Stress Surface as they include the effect of the angle between the principal strains and the material orthotropy directions (Figure 4-5). One of the main problems with this approach is the impossibility of using this surface if the angle θ between principal strains and orthotropy directions varies during the forming process.

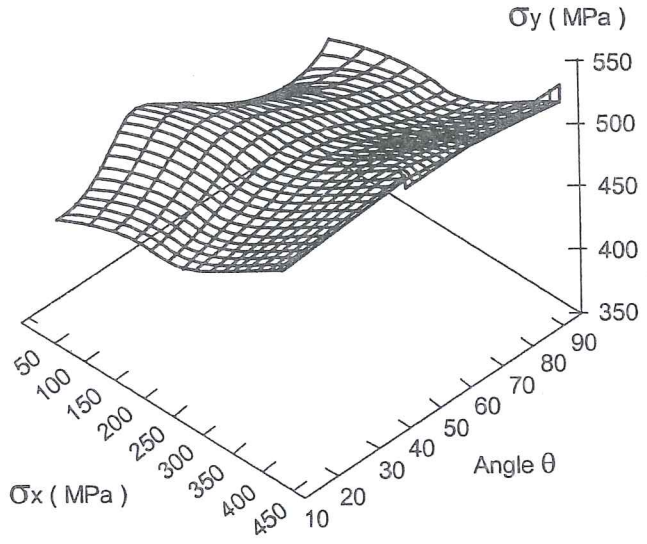

Figure 4-5 Forming Limit Stress Surface in and off axis solicitations, with direct paths, mild steel for deep drawing SEDDK A151 (from Vacher *et al.* 1988).

The FLD predictions also provide a very sensitive way to check analytical approaches coupled or not with FEM and adapted to different descriptions of the material behavior. The following references give only a small idea of the important effort dedicated to theoretical FLD prediction: Narasimhan & Wagoner 1991, Qiu *et al.* 1995, Boudeau *et al.* 1996a, Banabic 1996, Hora *et al.* 1996, Vegter *et al.* 1998, Cayssials 1998 and 1999, Hoferlin *et al.* 1998,Vegter *et al.* 1999, ... This proves the interest in FLD from the automotive or can deep drawing industries. Note that the model proposed by Cayssials 1998 and 1999 is very effective for classical steels. Coupling plastic instability theory with a damage approach, Cayssials's model accurately predicts FLD with data as simple as yield stress, hardening exponent, Lankford coefficient, and thickness of the metal sheet.

A complete review of approaches using MK model or analytical criteria to predict FLD is available in Esche *et al.* 1996. This represents a large amount of research as,

once the general computation principles are defined, they can be applied for numerous constitutive models: isotropic or not, with or without strain rate sensitivity, coupled to damage or not ... The following paragraph presents Marciniak & Kuczynski's approach. Then two examples of FEM models coupled with analytical stability criteria (Hora-Brunet and Boudeau-Gelin criteria) are summarized.

4.3.2. Marciniak & Kuczynski's approach.

Since localized necking under biaxial stretching of a uniform and homogeneous sheet is impossible when flow theories of plasticity with smooth yield loci are used, Stören & Rice 1975 pointed out that the development of a vertex on the yield locus is responsible for the onset of localized necking in thin sheets under biaxial tension. Marciniak & Kuczynski 1967 attempt to resolve this 'paradox' by another way. They assume pre-existing inhomogeneities in the sheet. Their method provides a well-known way to predict FLD by analytical developments (Barata da Rocha *et al.* 1984, Zhou & Neale 1995, Banabic 1996, Hoferlin *et al.* 1998, Vacher *et al.*1998, Vegter *et al.* 1999...) or even by FEM simulations (Narasimhan & Wagoner 1991, Qiu *et al.* 1995, Habraken *et al.* 1998, ...). The analytical way is summarized here. This approach postulates that an initial geometric imperfection exists in the form of a narrow band across the width of the sheet. As depicted in Figure 4-6, the initial thickness l_{30}^{b} of the band (zone b) is slightly less than the initial thickness l_{30}^{a} of the rest of the sheet (zone a).

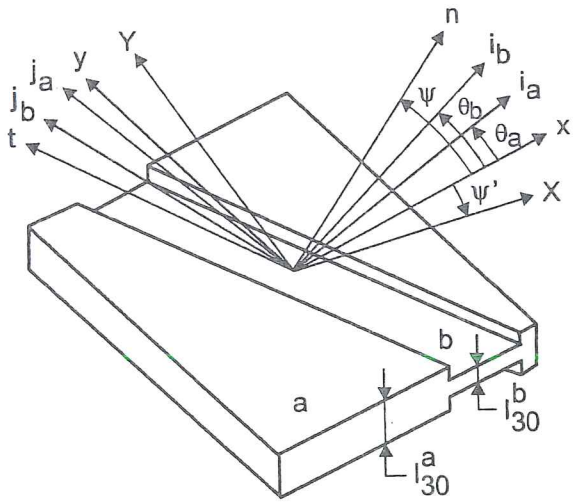

Figure 4-6 Marciniak and Kuczynski's model
X,Y principal stress directions; *x, y* principal strain directions; $i_a j_a$, $i_b j_b$ principal orthotropy axis in zone *a* and *b; n, t* initial orientation of the geometric defect (from Vacher *et al.* 1998).

The applications of MK method differ according to the orientation of the band, the imposition of principal stresses or strains at the edges of the sheet, the orientation of the material orthotropy axes. In their computation, Vacher *et al.* 1998 handle four

angles as defined in Figure 4-6. Generally, orthotropy axes and principal stresses or strains directions are set parallel and the orientation of the band is chosen. The simplest case (Zhou & Neale 1995, Banabic 1996) is to assume the band aligned with the minor-strain direction.

As studied by Barata da Rocha *et al.* 1984, for planar isotropic material and stretched zone of FLD, the critical neck orientation is effectively parallel to minor strain axis. Doghri & Billardon 1995 study the localization condition for homogeneous plane problems without shear. It depends on the material model and the stress-state but the orientation of the localization band only depends on the biaxiality ratio. Using a different approach, they recover the results of Hill 1950 for a tensile test. In this loading case, an angle of 54.7° separates the normal to the localization band from the normal to the tensile direction. This neck orientation is then assumed in the computation on FLD stretched zone by Vegter *et al.* 1999. The conservative approach used by Hoferlin *et al.* 1998 for predicting FLD is to compute the limit strains with various values of the initial band angle and to designate the minimum strain as the predicted forming limit. However Wu *et al.* 1998 have verified by simulations and experiments that FLD predictions are not very sensitive to the groove orientation.

Once these orientation choices are done, one must define the initial thickness ratio l^b_{30}/l^a_{30} . This ratio value (0.995, 0.986, ...) is often used as fitting parameter to get close to experimental results. Then, all authors apply the same procedure deduced from physical conditions:

- they impose principal stresses or strains in zone *a;*
- the yield locus and hardening law are respected in zones *a* and *b;*
- the normality rule is applied to derive strain from yield locus;
- the plastic incompressibility is used;
- the equilibrium across band boundary (1 or 2 equations according to its orientation) is respected;
- the equality of strain parallel to the band across its boundary is imposed;
- necking is assumed when the maximal principal strain rate in zone *b* is larger than the one in zone *a* by a factor of 10, 100, or even 1000 depending on the authors.

To be clear, the approach used by Hoferlin *et al.* 1998 is reproduced hereafter. The adopted choice of coordinates is presented on Figure 4-7. The stability analysis of plastic flow proceeds by an incremental loading of the homogeneous zone. During each increment, the strain rate tensor $\underline{\dot{\varepsilon}}^a$ is assumed to be constant and such that its principal directions are aligned with *X, Y, Z* axes. Furthermore, the major strain is assumed to occur along *X*-axis and the strain rate mode is characterized by the ratio β between $\dot{\varepsilon}^a_{xx}$ and $\dot{\varepsilon}^a_{yy}$. At each increment, the problem consists in determining the strain rate tensor $\underline{\dot{\varepsilon}}^b$ describing the plastic flow in the groove. For convenience, this latter is computed in the local reference frame *t, n*. In the following analysis, plastic

flow localization is supposed to occur when the maximal principal value of $\underline{\dot{\varepsilon}}^b$ is larger than $1000\,\dot{\varepsilon}^a_{xx}$. The corresponding strains $(\varepsilon^a_{xx}, \varepsilon^a_{yy})$ accumulated at that moment in the homogeneous zone are the limit strains. The analysis is actually repeated for different values of ψ ranging from 0 to 90° and the limit FLD point is obtained after minimization of ε^a_{xx} versus ψ.

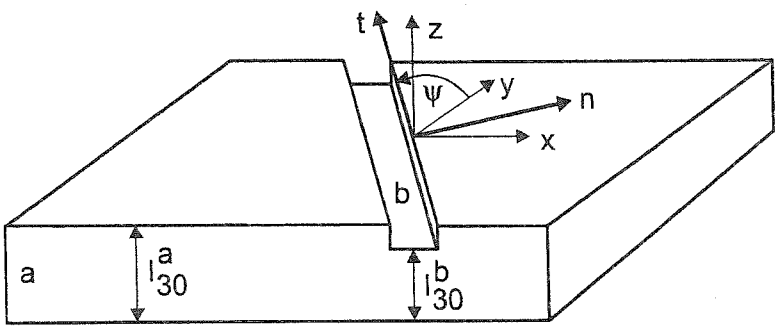

Figure 4-7 Marciniak and Kuczynski's model applied by Hoferlin *et al.* 1998. *xyz* principal strain directions, *x* is either the rolling direction or the transverse direction, *z* normal direction of the sheet; *n,t* initial orientation of the geometric defect (from Hoferlin *et al.* 1998).

The unknowns of the problem are the groove spin tensor $\underline{\Omega}$ and the groove strain rate tensor $\underline{\dot{\varepsilon}}^b$:

$$\underline{\dot{\varepsilon}}^b = \begin{bmatrix} \dot{\varepsilon}^b_{nn} & \dot{\varepsilon}^b_{nt} & 0 \\ \dot{\varepsilon}^b_{nt} & \dot{\varepsilon}^b_{tt} & 0 \\ 0 & 0 & \dot{\varepsilon}^b_{zz} \end{bmatrix} \quad \text{and} \quad \underline{\Omega} = \begin{bmatrix} 0 & \Omega^b_{nt} & 0 \\ -\Omega^b_{nt} & 0 & 0 \\ 0 & 0 & 0 \end{bmatrix} \tag{4-2}$$

The 5 unknowns of above equations are constrained by the following relations describing plastic incompressibility and geometrical compatibility:

$$\dot{\varepsilon}^b_{nn} + \dot{\varepsilon}^b_{tt} + \dot{\varepsilon}^b_{zz} = 0 \tag{4-3}$$

$$\dot{\varepsilon}^b_{tt} = \dot{\varepsilon}^a_{tt} \tag{4-4}$$

$$\Omega^b_{nt} = \dot{\varepsilon}^a_{nt} - \dot{\varepsilon}^b_{nt} \tag{4-5}$$

Finally, only 2 independent unknowns remain $(\dot{\varepsilon}^b_{nn}, \dot{\varepsilon}^b_{tt})$. They are solutions of the force equilibrium non linear equations (4-6) where stresses and strains are related by yield locus, normality rule and hardening law:

$$\sigma^b_{nn} l^b_3 = \sigma^a_{nn} l^a_3 \quad \text{and} \quad \sigma^b_{nt} l^b_3 = \sigma^a_{nt} l^a_3 \tag{4-6}$$

The updated thickness is computed by:

$$l_3^b = l_{30}^b \exp\left(-\int_0^t \dot{\varepsilon}_{xx}^b dt - \int_0^t \dot{\varepsilon}_{yy}^b dt \right) \quad (4\text{-}7)$$

The numerical necking prediction from the MK model depends on the value given to the initial geometrical defect. However it is often accepted to fit this parameter by one experiment and then to keep it constant for the other FLD points. As confirmed by numerous authors, Banabic 1996, Boudeau *et al.* 1998, Hoferlin *et al.* 1998, Narasimhan & Wagoner 1991, Vegter *et al* 1999, Zhou & Neale 1995, the initial yield shape and its evolution, the choice of a hardening law and the strain sensitivity formulation affect the FLD prediction produced by the MK method with fixed geometrical defect.
The use of MK method as a criterion to detect necking in general FEM deep drawing simulations is seldom considered because this method implies to solve a highly non linear problem at each incremental step and then leads to very long computation times (Boudeau *et al.* 1996a, Vacher *et al.* 1998). In conclusion, MK method is only dedicated to FLD prediction for direct or broken paths.

4.3.3. Hora & Brunet's criterion

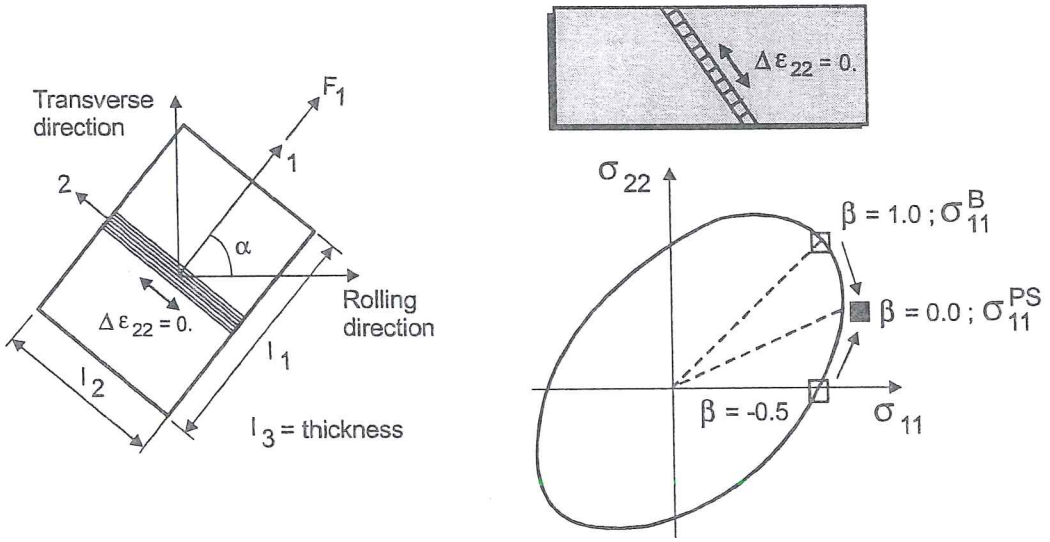

Figure 4-8 Model of sheet behavior when localized necking occurs (adapted from Hora *et al.* 1996).

The necking criterion proposed by Hora *et al.* 1996 has the great interest of not adding any parameter to the constitutive law to detect rupture. This criterion is based on physical considerations on the transition between a diffuse necking and a strain localization leading to necking and rupture. The strain ratio $\beta = \Delta\varepsilon_2 / \Delta\varepsilon_1$ (see Figure 4-8) has an evident influence on the internal damage of metal sheets. At the same level of deformation, it is generally noted that the damage increment is the largest in plane strain state. This indicates that plane strain is the most dangerous strain state for which strain localization is most likely to appear. Progressive development of

plane strain state after diffuse necking may be the common origin of strain localization appearance in tension-tension and tension-compression stress states. In both regions, the strains evolve towards the plane strain state such that $\Delta\varepsilon_2=0$, $\beta=0$ when localized necking occurs. The final criterion form is deduced from the following steps:

- assume plane stress state;
- Figure 4-8 defines the force F_1 and the directions 1 and 2. The sheet initial dimensions are l_{10}, l_{20}, l_{30} with l_1, l_2, l_3 being their updated value;
- the principal Cauchy stress σ_1, with $F_1 = \sigma_1 l_1 l_2$, and the natural strains are used:

$$\varepsilon_2 = ln\,(l_2/l_{20}) \qquad \varepsilon_3 = ln\,(l_3/l_{30}) \tag{4-8}$$

- so, the load instability ($dF_1<0$) gives:

$$\frac{d\sigma_1}{\sigma_1} + d\varepsilon_2 + d\varepsilon_3 \le 0 \tag{4-9}$$

- neglecting the elastic strain part, the plastic incompressibility leads to:

$$\frac{d\sigma_1}{d\varepsilon_1} \le \sigma_1 \tag{4-10}$$

- since the state of strain evolves towards plane strain due to the change of related stress state, there is an additional hardening effect such that :

$$d\sigma_1 = \frac{\partial\sigma_1}{\partial\varepsilon_1} d\varepsilon_1 + \frac{\partial\sigma_1}{\partial\beta} d\beta \tag{4-11}$$

- the final necking criterion takes the form:

$$\frac{\partial\sigma_1}{\partial\varepsilon_1} + \frac{\partial\sigma_1}{\partial\beta}\frac{d\beta}{d\varepsilon_1} \le \sigma_1 \tag{4-12}$$

Hora *et al.* 1996 apply this criterion on von Mises or general non-quadratic yield loci, while Brunet *et al.* 1997, 1998 compute it for anisotropic extensions of Gurson's model with Hill, Barlat or Lian's yield locus. The use of Gurson's type model requires some adaptation; for instance, relation (4-10) based on incompressibility is modified. Hora and Brunet's results demonstrate the efficiency of this criterion to determine strain Forming Limit Diagrams (Figure 4-9). This criterion is able to detect rupture for arbitrary paths by a direct implementation in FEM codes and does not require any arbitrary defect value as in MK approach. This model is unfortunately limited to 2D stress state.

Remark the similarity of this concept with the parameter P introduced by Sowerby & Duncan 1971 and telling that, for biaxial strain state, the higher is the P-ratio, the larger is the limiting strain. This P parameter is defined as the ratio between the

plane strain and the balanced biaxial flow stresses (see Figure 4-8, $P=\sigma_{11}^{PS}/\sigma_{11}^{B}$). Considering a MK model submitted to biaxial stretch ($\varepsilon_{11}=\varepsilon_{22}$) with a groove parallel to the "minor" strain axis and neglecting hardening, the stress states in the groove and in the homogeneous zone belong to the same yield locus. As deformation proceeds, the ratio between the thickness of the groove and the homogeneous zone decreases. Consequently, in order to fulfill the force equilibrium along the groove interface, the stress in the groove has to increase. Therefore it rotates towards the plane strain yield point ($\beta=0$) where the normal to the yield locus is "horizontal" (parallel to σ_{11}). Since the strain rate in the vertical direction (parallel to σ_{22}) remains constant (MK hypothesis), it implies an infinite horizontal strain rate in the groove, *i.e.* plastic flow localization or necking. So, the additional shape hardening of the yield surface, indicated by the β parameter in Hora and Brunet's approach, was already present in the P–ratio approach. Note that, when isotropic hardening occurs, the rotation of the stress point toward plane strain-state is slowed down. Finally, if kinematic hardening is introduced, it reduces the effect of the shape hardening (Hiwatashi *et al.* 1998).

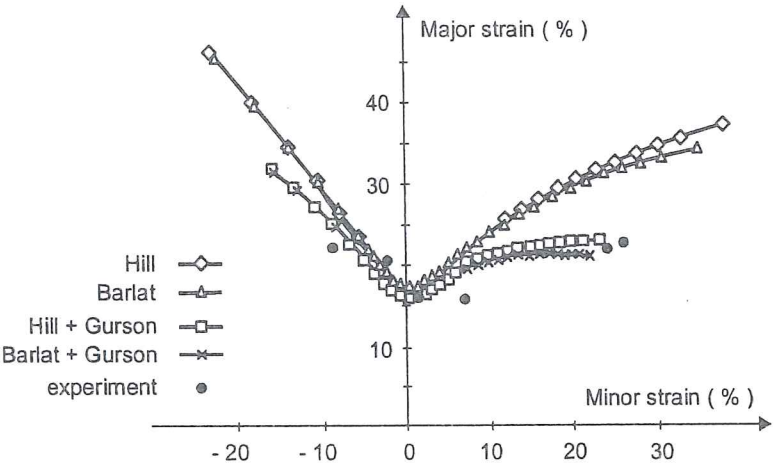

Figure 4-9 Experimental and theoretical FLD predicted by Hora-Brunet's criterion applied to Hill's or Barlat's models coupled or not with damage, Al5182 (from Brunet *et al.* 1998).

4.3.4. Boudeau-Gelin's criterion.

Since 1992, Boudeau and Gelin have presented a criterion, which considers the necking phenomenon as an instability phenomenon. The proposed method is the linear perturbation technique largely employed in physics and engineering sciences. It consists in perturbing the equilibrium and examining if the perturbed solution remains close to the initial one or, on the contrary, increases indefinitely when time goes on. The particularities of this approach are that it does not require to study the evolution of an assumed defect and that the analysis can be done at any instant regardless of the previous one. Initially, developed in plane stress state, this approach

has been extended to 3D stress state (Boudeau *et al.* 2001). For 2D stress state, Boudeau & Gelin 1994 can be summarized by the following steps:

- The equilibrium of a material point is locally governed by nine equations defining nine variables represented by the vector $\underline{u}$:

$$\underline{u} = \{ \sigma_{11}, \sigma_{22}, \sigma_{12}, \sigma_{eq}, \dot{\varepsilon}_{11}, \dot{\varepsilon}_{22}, \dot{\varepsilon}_{12}, \dot{\varepsilon}_{33}, \dot{\varepsilon}_{eq} \}$$

  Note that σ_{eq} and $\dot{\varepsilon}_{eq}$ are not the equivalent von Mises' expressions but are related to the anisotropic yield locus formulation (see respectively sections 3.5.5 and 2.2 of part B). The nine relations to fulfill are the following ones:

  - The hardening law defining the plastic reference yield curve σ_F, for instance:

$$\sigma_F = K(\varepsilon_o + \varepsilon_{eq}^p)^n (\dot{\varepsilon}_{eq}^p)^m \qquad (4\text{-}13)$$

  - The yield surface: $F_p(\underline{\sigma}, \sigma_F) = 0$ (4-14)

  - The plastic flow law (3 equations): $\underline{\dot{\varepsilon}}_p = \dot{\lambda}_p \dfrac{\partial F_p}{\partial \underline{\sigma}}$ (4-15)

  - The equilibrium:

$$(l_3\ \sigma_{11})_{,1} + (l_3\ \sigma_{21})_{,2} = 0 \qquad (4\text{-}16a)$$

$$(l_3\ \sigma_{12})_{,1} + (l_3\ \sigma_{22})_{,2} = 0 \qquad (4\text{-}16b)$$

  - The plastic incompressibility assumption: (4-17)

$$\dot{\varepsilon}_{33} = -\dot{\varepsilon}_{11} - \dot{\varepsilon}_{22}$$

  - The compatibility of the strain rate: (4-18)

$$\dot{\varepsilon}_{11,22} + \dot{\varepsilon}_{22,11} = 2\dot{\varepsilon}_{12,22}$$

- The elastic strain is neglected.
- The above set of equations defines a non linear system: $A(\underline{u})=0$.
- If $\underline{u}^0$ is a solution of $A(\underline{u})=0$, its stability, in the sense of linear perturbation technique, is verified using the perturbed solution $\underline{u}$:

$$\underline{u} = \underline{u}^0 + \delta\underline{u} \qquad (4\text{-}19)$$

  with $\delta\underline{u} = \delta\underline{u}^0 \exp(\eta t) \exp(\xi\, o\underline{M} \,.\, \underline{n})$

  where $\delta\underline{u}^0$ is the amplitude of the perturbation;
  η is the temporal part of the instability;

ξ is the spatial part of the instability;
M is the point where instability could occur;
o is the center of the global frame (o,x,y);
$\underline{n}$ is the normal to the direction $\underline{t}$ along which necking could occur.

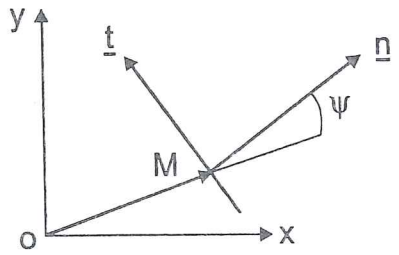

Figure 4-10 Representation of $\underline{oM}$, $\underline{n}$, $\underline{t}$ vectors in global frame x,y, (from Boudeau & Gelin 1996a).

- The above system is linearized, and the perturbed solution must satisfy:

$$A(\underline{u}^0, \eta, \xi).\ \delta\underline{u}^0 = \underline{0} \tag{4-20}$$

A non trivial solution only exists if:

$$det\ A(\underline{u}^0, \eta, \xi) = 0 \tag{4-21}$$

Knowing $\underline{u}^0$ and fixing ξ, this equation allows computing η. If the real part of η becomes positive, instability occurs.

The numerical implementation has been carried out in the FE code developed by Gelin's laboratory (Boudeau & Gelin, 1994). It has been extended to 3D stress state in Boudeau *et al.* 2001. The code does not consider strain rate sensitivity in the hardening law. However, this parameter is required for the establishment of the necking criterion. At last, the strain rate sensitivity parameter will be imposed to be equal to 0. Above equations are transformed into an incremental form and a loop on various orientations of the necking zone ψ is necessary to find the lowest root η with positive real part. Numerous numerical results, compared to experimental ones, show the validity of such an approach (Boudeau *et al.* 1992, 1994, 1996, 2001). The necking phenomenon is detected even when no critical thinning is observed. The investigations also prove the ability of this criterion to detect the formation of wrinkles too. The two kinds of instability can be distinguished by the sign of the two principal stresses in the sheet plane, but also by the range of the instability parameter η. For necking, this parameter is in the range 0.01 to 0.1, while it reaches unit value in case of wrinkling. This criterion has been applied with the classical Hill's yield locus but also with a polycrystalline model taking into account crystallographic slips, work hardening at microstructural level and lattice rotations, which induce texture evolution (Boudeau *et al.* 1996b, 1998, 2001). Note that Cayssials' 1998 "new" criterion is very similar to Boudeau-Gelin's approach.

4.3.5. Conclusion

To detect necking in sheet FEM simulations, the use of criteria such as Brunet-Hora's or Boudeau's ones seems promising. Such approaches require no additional assumption and are closely connected to stress and strain fields, which should be more sensitive in any finite element code than the global thickness reduction. Moreover, these approaches are adapted to complex strain paths as demonstrated by their authors. Interesting applications can be found in Knockaert 2001.

4.4. Criteria based on microscopic phenomena analysis

The study of the coalescence of cavities in porous plastic solids is important for the definition of macroscopic models describing the mechanical behavior of ductile metals. Unfortunately, a number of factors contribute to make it a difficult problem, notably the fact that coalescence is sensitive to many parameters such as void shape, spacing and distribution, nucleation of cavities, presence of smaller, secondary voids, etc... The hereafter collected criteria result from the application of a mechanical theory, like the upper-bound theorem, localization condition or just geometric conditions, applied on representative cell models (matrix + voids or matrix + inclusions).

The work of Rice & Tracey 1969 based on the study of a cell model with initial spherical void yields an approximate relation, where void growth rate is linked to triaxiality ratio. First, a variational principle was established by Rice and Tracey to characterize the flow field in a plastic rigid incompressible material containing internal voids and subjected to a remote uniform stress-strain field. Then, an approximate Rayleigh-Ritz procedure is applied to the enlargement of an isolated spherical void in a non-hardening material and approximate relations are deduced for linear hardening material. This work establishes that, for any remote strain field, the ratio of the void enlargement rate over the remote strain rate is amplified by a factor rising exponentially with triaxiality ($T = \sigma_m/\sigma_{eq}$). Recalling relation (2.11), already presented in section 2.1, it covers the simple case of a tension remote field and gives the average spherical growth rate:

$$\frac{dR}{R} = A\, exp\left(\frac{3\sigma_m}{2\sigma_{eq}}\right) d\varepsilon_{eq} \qquad (4\text{-}22)$$

The first work of Rice & Tracey set A to 0.283; however further research shows that this factor should be increased (Marini 1985). In practice the factor A is adjusted to fit the experimental data obtained with different triaxialities.

The ellipsoidal shape can be estimated by the general relation (2.12) using a void shape parameter E or, in the case of linear isotropic hardening materials, is directly given by:

$$\dot{R}_k = \left(\frac{5}{3} \dot{\varepsilon}_k^p + \frac{3}{4} \frac{\sigma_m}{\sigma_{eq}} \dot{\varepsilon}_{eq}^p \right) R \qquad (4\text{-}23)$$

where $\dot{R}_k$ denotes radial velocities of the void boundary at points aligned with the remote principal directions, $\dot{\varepsilon}_k^p$ are the principal plastic strains. As reported by Boyer & Staub 1997, relation (4-23) gives useful estimates of the change in shape and volume of an initial spherical void. Some extensions have already been proposed by Thomason 1990. However, this type of approach does not handle pure shear stress states.

The critical ratio $(R/R_0)_c$ can be used as rupture criterion. The determination of this value links numerical FEM simulation and fracture mechanics experiments. A large literature review of $(R/R_0)_c$ is proposed by Wilsius 1999.

It is worth to mention Rice & Tracey's relation since principal radii of ellipsoidal voids are necessary to use coalescence criteria of Brown & Embury or Thomason for instance.

Based on a number of experimental studies, Brown & Embury 1973 found that after nucleation, cavities elongate along the major tensile axis and that two neighboring cavities coalesce when their length has grown to the order of magnitude of their spacing. This local failure occurs by the development of slip planes between the cavities or simply by necking of the ligament. As presented by Pardoen 1998, Brown & Embury's criterion can be of practical application in numerical macroscopic computations :

- the porosity f is computed by a Gurson's type model, relation (2-10) allows to estimate the updated void radius; relations (2-11) and (2-12) assume an ellipsoidal void growth and help to compute characteristic sizes of the ellipse (R_1, R_3) (see Figure 1-1 for axes definition).
- the updated distance l_c between the centers of neighboring voids is deduced from the local strain ε_1 and the initial intervoid length l_{c0}:

$$l_c = l_{c0} \ exp(\varepsilon_1) \qquad (4\text{-}24)$$

- Brown & Embury's criterion is fulfilled if: $l_c = 2\sqrt{R_1^2 + R_3^2}$ (4-25)

Koplik & Needleman's 1988 work, already described at section 4.1, verifies that this criterion provides a good approximation in case of a triaxiality ratio $(T = \sigma_m / \sigma_{eq})$ close to 1 and of predominant axial stress loading. However, they show that it detects coalescence too late at a higher triaxiality value ($T = 2$). The experimental and numerical work of Pardoen 1998 confirms this conclusion. The cell model easily explains this observation: the void initially grows into a prolate ellipsoid as expected from predominant axial stress, then suddenly turns back to more oblate shapes as coalescence results in a strong straining and necking of the horizontal ligament

separating nearby cavities. Of course, the intensity of the lateral stresses and hence the triaxiality value modify this event appearance.

As verified by Brocks *et al.* 1995, the critical void volume fraction f_{cr} decreases with increasing triaxiality. Gologanu *et al.* 1994 also use a cell model to study lower triaxiality cases (T = *1/3; 2/3; 1*) and different loading characteristics such as predominant lateral axisymmetric stress or axial stress. In the case of predominant axial stress and high value of triaxiality (T = *2/3 and 1*), their conclusions recover those of Koplik & Needleman's work. However in the case of no lateral stress and T=*1/3*, which corresponds to uniaxial tension, the shape parameter (equal to $ln(R_3/R_1)$, where R_3 and R_1 respectively denote the semi-axes of the void along the vertical-axial and horizontal-transversal direction) can be observed to increase without any apparent bound. This means that the cavity grows into cylindrical hole, the porosity tends towards some asymptotic value and no coalescence occurs in pure tensile state. Note that tensile bars (for which T=*1/3*) usually fail after necking, which locally increases the stress triaxiality. In the case of predominant lateral stresses, intervoid straining and coalescence were observed to occur along vertical columns (see Figure 4-11b) instead of horizontal layers (see Figure 4-11a). Since the overall weakening effect resulting from the formation of a damaged zone is considerably less dramatic in the case of a column than in that of a layer, the macroscopic equivalent stress at fracture decreases in a much more gradual way than in the case studied by Koplik & Needleman (see Figure 4-3). In conclusion, the cell model helps to understand the limits of Brown & Embury's criterion.

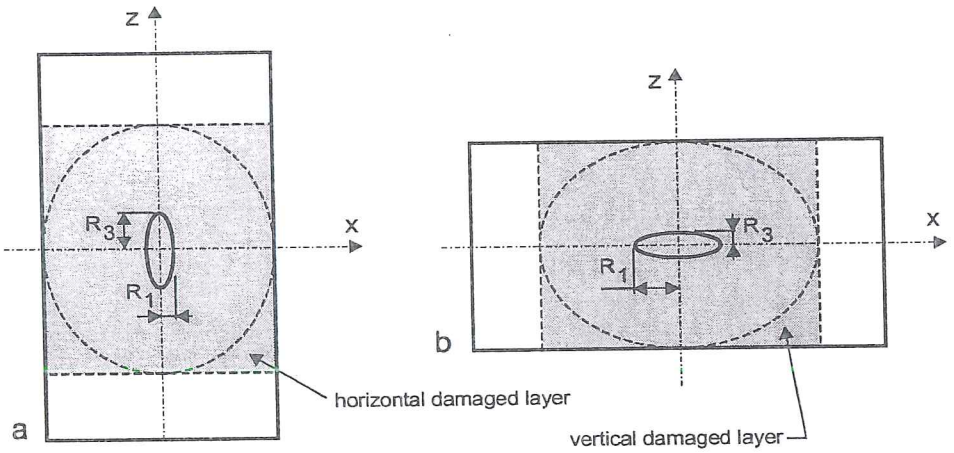

(a) predominant axial stress (b) predominant transversal stress

Figure 4-11 Composite cell models to simulate the coalescence event with sound material (not shaded) described by von Mises criterion and highly porous material (shaded) represented by Gurson-Gologanu's model accounting for void shape effects (from Gologanu *et al.* 1994).

Thomason's criterion (Thomason 1985a, 1985b, 1993) is issued from a sophisticated micromechanical model of void coalescence. For a non-hardening rigid plastic solid,

which contains a regular three-dimensional distribution of spherical microvoids in the initial state, this model considers that the necking of ligaments separating the cavities results from the attainment of a maximal load withstood by these ligaments. Recall that Koplik & Needleman 1988 cell computations give further support to Thomason's idea about this fracture mechanism. The updated size and shape of microvoids are computed by Rice-Tracey's equations. The limit load depends on the current yield stress of the matrix, the updated shape of the voids, their size and spacing, which are related to the strain state. This load, estimated by means of the upper-bound theorem[1], is then compared to the maximal principal stress effectively applied (Figure 4-12). When both terms are equal, failure is predicted. In three dimensions, assuming axisymmetry and ellipsoidal void growth and collecting various results from Thomason, Pardoen 1998 expresses this criterion by the following equation:

$$\left(\frac{0.1}{\left(\frac{R_3}{\frac{l_c}{2} - R_1} \right)^2} + \frac{1.2}{\sqrt{\frac{R_1}{\frac{l_c}{2}}}} \right) (1 - f_0)^{-1} \left(1 - \left(\frac{3\sqrt{\pi}}{4} f_0 \right)^{2/3} \left(\frac{R_1}{R_{10}} \right)^2 \exp \varepsilon_3 \right) = \frac{\sigma_{max\ princ}}{\overline{\sigma}_{eq}} \qquad (4\text{-}26)$$

where l_c is the current transversal distance (see Figure 1-1) between the centers of two cavities, ε_3 is the longitudinal strain, $\sigma_{max\ princ}$ is the value of maximal principal stress and $\overline{\sigma}_{eq}$ is the current yield stress of the matrix.

Figure 4-12 from Pardoen 1998 illustrates how the two sides of equation (4-26) behave in the case of the finite element simulation of a notch test. He uses the improved version of Gurson's model proposed by Leblond *et al.* 1995 to compute the macroscopic stress-strain state. The updated radii of cavities are computed as explained above for Brown & Embury's criterion. As shown by Figure 4-12, at the beginning of void growth, the applied stress state is much lower than the stress state required to cause plastic failure of the ligament (left-hand side of equation (4-26)). As void size increases, the stress state required to induce ligament failure decreases to a point where it becomes equal to the applied stress and the fracture strain is predicted.

[1] From the upper-bound theorem for rigid-plastic non-hardening solids, an overestimated plastic load for incipient internal necking of the intervoid matrix is obtained by equating the rate of internal energy dissipation, for a kinematically admissible velocity field, to the rate of work of the external loads.

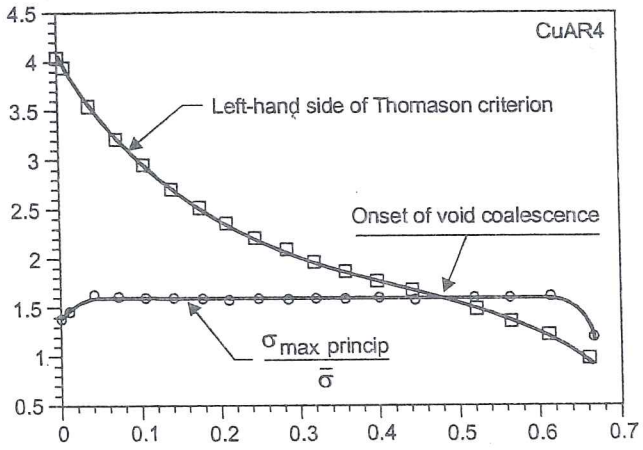

Figure 4-12 Example of Thomason's criterion application; variations of both sides of equation (4-26) are locally computed thanks to FEM simulation of a notch test (from Pardoen 1998).

To be clear, Thomason's criterion for coalescence is purely based on geometrical consideration and upper-bound theorem. To be used, it requires other models that provide the evolution of the porosity, the void shape and the stress and strain fields.

Pardoen's 1998 work dedicated to experimental and numerical study of copper bars concludes that, among the four void growth models studied (Rice & Tracey's approach coupled with von Mises' law, Gurson-Tvergaard's model, Gurson-Leblond-Perrin's model, Lemaître's model) and the four void coalescence criteria (threshold value of damage parameter, Brown & Embury's criterion, Thomason's criterion and a criterion based on the decrease of macroscopic stress), *the Gurson-Leblond's void growth model coupled with the Thomason's void coalescence criterion was found the most pertinent for modeling the porosity variation and cracking initiation in copper bars.*

Another aspect of Thomason's work concerns his study on ductile fracture by the growth and coalescence of microvoids of non-uniform size and spacing (Thomason 1993). The theoretical void-growth strains at ductile fracture for a wide variation in void diameters and spacing show that, for a given volume fraction of voids, the minimum ductile-fracture strain occurs when the voids are of uniform size and spacing. Such a result is quite interesting as most of the models are developed on the assumption of uniform void size and spacing and should accordingly give safe predictions. However, this conclusion is opposite to common physical sense and to the work of Benzerga *et al.* 1999 or Koplik & Needleman 1988 commented in this thesis. Thus Thomason's results are probably of limited generality since they were reached by means of a two-dimensional plane strain model of void growth and coalescence in a rigid/plastic solid.

Another coalescence model considers the coalescence as a bifurcation behavior in a pressure-sensitive material. As summarized by Benzerga *et al.* 1999, various scientists have followed such approach. The first trials to apply strain-localization

analyses on simulations performed with Gurson's models lead to excessive ductility predictions. To find results in correlation with experiments for axisymmetric loading with predominant axial stress, Leblond & Perrin 1991 use a doubly periodic array of voids (Figure 4-13). Let us remark that such an assumption is connected to the one chosen by Gologanu and represented on Figure 4-11. The non-homogeneity of the void distribution during deformation has been confirmed by experimental observations (Pineau 1981).

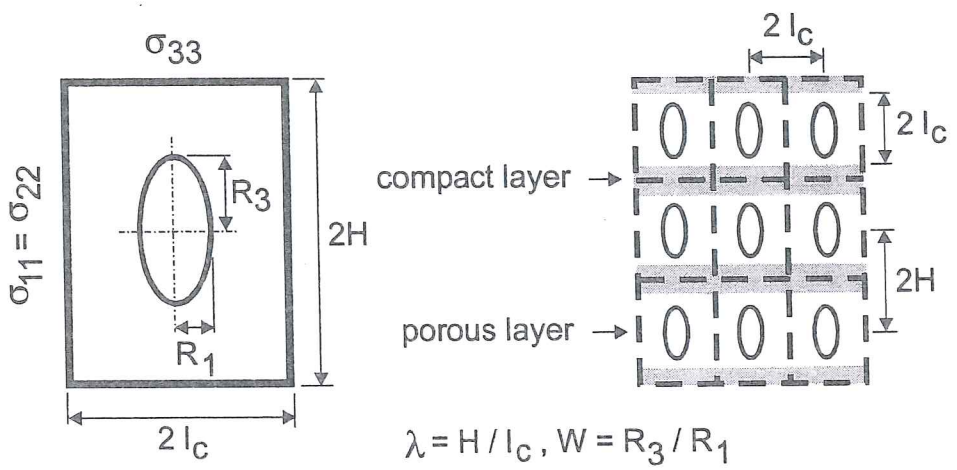

Figure 4-13 Axisymmetric unit cell submitted to macroscopic stress (σ_{11} σ_{22} σ_{33}), definition of compact and porous layers and geometric parameters (from Benzerga *et al.* 1999).

According to Leblond & Perrin 1991, the overall behavior of the material is supposed to obey a Gurson like criterion. Coalescence arises from the progressive concentration of voids in some highly porous layers separated by compact regions (Figure 4-13). Coalescence is detected by the localization condition of Rudnicki & Rice 1975 applied on a mesoscopic stress state present in this porous layer. This mesoscopic stress state must be compatible with the macroscopic one and is computed according a Gurson's criterion written with a local porosity. Such final coalescence condition is of course not straightforward.

Benzerga *et al.* 1999 compares the hereabove described Leblond-Perrin model coupled with a localization criterion and three models coupled with Thomason's criterion. The first one is a simple law with fixed porosity and perfect plasticity which uses Rice and Tracey's assumptions to model void shape modifications. The second one is the classical Gurson's model with spherical voids and the third one, proposed by Gologanu *et al.* 1994, takes void shape into account. Some conclusions from Benzerga *et al.* 1999 are now summarized.

For highly clean materials ($f_0 < 0.01\%$), the onset of coalescence (f_{cr}) is almost independent of the stress state for mean to high triaxiality ($T>1.5$); however for higher initial porosity, the dependence is not negligible (Figure 4-14). This figure

helps to understand why, depending on the studied cases, authors like Koplik & Needleman 1988, Brocks *et al.* 1995, Brethenoux, *et al.* 1997 ... have concluded to different influence of triaxiality on the critical porosity.

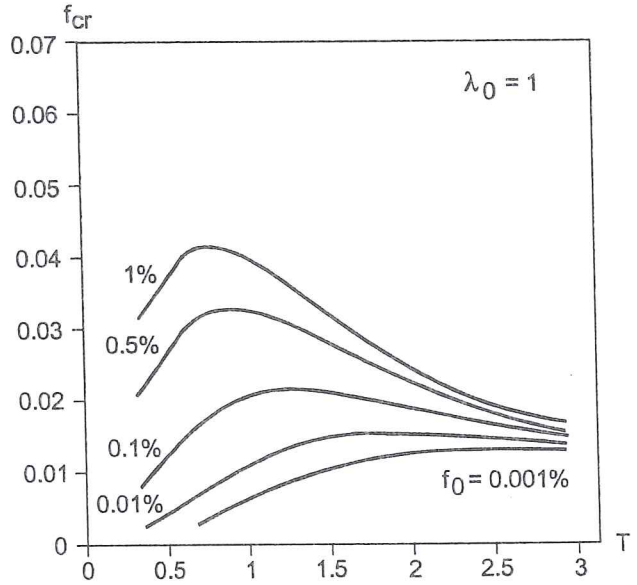

Figure 4-14 Critical porosity-triaxiality curve according to Thomason's criterion and Gurson's model (from Benzerga *et al.* 1999).

The coalescence models predict a drastic effect of void distribution (λ_0) on the critical porosity (Figure 4-15), as already checked on Figure 4-2 from Koplik & Needleman 1988. High λ_0 means that porous layers are separated by large sound layers.

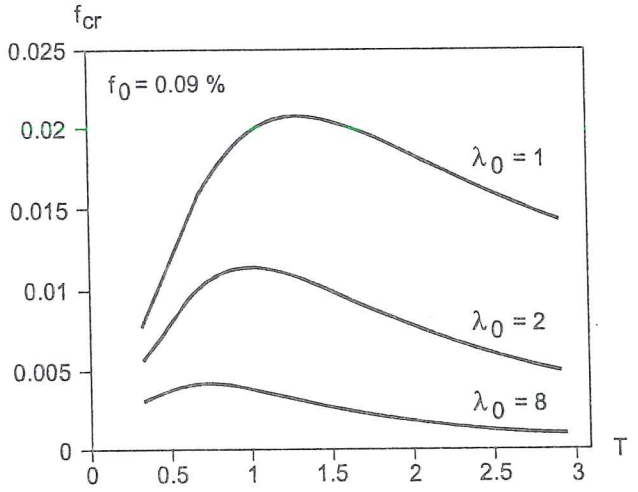

Figure 4-15 Critical porosity-triaxiality curve according to Thomason's criterion and Gurson's model for various initial void distributions (from Benzerga *et al.* 1999).

For initial spherical voids, the assumption of spherical void growth leads to underestimate both critical porosity f_{cr} and strain at coalescence. However, for high triaxiality ($T=3$), frequently encountered at a blunted crack tip in plane strain conditions, the void shape evolution has little effect. The effect of inclusion morphology appears to be negligible at high triaxiality ($T=10/3$) but crucial for low triaxiality.

To complete this section about microscopic phenomena analysis, one cannot forget the work at the atomic level. Using massive parallel computers, scientists like Abraham 1996 use *molecular dynamics simulation technique* to learn about fracture process in ductile or brittle materials. This technique is based on the motion of a given number of atoms governed by their mutual interatomic interactions described by continuous interatomic potentials. It requires the numerical integration of Hamilton's equation of motion. For instance, Abraham models the fracture of two-dimensional notched solids under tension using a million of atoms. Even if his results such as the order of magnitude of the fracture strain or the crack tip speed do not agree with experimental values, ductile or brittle fractures are effectively reproduced. Such approaches are still far from producing macroscopic fracture criteria, but help to understand fracture events more deeply. As developed by Ceder 1999, the gap between time scale and length scale of atomistic level (10^{-13} sec, 10^{-10} m) to macroscopic properties (10^{4} sec, 1 m) can only be overcome with knowledge of the relevant phenomena at each scale. According to Ceder's point of view, even if practical results of atomistic computations can already be presented in the designing of rechargeable Lithium batteries, the field of mechanical properties seems to need further investigation.

4.5. Criteria issued from fracture mechanics

Presenting the links between continuum damage mechanics and fracture mechanics was one aim of the Symposium on "Continuous Damage and Fracture" (Benallal, 2001) held in Cachan on October 2000 to celebrate Professor Jean Lemaître's 66th birthday. Such a symposium underlines the connections between these two fields that are now of common use not only in the academic world but also in the industry. For instance, Mudry 2000 has given practical examples in his presentation.

Chaouadi 1996 from Katholieke Universiteit Leuven, Marchal 1997, Pardoen 1998 from Université Catholique de Louvain, and Wilsius 1999 from Université des Sciences et Technologie de Lille are Ph.D. theses that cover fracture mechanics, continuum damage ductile fracture models and important experimental work. Their state-of-the-art summaries of fracture mechanics are used here to present its general concepts, then to underscore the interest of its coupling with continuum damage mechanics.

4.5.1. Fracture Mechanics

Materials possess a fracture resistance, which is an intrinsic property. Fracture propagation occurs when the loading imposed to the crack exceeds the material fracture resistance. As presented on Figure 4.16, a crack can experience three loading modes or a combination of these modes.

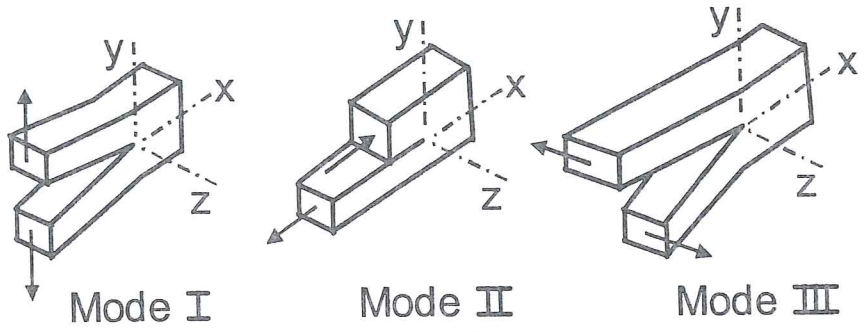

Figure 4-16 Fracture modes; mode I: opening mode, mode II: sliding mode, mode III: tearing mode (from Chaouadi 1996).

In practice, mode I is the most severe. Typical stress-strain zones appear at the crack tip in a finite cracked specimen; they are represented on Figure 4-17.

Linear elastic fracture mechanics is shown on Figure 4-17a. For mode *I*, the stress and strain fields near the crack tip are defined by:

$$\underline{\sigma} = \frac{K_I}{\sqrt{2\pi r}} \underline{\tilde{\sigma}}(\theta) \qquad \underline{\varepsilon} = \frac{K_I}{\sqrt{2\pi r}} \underline{\tilde{\varepsilon}}(\theta) \tag{4-27}$$

where r and θ are the polar coordinates, with r the distance from the crack tip and θ the angle relative to the crack plane, $\underline{\tilde{\sigma}}(\theta)$ and $\underline{\tilde{\varepsilon}}(\theta)$ are functions, dependent on the angle θ. Similarly, the same expressions can be obtained for mode *II* and *III*. That means that one parameter, the stress intensity factor *K*, is sufficient to determine the material stress or strain field near the crack tip. The critical condition for fracture corresponds to a critical value of stress intensity factor, K_{IC} for mode *I*. This parameter is related to *G*, the energy released per unit extension of crack front per unit thickness of the body, also called crack extension force:

$$G = \frac{K_I^2}{E} \text{ (plane stress)} \qquad G = \frac{K_I^2}{E(1-\nu^2)} \text{ (plane strain)} \tag{4-28}$$

The stress and strain distributions ahead of a crack are similar for any geometry and loading provided similar *K* are reached. This is true when small scale yielding prevails: the plastic zone is very small compared to the geometrical dimensions. Such situations are found in brittle materials or for very low load levels.

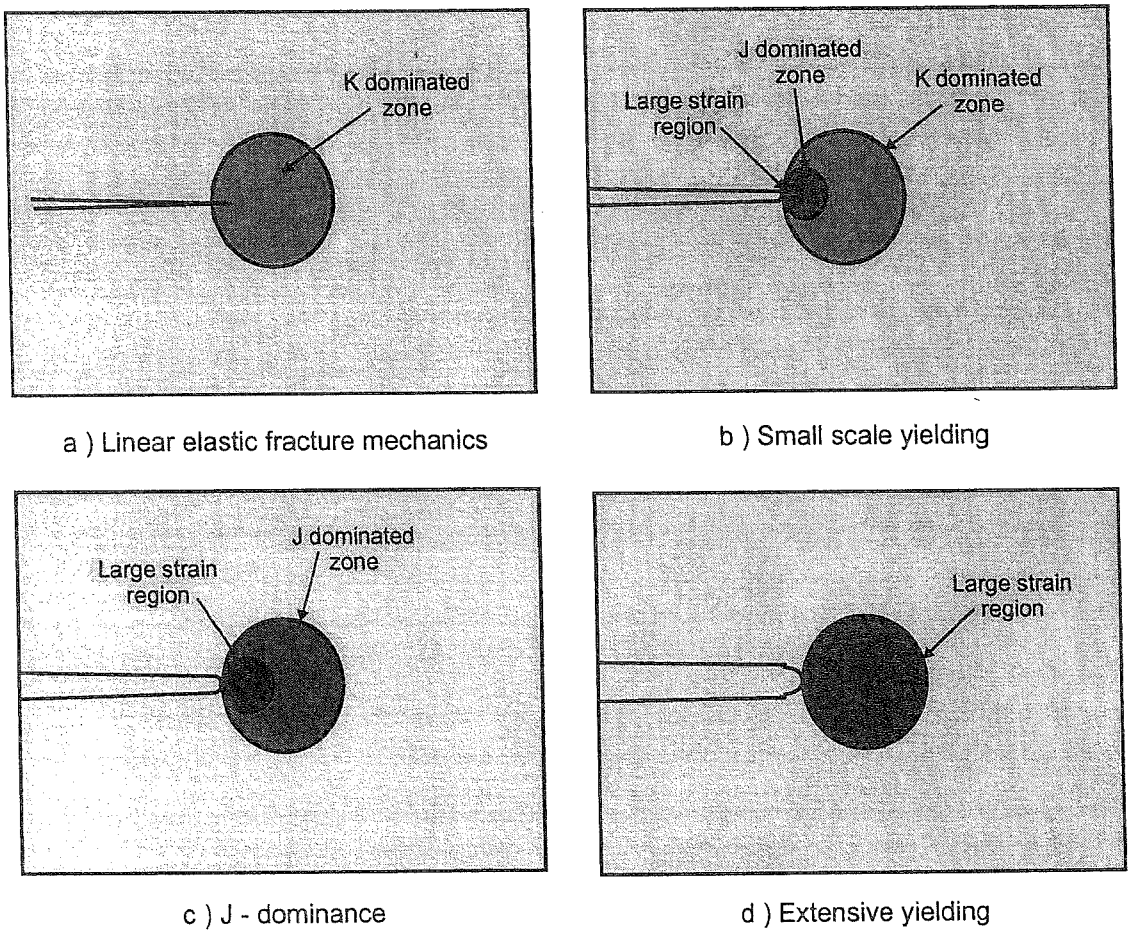

Figure 4-17 Typical stress-strain zones at the crack tips for different types of material (from Anderson 1995).

When working with *elastic plastic fracture mechanics*, the *J*-integral parameter appears. Rice 1968 defines the *J*-integral for non-linear elastic material by:

$$J = \int_{\Gamma} \left(W dy - T_i \frac{\partial u_i}{\partial x} \right) ds \qquad (4\text{-}29)$$

where $W = \int_0^{\varepsilon_{ij}} \sigma_{ij}\, d\varepsilon_{ij}$ is the strain energy density, u_i are the components of the displacement vector, n_j is the component j of a unit vector perpendicular to the contour line, Γ is the path followed in anti-clockwise direction, $T_i = \sigma_{ij} n_j$ are the components of the normal stresses acting at the boundaries, x, y and s coordinates are defined on Figure 4.18. Rice derived this parameter from a non-linear elastic material, so its application to elastic-plastic material assumes radial loading without unloading.

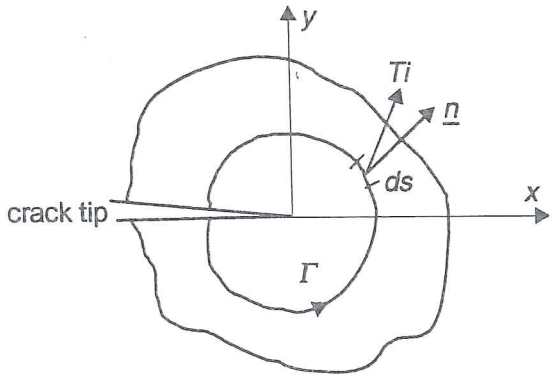

Figure 4-18 *J*-integral evaluation along an arbitrary contour (from Chaouadi 1996).

The interesting properties of *J*-integral are:

- *J*-integral is path independent except very near the crack tip.
- *J* can be interpreted as a pseudo energy release rate. *J* should be considered as the difference of the energies absorbed by 2 specimens with crack sizes a and $a+\Delta a$ loaded up to a given displacement u rather than as the variation of the potential energy of the sample for an increment of crack advance (see Figure 4-19).

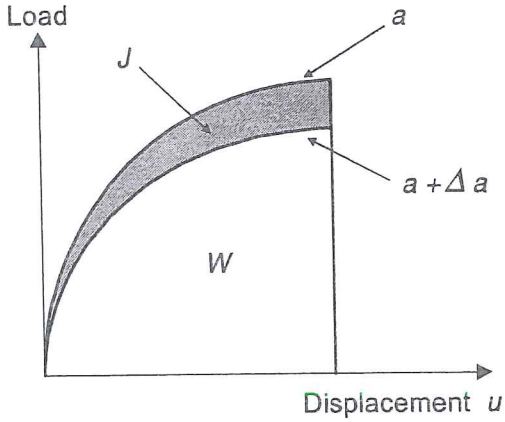

Figure 4.19 Energy release rate interpretation of *J* (from Pardoen 1998).

- The stress and strain fields ahead of a crack tip can be represented by functions known as the HRR fields. These relations due to Hutchinson 1968 and Rice & Rosengren 1968 use material constants such as the yield stress and strains, *J*-integral and dimensionless functions tabulated by Shi 1983. The HRR (Hutchinson-Rice-Rosengren) singularity fields define the stress and the strain fields ahead of a crack tip for loading levels such that the plastic zone size is small in comparison to the specimen dimension (see Figure 4-17b). HRR fields are accurate in the *J* dominated zone except very near the crack tip (large strain zone). This means that the fields in crack tip region are independent on specimen geometry and loading type.

Since World War II, testing standards to measure fracture toughness have been established (see ASTM, American Society for Testing and Materials, and ESIS, European Structural Integrity Society). Wilsius 1999 summarizes the methods generally applied to measure J and Figure 4-20 presents sample geometries commonly used. In small scale yielding situations, where the plastic zone does not influence the elastic stress field, J-integral is equal to G and relation (4-28) directly gives the link between J-integral and K stress intensity factor.

The case shown on Figure 4-17c presents a large plastic zone with respect to specimen dimension. In such a case, the geometry can induce a highly constrained crack, corresponding to high stress triaxiality near the crack tip. In this condition, the HRR fields still apply. So J-integral alone still suffices to characterize the stress and strain fields in the zone called "J-dominance".

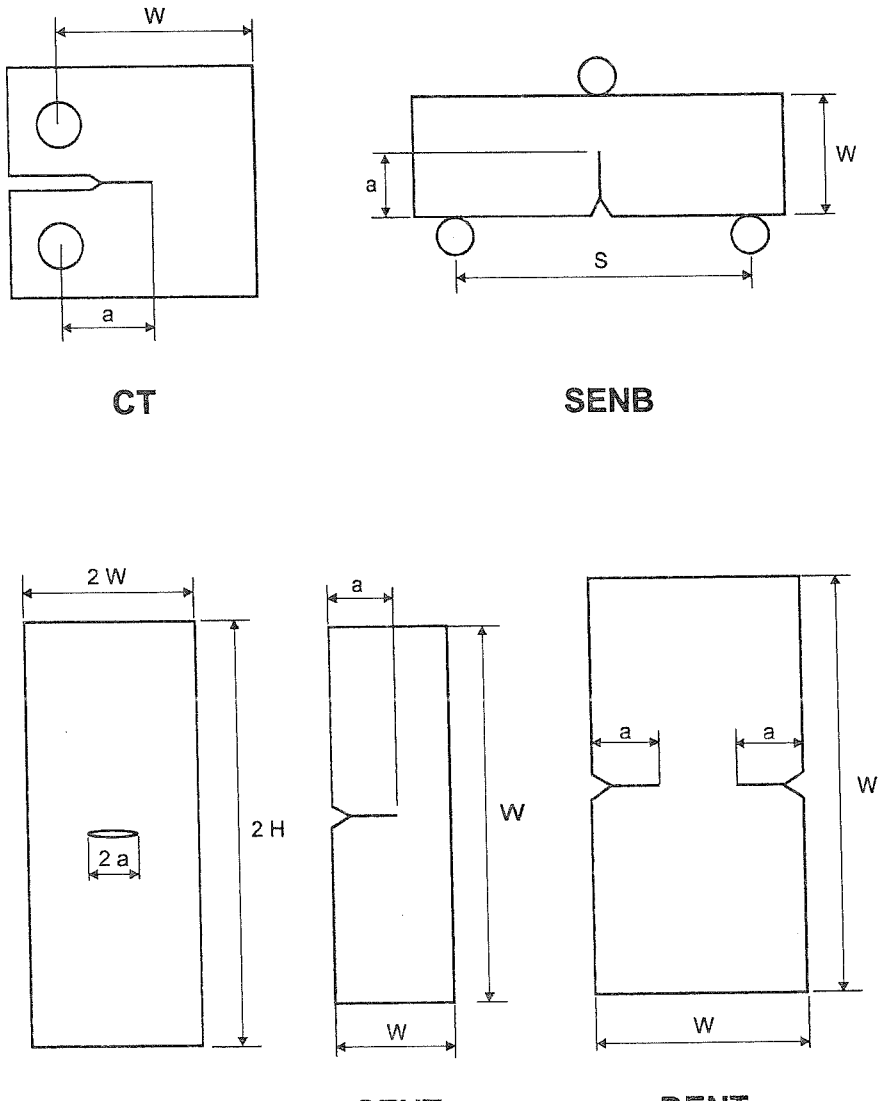

Figure 4.20 Fracture samples used to characterize fracture toughness estimated by J-integral (from Wilsius 1999).

For less constrained crack, Figure 4-17d shows an extensive finite strain region at the crack tip. In this case, *J*-integral alone cannot characterize univocally the stress and strain fields anymore because they exhibit size and geometry dependence.

Brocks *et al.* 1995 underlines the geometry dependence of the toughness results:

$$J_{CCP} \geq J_{DENT} \geq J_{SENT} \geq J_{SENB} \geq J_{CT} \tag{4-30}$$

where the geometries CCP, DENT, SENT, SENB and CT are defined of Figure 4-20. So additional parameters are required to characterize the fracture; common choices are either Q parameter or T parameter. Q is the difference field between a FEM solution and a reference field (HRR field for instance). T characterizes the stress conditions, including specimen geometry effect, on stress triaxiality under well contained yielding. Wilsius 1999 reviews the determination methods of T and Q.

The thickness of engineering structures is usually larger than the size of the laboratory samples with which the fracture toughness is determined. When J uniquely characterizes the crack tip field in specimen and structure, the onset of crack initiation can be identified, when one reaches a same critical value J_{IC}. However, in other cases, different fracture toughness values appear between specimen and real piece, so additional parameters are required. This leaves a field where fracture mechanics and continuum mechanics can cooperate.

4.5.2. Continuum damage mechanics criteria imbued from fracture mechanics

Considering fracture mechanics where critical values of *J*-integral or K stress intensity factor determine fracture occurrence, the concept of critical energy as an intrinsic property of the material appears. A lot of authors, such as Lemaître 1986, Rabier 1989, Chaboche 1988, Bruhns & Schiesse 1996, use a critical value of the elastic energy release rate, often called Y in the damage models (see section 3.2.2) as fracture criterion.

Another example is given by Chaouadi's 1996 work devoted to the fracture of steels for reactor pressure vessels in the ductile regime. Like many other scientists (Cotterel & Reddel 1977, Atkins & Mai 1985, Knockaert *et al.* 1996), Chaouadi proposes an energy criterion. He first validates it using notch experiments, then applies it to predict crack toughness data, in cases where experiments are not possible. He assumes that the total energy is a constant at rupture. Neglecting the elastic part, this energy consists in two terms: the plastic strain work and the void expansion work. This latter damage energy is simply evaluated by the hydrostatic stress multiplied by the hydrostatic strain related to Rice & Tracey's relation (4-22). This gives:

$$W^t = \int_0^{\varepsilon} \sigma_{eq}\, d\varepsilon_{eq}^p + 3A\sigma_m \exp\left(\frac{3}{2}\frac{\sigma_m}{\sigma_{eq}}\right) d\varepsilon_{eq}^p \tag{4-31}$$

where A is a "constant" reflecting the particle distribution in the material, it can be replaced by a statistical distribution. Numerous comparisons with tensile experiments on notched tests show that a critical value of W^t, independent of the sample geometry or the stress triaxiality appears. So this critical energy is an intrinsic material property. To reach this conclusion, Chaouadi has introduced a critical length: a distance over which the energy should reach its critical value to initiate the crack. The evaluation of this distance shows that it is always larger than the blunting affected region. A correlation between W^t and J-integral is established with the objective to define fracture toughness derived from the tensile test. In practice, the size of irradiated samples available from nuclear power plants does not allow valid toughness measurements and Chaouadi's approach, using total energy, allows extrapolating reasonable values.

Pardoen 1998 proposes another thesis using both fracture mechanics and continuum damage mechanics. He works on cold-drawn copper bars of 10 or 20 mm diameter and studies two states of the material: the As-Received state, called "CuAR" and the annealed state, called "CuA". He reaches J-integral by means of tensile tests on circumferentially cracked bar (CBR) geometries, which is an approach not yet standardized. He finds that for CuAR material, the J-integral is valid (path independent) and dominant (no constraint effects) until cracking, in spite of large scale yielding. However for CuA material, which is very ductile, even if CRB geometry provides highly constrained fracture, path independence of J-integral is not valid. Pardoen checks that the J-Q approach cannot be applied in this case. So, fracture mechanics does not provide an efficient way to predict fracture. To solve this problem, Pardoen, as Chaouadi, tries to find an energy criterion with success. He assumes that the work density spent in the Fracture Process Zone (FPZ) until crack initiation is a material constant. Broberg 1975 has proposed the occurrence of a physical uncoupling between an "essential" work for fracture, consumed in a crack tip zone (FPZ), and a "non-essential" work, dissipated around FPZ. This means that the FPZ zone is defined more precisely as the smallest zone where specific work until fracture is constant, independent of specimen geometry. Marchal's 1997 thesis particularly investigates and develops the "essential" work of fracture. In Pardoen's thesis, the FPZ is assumed to cover the major part of the ligament area in deeply cracked specimens CuA or, in other words, all work spent in the test would be "essential". Numerical simulations and experiments confirm this assumption and the efficiency of this energy criterion to predict fracture for different sizes of specimen.

The last example presented here is Wilsius 1999. This thesis proposes a synthesis of criteria to detect rupture and a practical introduction to fracture mechanics, which summarizes not only the theory but also the methods to measure introduced variables. Wilsius studies three materials with very different volume fraction of inclusions: a CMn steel with welding, an aluminum alloy 2024 T351 and a NiCr 12 NC6 steel. Classical fracture tests to determine toughness and classical tensile tests to reach material behavior are performed. Three different models are applied to simulate toughness tests:

- a rigid plastic von Mises' approach coupled with Rice & Tracey's criterion (see relation 4.22);
- Rousselier's model (see section 3.2.3);
- Gurson-Tvergaard-Needleman (see Chapter 2).

To reach a good simulation of fracture tests, Wilsius shows that the mesh size at the crack tip is an important parameter. The set of material parameters describing material behavior and enabling to recover the curve "*J*-integral versus fracture opening" strongly depends on this information. The fracture criteria used to simulate the fracture development are either Rice & Tracey's criterion or a critical value of the damage parameter. These simulations also require the use of a characteristic length (different from the element size) where the criterion is fulfilled to determine crack propagation. This research shows that continuum damage mechanics can reproduce the curves measured in fracture mechanics.

4.5.3. Summary of links between Fracture Mechanics and Continuum Damage Mechanics

Energy criteria suggested by fracture mechanics are interesting to use in continuum mechanics. For ductile rupture with large plastic zone, the critical value of one parameter proposed by fracture mechanics cannot provide a solution to detect fracture anymore. So, a continuum damage approach can complete fracture mechanics to find efficient ways to predict fracture in these cases.

Note that an important feature appears in this section: a material length scale. The critical density energy or the critical damage value must be reached not at a single point but in a zone to induce crack propagation. This feature seems logical when one looks at numerical simulations near the crack tip with refined finite elements. Such refined simulations are necessary if one intends to study crack propagation, as cracks introduce singularities in the stress and strain fields at a very small length scale.

The rupture criteria described in previous sections were more dedicated to the detection of the initiation of rupture, which explains why this length scale did not so clearly appear.

References

Abraham F.F. (1996) Parallel molecular dynamics investigation fracture. *Computer simulation in materials science*, Kluwer Academic Publishers, 211-226.

Arrieux, R. (1990) Détermination théorique et expérimentale des courbes limites de formage en contraintes, Thèse de docteur d'état en sciences, Institut national des sciences appliquées de Lyon et l'université Claude Bernard Lyon I.

Anderson, T.L. (1995) Fracture Mechanics – Fundamentals and Application, CRC Press, Boca Raton.

Atkins, A.G. (1981) Possible explanation for unexpected departures in hydrostatic tension-fracture strain relations. *Metal Sci*, **15**, 81-83

Atkins, A.G., Mai, Y.W., (1985) Elastic and Plastic Fracture, Ellis Horwood Limited, Chicheester, England.

Banabic, D. (1996) Forming limit diagrams predicted by using the new Hill's yield criterion, *Proceedings of the 3rd Int. Conf. Numisheet' 96 Numerical Simulation of 3-D Sheet Metal Forming Processes – Verification of Simulations with Experiments*, ed. Lee, Kinzel, Wagoner, the Ohio State University.

Barata da Rocha, A., Barlat, F., Jalinier, J.M. (1984) Prediction of the forming limit diagrams of anisotropic sheets in linear and non-linear loading, *Mat. Sci. Eng.*, **68**, 151-164.

Barata da Rocha, A. (1985) Mise en forme des tôles minces, instabilité plastique, anisotropie et endommagement, Thèse de Doctorat, Institut National Polytechnique de Grenoble.

Bauvineau, L. (1996), Approche locale de la rupture ductile: application à un acier au carbone –manganèse, Thèse de Doctorat, Ecole Nationale Supérieures des Mines de Paris.

Benallal, A., (2000), Continuous Damage and Fracture, Elsevier.

Benzerga, A., Besson, J., Pineau, A. (1999) Coalescence-controlled anisotropic ductile fracture. *J. of Eng. Mat. & Techn.* (soumis pour publication).

Boudeau, N., Gelin, J.C. (1992) Finite element simulation of the ductile fracture in 3-D sheet metal forming process, *Journal of Materials Processing Technology*, **32**, 521-530.

Boudeau, N., Gelin, J.C. (1994) Prediction of the localized necking in 3D sheet metal forming processes from FE simulations. *J. of Materials Processing Technology*, **45**, 229-235.

Boudeau, N., (1995) Prédiction des instabilités élasto-plastiques. Application à l'emboutissage, Ph. D. Thesis, Université de Franche – Comté, France.

Boudeau, N., Gelin, J.C. (1996a) Post-processing of finite element results and prediction of the localized necking in sheet metal forming, *J. of Materials Processing Technology*, **60**, 325-330.

Boudeau, N.,Salhi, S., Gelin, J.C. (1996b), Necking in sheet metalforming, prediction from finite element simulations and computations based on crystalline plasticity, *NUMISHEET 96 Numerical Simulation of 3-D Sheet Metal Forming Processes – Verification of Simulations with Experiments,* ed. Lee, Kinzel, Wagoner,,the Ohio State University.

Boudeau, N., Gelin, J.C., Salhi, S. (1998) Computational prediction of the localized necking in sheet forming based on microstructural material aspects, *Computational Materials Science*, **11**, 45-64.

Boudeau, N., Lejeune, P., Gelin, J.C. (2001) Damage in sheet metal forming : prediction of necking phenomena, *Journal of Finite Elements*, Hermes, to appear.

Boyer, J.C., Staub, C., (1997) A ductile damage model including shear stress effects. *Advanced Methods in Materials Processing Defects*, Predeleanu, M., & Gilormini, P., Eds Elsevier, 13-22.

Brethenoux, G., Mazataud, P., Bourgain, E., Muzzi, M. & Giusti, J. (1997) A mesoscopic approach of ductile damage during cold forming processes, *Advanced Methods in Materials Processing Defects*, Predeleanu, M., & Gilormini, P., 23-32.

Broberg, K.B. (1975) On stable crack growth, *J. Phys. Mech. Solids* **23**, 215-237.

Brocks, W., Sun, D.Z., Honig, A. (1995) Verification of the transferability of micromechanical parameters by cell model calculations with visco-plastic materials, *Int. J. Plasticity*, **11-8**, 971-989.

Brown, L.M. , Embury, J.D. (1973) The initiation and growth of voids at second phase particles. *Proceedings of the 3rd Int. Conf. on the Strength of Metals and Alloys, ICSMA3*, Cambridge, England, 164-169.

Brozzo, P. de Luca, B. & Rendina, R. (1972) Eine neue Methode zur Vorhersage der Umformbarkeit von Metallfeinblechen. *Proc. 7th Biennial Congress IDDRG*, 9-13.Cayssials, F. (1998) A new method for predicting FLC, *IDDRG, Conference Geneval*, Brussel 6/98.

Bruhns, O.T., Schiesse, P. (1996) A continuum model of elastic-plastic materials with anisotropic damage by oriented microvoids. *Eur. J. Mech. A/Solids*, **15-3**, 367-396.

Brunet, M., Mguil-Touchal, S., Morestin, F. (1997) Numerical and experimental analysis of necking in 3D sheet forming processes using damage variable, *Advanced Methods in Materials Processing Defects*, Predeleanu M. & Gilormini P. Eds, 205-214.

Brunet, M., Mguil-Touchal, S., Morestin, F. (1998) Analytical and experimental studies of necking in sheet metal forming processes, *J. of Materials Processing Technology*, **80-81**, 40-46.Cayssials, F., (1999) The new version of the Sollac model, *Working Group of the IDDRG 99*, Birmingham.

Cayssials, F. (1998) A new method for predicting FLC, IDDRG, Conference Geneval, Brussel 6/98.

Cayssials, F., (1999) The new version of the Sollac model, Working Group of the IDDRG 99, Birmingham.

Ceder G. (1999) Designer materials, *Res metallica'99*, Chair Framework Agreement, KUL, MTM-Bekaert, Sidmar, Union Minière.

Chaboche, J.L., (1988a) Continuum damage mechanics. Part I – General concepts, *J. Appl. Mech.*, **55**, 59-64.

Chaboche, J.L., (1988b) Continuum damage mechanics. Part II – Damage growth, crack initiation, and crack growth, *J. Appl. Mech.* **55**, 65-72.

Chiou, J.M. (1996) A study of ductile damage in metal forming. Ph. D. thesis, the University of Birmingham.

Chaouadi, R. (1996), Micromechanically based damage modelling of crack initiation in reactor materials, Ph. D. Thesis Katho. Universiteit Leuven.

Cockroft, M.G. & Latham, D.J. (1968) Ductility and the workability of metals, *J. Inst. Met.*, **96**, 33-39.

Cotterell, B., Reddel, J.K., (1977) The essential work of plane stress ductile fracture. *Int. J. Fract.* **13**, 267-277.

Doege, E., Bagaviev, A. & Dohrmann, H. (1997) Formability analysis based on the anisotropically extended Gurson model, *Advanced Methods in Materials Processing Defects*, Predeleanu, M. & Gilormini P., 281-288.

Doghri, I. Billardon, R.(1995), Investigation of localization due to damage in elasto-plastic materials, *Mechanics of Materials,* **19**, 129-149.

Eckstein, A., Basar, Y. & Konke, C. (1997) Damage analysis of ductile metallic shells. Computational plasticity – *Fundamentals and Applications*, Owen, D.R.J, Onate, E. Hinton, E., editors, CIMNE, Barcelona.

Esche Sven K, Kinzel Gary L., Altan, T. (1996) Review of failure analysis in sheet metal forming simulations. *Proceedings of the 3rd Int. Conf. Numisheet' 96 Numerical Simulation of 3-D Sheet Metal Forming Processes – Verification of Simulations with Experiments*, ed. Lee, Kinzel, Wagoner, the Ohio State University.

Freudenthal, A.M. (1950) The inelastic behaviour of engineering materials and structures, John Wiley & Sons, New-York.

Gologanu, M., Leblond, J.B., Devaux, J. (1994) Numerical and theoretical study of coalescence of cavities in periodically voided solids, *Computational Material Modeling, ASME*, AD-vol. **42/PVP**-Vol. 294.

Gosh, A.K., (1976) A criterion for ductile fracture in sheets under biaxial loading, Metallu. Trans. , **7A**, 523-533.

Habraken, A.M., Radu, J.P., Duchêne. L., Wauters, M. (1998) Simulation of Materials processing : Theory, methods and Applications, *Proceedings of the sixth international conference on numerical methods in industrial forming processes – Numiform '98, June*, Huétink, J., Baaijens, F.P.T., Balkema, A.A., Eds.

Hill, R. (1950) *The Mathematical Theory of Plasticity*, Clarendon Press, UK.

Hiwatashi, S., Van Bael, A., Van Houtte, P., Teodosiu, C. (1998) Prediction of forming limit strains under strain-path changes : application of anisotropic model based on texture and dislocation structure. *Int. J. of Plasticity*, **14-7**, 647-669.

Hoferlin, E., Van Bael, A., Hiwatashi, S., Van Houtte, P. (1998) Influence of texture and microstructure on the prediction of forming limit diagram, *19th RISO Symposium on Materials Science*, 7-11 Sept. 1998.

Hora, P., Tong, L., Reissner, J. (1996) A prediction method for ductile sheet metal failure in f.e. simulation, Proceedings of the 3rd Int. *Conf. Numisheet' 96 Numerical Simulation of 3-D Sheet Metal Forming Processes – Verification of Simulations with Experiments*, ed. Lee, Kinzel, Wagoner, the Ohio State University.

Hutchinson, J.W. (1968) Singular behaviour at the end of a tensile crack in a hardening material, *J. Mech.A/Solids*, **16**, 13-31.

Knockaert, R., Doghri, I., Marchal, Y., Pardoen, T., Delannay (1996) Experimental and numerical investigation of fracture in double-edge notched steel plates. *Int. J. Fract.* **81**, 383-399.

Knockaert, R. (2001), Etude expérimentale et numérique de la localisation de la déformation lors de la mise en forme de produits minces, Thèse de Doctorat, Ecole Nationale Supérieure des Mines de Paris, Sophia Antipolis.

Koplik, J., Needleman, A. (1988) Void growth and coalescence in porous plastic solids. *Int. J. Solids Structures*, **24-8**, 835-853.

Komori, K. (1998) Simulation of chevron crack in drawing : effect of parameter in fracture criterion, *Simulation of Materials Processing: Theory, Methods and Applications*, Numiform, Huetink & Baaijens Eds, Balkema.

Leblond, J.B., Perrin, G. (1991) Analytical study of the coalescence of cavities in ductile fracture of metals, *Plasticity 3rd Symposium*, 233-236.

Leblond, J.B., Perrin, G., Devaux, J. (1995) An improved Gurson-type model for hardenable ductile metals, *Eur. J. Mech. A/Solids*, **14**, 499-527.

Lemaître, J. (1985) Coupled elastoplasticity and damage constitutive equations, *J. Comp. Meth. in Appl. Mech. and Eng.* **51**, 31-49.

Lemaître, J. (1986), Local approach of fracture, *Eng. Fracture Mech.*, **25**, 523-537.

Marchal, Y. (1997), Mechanics and Physics of the ductile fracture of thin plates, Thèse de doctorat, Université de Louvain-La-Neuve.

Marciniak, Z., Kuczynski, K., (1967) Limit strains in the processes as stretch-forming sheet metal, *Int. J. Mech. Sci.*, **9**, 609-620.

Marini, B., Mudry, D., Pineau, A. (1985), Experimental study of cavity growth in ductile rupture, *Eng. Fracture Mech.*, **22/6**, 989-996.

Narasimhan, K., Wagoner, R.H. (1991) Finite element modeling simulation of in-plane forming limit diagrams of sheets containing finite defects. *Metallurgical Transaction A*, 22A, 1991, 2655.

Needleman, A., Tvergaard, V. (1984) An analysis of ductile rupture in notched bars, *J. Mech. Phys. Solids*, **32**, 461-490.

Mudry, F.(2000), Some examples of the use of continuous damage and fracture mechanics in the steel industry, *Continuous Damage and Fracture*, Benallal, A, editor, Elsevier.

Pardoen, T. (1998) Ductile fracture of cold-drawn copper bars : experimental investigation and micromechanical modelling, Doctorat en sciences appliquées, Université de Louvain-La-Neuve.

Oh, S.I., Chen, C.C. & Kobayashi, S. (1979) Ductile fracture in axisymmetric extrusion and drawing. *J. Eng. Ind. Trans. ASME*, **101**, 36-44.

Oyane, M. (1972) Criteria of ductile fracture strain. *Bull. Jpn. Soc. Mech. Eng.*, **15**, 1507-1513.

Picart, P., Piechel, G. & Oudin, J. (1997) Damage influence in the finite element computations for large strains elastoplastic mechanical structures, *Advanced Methods in Materials Processing Defects*, Predeleanu, M. & Gilormini, P., Eds. Elsevier, 175-184.

Pineau, A. (1981) Review of fracture micromechanisms and a local approach to predicting crack resistance in low strength steels., *Advances in Fracture Research*, Pergamon Press, 553-577.

Qiu, Y., Neale, K.W., Makinde, A., MacEwen S.R. (1995) Numerical modelling of metal formability using polycrystal plasticity, *IDDRG Genval*, juin 1998.

Rabier, P. J. (1989) Some remarks on damage theory, *Int. J. Engng. Sci.*, **27**, 29-54.

Rice, J.R. (1968) A path independent integral and the approximate analysis of strain concentration by notches and cracks, *J. Appl. Mech.*, **35**, 379-386.

Rice, J.R. , Tracey, D.M. (1969) On the ductile enlargement of voids in triaxial stress fields, *J. Mech. Phys. Solids*, 17, 201-217.

Rice, J.R., Rosengren, G.F. (1968), Plane strain deformation near a crack tip in a power-law hardening material, *J. Mech. Phys. Solids,* **16**, 1-12.

Rousselier, G., Devaux, J.C., Mottet, G., Devesa, G. (1989) A methodology for ductile fracture analysis based on damage mechanics : an illustration of a local approach of fracture, *Nonlinear Fracture Mechanics : vol. II – Elastic-Plastic Fracture, ASTM STP 995,* J.D. Landes, A. Saxena, J.G. Merkle Eds, American Society for Testing and Materials, Philadelphia, 332-354.

Rudnicki, J.W., Rice, J.R. (1975) Conditions for the localization of deformation in pressure-sensitive dilatant materials, *J. Mechs. Phys. Solids*, **23**, 371-394.

Shi, C.F. (1983) Tables of Hutchinson-Rice-Rosengren singular field quantities, *Report MRL E-147,* Brown University.

Sowerby, R., Duncan, J.L. (1971) Failure in sheet metal in biaxial tension, *Int. J. Mech. Sci.*, **13**, 217-229.

Storen, S. & Rice, J.R. (1975) Localized necking in thin sheets, *J. Mech. Phys. Solids*, **23**, 421-441.

Thomason, P.F. (1985a) Three-dimensional models for the plastic limit-load at incipient failure of the intervoid matrix in ductile porous solids, *Acta Metall.*, **33**, 1079-1085.

Thomason, P.F. (1985b) A three-dimensional model for ductile fracture by the growth and coalescence of microvoids, *Acta metall.*, **33**, 1087-1095.

Thomason, P.F. (1990) Ductile fracture of metals, Pergamon Press.

Thomason, P.F. (1993) Ductile fracture by the growth and coalescence of microvoids of non uniform size and spacing, *Acta Metall. Mater*, **41-7**, 2127-2134.

Tvergaard, V. (1982) Material failure by void coalescence in localized shear bands, *Int. J. Solids & Struct.* **18**, 659-672.

Vacher, P., Arrieux, R., Tabourot, L. (1998) Analysis of a criterion of deep drawing operation capability for thin orthotropic sheets, *Journal of Materials Processing Technology*, **78**, 190-197.

Vegter, H., An Y., Pijlman H.H., Carlee B.D., Huetink J. (1998), Advanced material models in simulation of sheet forming processes and prediction of forming limits, *1st ESAFORM Conference on Material Forming*, Sophia Antopolis, Eds. Chenot, Agassant, Montmitonnet, Vergnes, Billon.

Vegter, H., An Y., Pijlman H.H., Huetink J. (1999), Different approaches to describe the plastic material behaviour of steel and aluminium-alloys in sheet forming, *2nd ESAFORM Conference on Material Forming*, Guimaraes, Portugal, Covas J.A. Ed.

Wilsius, I., (1999) Etude expérimentale et numérique de la déchirure ductile basée sur des approches locales en mécanique de la rupture. Ph. D. Thesis Université des Sciences et Technologie de Lille.

Wu, P.D., Neale, K.W., Van Der Giessen, E. (1998) Effects of strain paths on sheet metal limit strains, Material Instabilities in Solids, John Wiley & Sons Ltd, de Borst R. & Van der Giessen EK, Eds.

Zhou, Y., Neale, K.W. (1995) Prediciotns of Forming limit Diagrams using a rate sensitive crystal plasticity model, *Int. J. Mech. Sc.*, 37-1, 1-20.

Zhu, Y.Y. (1992) Contribution to the local approach of fracture in solid dynamics, Ph. D. thesis, University of Liège, MSM Department .

Zhu, Y.Y., Cescotto, S. and Habraken, A.M. (1992) A fully coupled elastoplastic damage modeling and fracture criteria in metalforming processes, *J. of Mater. Processing Technology* **32**, 197-204.

5. MESH DEPENDENCE IN DAMAGE MODELING

5.1. Introduction

To model the behavior of a structure or a specimen up to rupture, a descending branch in the stress-strain curve is introduced, at a generic stage of the deformation process, to simulate the loss of load-carrying capacity at progressive straining. Examples of such models applied to ductile metals were given in Chapters 2 and 3; however this approach also appears in soils or more brittle materials like concrete, polymers, ceramics, ... So, the global answer, "load-deflection curve", is translated into local description by a "softening" stress-strain relation.

A mathematical consequence of such softening models is that, at certain threshold levels of loading, in the static case, the governing differential equations locally lose their elliptic character. In the dynamic case, a change of the hyperbolic equations into an elliptic set is typically observed. Consequently, the boundary or initial value problem becomes ill-posed and analytical as well as numerical solutions become meaningless. For instance, the numerical solution appears to be fully determined by the refinement and the direction of the mesh discretization. For instance, de Vree *et al.* 1995 apply a simple elastic isotropic model of local damage to a square plate with a central hole. This plate is supported along one side and a prescribed displacement is defined along the opposite side. Because of symmetry, only the upper right quarter of the plate is discretized with 5 different meshes (Figure 5.1).

Figure 5-1 Meshes for the quarter plate (from de Vree *et al.* 1995).

The results of the local damage approach are clearly mesh dependent as shown by the force-displacement curves presented on Figure 5.2.

Typical differences in the distributions of the damage variable determined by a coarse and a refined mesh are visualized on Figure 5.3. Mesh refinement leads to

a vanishing energy dissipation and the deformation localizes in an zone of decreasing volume.

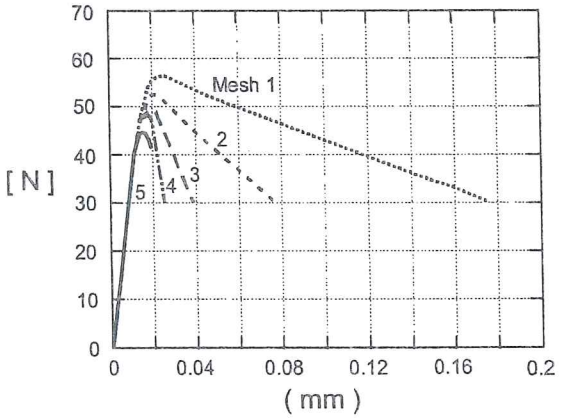

Figure 5-2 Force- displacement curves, local damage model (from de Vree *et al.* 1995).

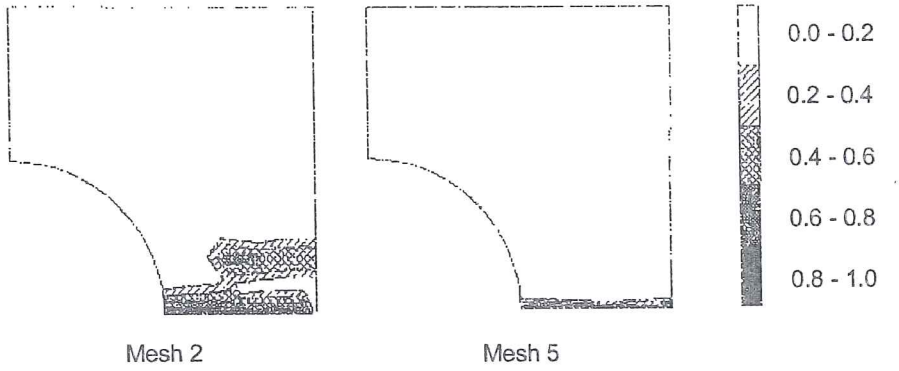

Figure 5-3 Damage distribution, local damage model (from de Vree *et al.* 1995).

Starting in the early 1980s, a tremendous amount of activity has been devoted to remedying this deficiency of the standard continuum approach.

A good review of all possible solutions was proposed by de Borst *et al.* 1998 and presented for instance during de Borst's 1999 plenary lecture at the 5th United States National Congress on Computational Mechanics; or one can also read the review by Desoyer 1995. Both authors underline that softening materials can predict strain localization, which in most engineering materials precedes failure by the emergence of narrow zones of intense straining. For rate insensitive materials, localization is interpreted as a bifurcation phenomenon (Rice 1976): for a given homogeneous strain rate, the material constitutive equation allows for a

non homogeneous solution to develop. A material instability occurs and strain localization takes place. Standard, rate independent continuum models are able to determine the behavior in the pre-localization regime and some properties at incipient localization, such as the direction of shear bands in tensile tests or in biaxial and triaxial states (Doghri & Billardon 1995). However in the post-localization regime, or in the softening branch of the material behavior, a possible change appears for the character of the governing set of partial differential equations. Numerical solutions suffer from spurious mesh sensitivity and become meaningless.

Scientists (Belytscko & Fish 1989, Wang 1993) have first tried to "enrich" finite elements but this does not tackle the basic problem of loss of ellipticity. Upon mesh refinement, the solution converges to a localization zone with zero dimension. No energy is dissipated and the results become meaningless. A more efficient approach is to modify the FEM formulation or the constitutive law of the material in such a way that, even when localization occurs, the problem remains well posed. Different ways to achieve this second approach have been followed:

The Non-Local Approach. It basically consists in using classical laws with non-local variables computed by a weighted average over a volume of material with characteristic dimension l. This length introduced in the formulation proves to be an essential feature to restore the objectivity of the numerical models during localization (Bazant & Chang 1984). The choices of the characteristic volume (size and shape), weighting function and variables on which averaging is made are not simple.

The Cosserat Continuum Theory. In this approach, moment and rotation degree of freedom are used in addition to the classical stress components and translation degrees of freedom. It constitutes an elegant way to induce an internal length in the material constitutive law (de Borst 1991). It may be justified in the case of granular materials like sand. For polycrystalline materials, one can link rotations to grain motion (Lippman 1995). Unfortunately, this approach is totally effective in pure shear, only when the rotations are predominant. For instance, Sluys 1992 shows that, for a compression test, only partial regularization is achieved.

The Viscous Regularization. Some authors (Simo 1989, Loret 1990, Zhu 1992) use classical continuum theory but they include some viscous effects in the material constitutive equations. It appears that the mesh independency can be achieved but is conditional to the amount of viscosity introduced in the model.

The Gradient Approach. The basic idea is to introduce some gradients of the pertinent state variables in the formulation of constitutive laws. Bazant 1984 has presented the non-local gradient formulation with a Laplacian of strain and has applied this formulation in solving a one dimensional localization problem. Aifantis 1988, 1992 show that the introduction of the second gradient of deformation into the expression of the flow stress for plastic materials can

preserve ellipticity of the governing equations. de Borst & Mulhaus 1992 have presented the formulations and algorithms for the gradient plastic continuum in a two-dimensional and three-dimensional finite element context, where the yield strength depends not only on the effective plastic strain but also on its Laplacian. This method has been widely used in plastic models (Pamin 1994, Li & Cescotto 1996), in elastic damage models (Geers 1997) or elastic-plastic-damage models (Zbib & Aifantis 1988); it keeps efficiently ellipticity of the equations when localization occurs.

It seems that all the different proposed numerical solutions and the physical reality have in common the existence of an internal material length scale parameter. It characterizes the range and the amplitude of the micromechanical non-local bindings between the material particles. This length scale parameter can only be identified when inhomogeneous deformations occur; so standard material tests do not suffice. Structural tests must be considered and the length scale parameter must be determined by inverse modeling (Geers 1997). Note that it is interesting to couple non-local continuum damage model to random field theory and stochastic finite-element analysis. This yields a probabilistic formulation of the damage evolution (Carmeliet 1996). This approach introduces two different length parameters: the characteristic length of the non-local damage model and the correlation distance of the random field.

The Euromech 417 conference entitled "Numerical Modelling in Damage Mechanics" held in Troyes or the Symposium on "Continuous Damage and Fracture" (Benallal, 2000) held in Cachan, both in October 2000, help to summarize the state-of-the-art. They demonstrate clearly that the non-local and gradient approaches have the largest range of applications and solve efficiently the problem of mesh dependency. So these solutions will be shortly presented hereafter.

If the softening effect is not too strong and in applications where the non-homogenous strain and stress fields induce well localized shear zone, one can hope to avoid more or less mesh dependent results. It is then possible to detect fracture location and to identify the fracture moment of occurrence (pre-localization regime). For instance, Brunet *et al.* 1997, with his anisotropic extension of Gurson's model, but also Picart *et al.* 1997, Lazzaretto *et al.* 1996, with a classic isotropic Gurson's model, or Hartley *et al.* 1997, with a Lemaître's type law, look for fracture occurrence and do not bother with mesh dependence problems. It is difficult to know if these authors have checked the mesh independence of their results with their particular data or if the regularization issued from damage strain rate dependence preserves the ellipticity of their equations. However for metal modeling, the work of Stainier 1996 with Gurson's law and Castagne 1998 with Lemaître's type model proved the importance of the mesh dependence on results. To follow crack development it is really not possible to neglect this problem.

In the applications of Chapter 6, the conclusion is that, because of the non homogeneous field, the fracture location is well predicted but its occurrence instant is mesh dependent, at least in cases of strong damage localization like the notch test with sharp radius or the notched bending rod test. In the research described in section 6.2, even if the material viscosity is low, it generally seems to be sufficient to prevent strain localization before experimental crack appears. This was not the case with Castagne's 1998 work, summarized in section 6.3, where a damage elasto-plastic model was fitted on the same set of experiments. Her elasto-plastic simulations clearly show bifurcations long before experimental cracks appear.

5.2. Non-Local approach

In this method, the length range of the microscopic interaction forces is taken into account at macroscale, by expressing the material constitutive law in terms of one or more non-local variables defined as suitably weighted averages of their local values over the interaction domain.

The case of a simple isotropic elastic local model of damage is presented here. The stress-strain relation is given by:

$$\underline{\sigma} = (1 - D)\,\underline{\underline{C}}^{e} : \underline{\varepsilon} \tag{5-1}$$

where the scalar damage variable D is limited by:

$$0 \le D \le 1 \tag{5-2}$$

This damage parameter D is coupled to the deformation history of the material through the use of a monotonically increasing deformation history parameter κ. Geers' 1997 choice is presented here:

$$\kappa(\underline{x},t) = max\left[\varepsilon^{d}_{eq}(\underline{x},\tau)\ with\ \tau \le t\ ),\kappa_{i}\right] \tag{5-3}$$

where ε^{d}_{eq} is a damage equivalent strain derived from the different strain components of the local strain tensor. The chosen mathematical function for ε^{d}_{eq} offers various possibilities to quantify the effect of the local strain on the damage process, and constitutes one of the characteristics of the failure behavior. $\underline{x}$ identifies the position of the point in consideration, t is the time, κ_i is the threshold value for damage initiation at time $t = 0$. The evolution of κ can be mathematically expressed by Kuhn Tucker's relations:

$$\dot{\kappa} \ge 0 \quad \varepsilon^{d}_{eq} - \kappa \le 0 \quad \dot{\kappa}\,(\varepsilon^{d}_{eq} - \kappa) = 0 \tag{5-5}$$

An example of damage evolution law is:

$$D = 1 - \frac{\kappa_i}{\kappa}((1-\alpha) + \alpha\, e^{-\beta(\kappa-\kappa_i)}) \tag{5-6}$$

where α and β are material parameters.

In the non-local version of this model, the damage equivalent strain is just replaced by a non-local equivalent strain, which characterizes the deformation in a material volume surrounding the focused point:

$$\bar{\varepsilon}^{d}_{eq}(\underline{x}) = \frac{1}{V}\int_{V} g(\underline{y})\,\bar{\varepsilon}^{d}_{eq}(\underline{x}+\underline{y})\,dV \tag{5-7}$$

where $\underline{x}$ characterizes the position of the analyzed point, $\underline{y}$ the relative positions of the material points in a surrounding volume V. The function $g(\underline{y})$ is a weighting function defining the intensity and the radius of the spatial non-local effect. It introduces the material internal characteristic length scale. It should satisfy:

$$\frac{1}{V}\int_{V} g(\underline{y})\,dV = 1 \tag{5-8}$$

The definitions of the non-local variable(s), weight function and interaction domain have important consequences in finite element implementations. For instance, depending on the choice of non-local variables, the corrector phase in standard finite element iterative procedure, typically carried out separately at each Gauss point, may cease to be local. The choice of a non symmetric weight function implies that the consistent tangent matrix becomes non-symmetric. These two drawbacks are suppressed in the final proposal by Comi & Perego 2001. In this article, they first choose as non-local variable the elastic energy release rate. It has the advantage that the constitutive calculations can be separately conducted during the corrector phase but suffers the drawback of yielding a non-symmetric consistent tangent matrix. Following the thermodynamically founded, non-local theory recently developed by Borino *et al.* 1999, a second version of the model is proposed. A new term is added in the dissipation rate density: a non-local residual. It represents the energy due to the intrinsic non-locality of the developing damage mechanism. This energy is exchanged between the considered material point and other points belonging to its interaction domain. In the final proposal by Comi & Perego 2001, the non-local nature, originally conferred to the damage variables, is transferred to their conjugate variables, the energy release rates, on the basis of an energy equivalence, which helps to eliminate the so-called non-local residual. The explicit expression of the finite element tangent stiffness matrix for this new non-local model has been derived and is symmetric.

5.3. Gradient approach

5.3.1. Gradient damage method

As proposed by Bazant *et al.* 1984 and applied for instance by Geers 1997, Peerlings 1999, one way to reach gradient theory is to expand the local damage equivalent strain ε_{eq}^{d} into a Taylor series, then to compute its integral (5-7) in a material volume surrounding the focused point. Neglecting the high-order terms, this substitution allows to transform relation (5-7) into:

$$\bar{\varepsilon}_{eq}^{d} = \varepsilon_{eq}^{d} + c\nabla^2 \varepsilon_{eq}^{d} \tag{5-9}$$

The remaining gradient parameter c represents the square of the average internal length. It only depends on the selected weighting function and the averaging volume V. In practice, if no term of the Taylor series was neglected and the same weighting function was applied, the integral (5-7) and differential (5-9) formulation should be fully equivalent. However, neglecting higher-order gradient coefficients is one way to choose implicitly another weighting function, so the integral and differential formulations differ. As formulation (5-9) relates explicitly $\bar{\varepsilon}_{eq}^{d}$ to the Laplacian of ε_{eq}^{d}, it inevitably requires C^1 continuity of the displacement shape functions in finite element formulations. To tackle this drawback, Peerlings *et al.* 1996 propose to use another formulation reached by some algebraic transformation of (5-9), where higher order term are dropped:

$$\bar{\varepsilon}_{eq}^{d} = \varepsilon_{eq}^{d} + c\nabla^2 \bar{\varepsilon}_{eq}^{d} \tag{5-10}$$

In practice, it can be considered as another approximation deduced from the differential formulation (5-7). It implicitly defines another weighting function than in equation (5-9). Using a Galerkin finite element scheme, Peerlings *et al.* 1996 present a consistent incremental iterative Newton-Raphson solution procedure of the discretized weak form of the governing field equations, which are the equilibrium and the non-local formulation:

$$div\,\underline{\sigma} + \underline{f} = 0$$

$$\bar{\varepsilon}_{eq}^{d} - c\nabla^2 \bar{\varepsilon}_{eq}^{d} = \varepsilon_{eq}^{d} \tag{5-11}$$

As checked by Geers 1997, this formulation, called "**constant gradient damage model**", uses a constant c parameter and suffers from some inherent deficiencies, which render the method unable to describe a discontinuous crack evolution. In the final failure stage, the damage computed by this method propagates in a direction normal to the crack, which causes widening of the damaged zone (Figure 5-4).

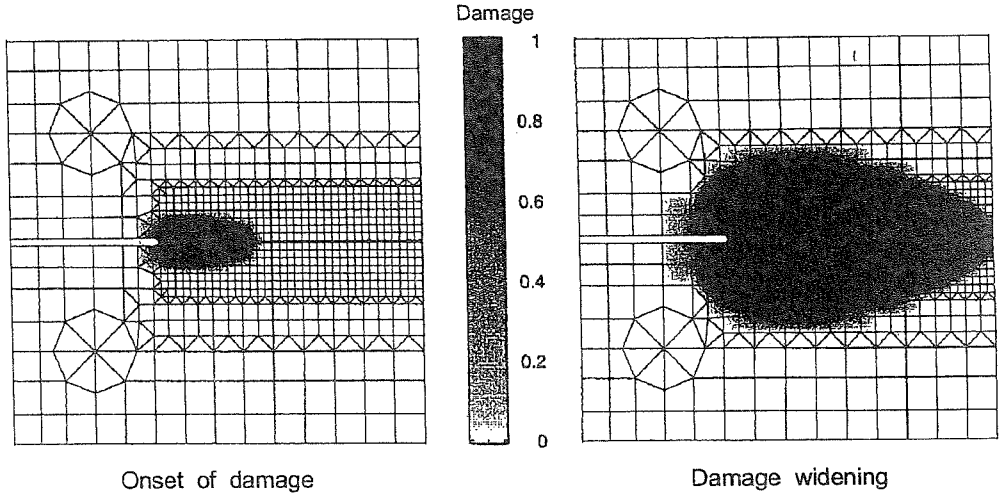

Figure 5-4 Damage distribution of a compact tension experiment on a short glass-fiber-reinforced polypropylene simulated by constant gradient damage model (from Geer's 1997).

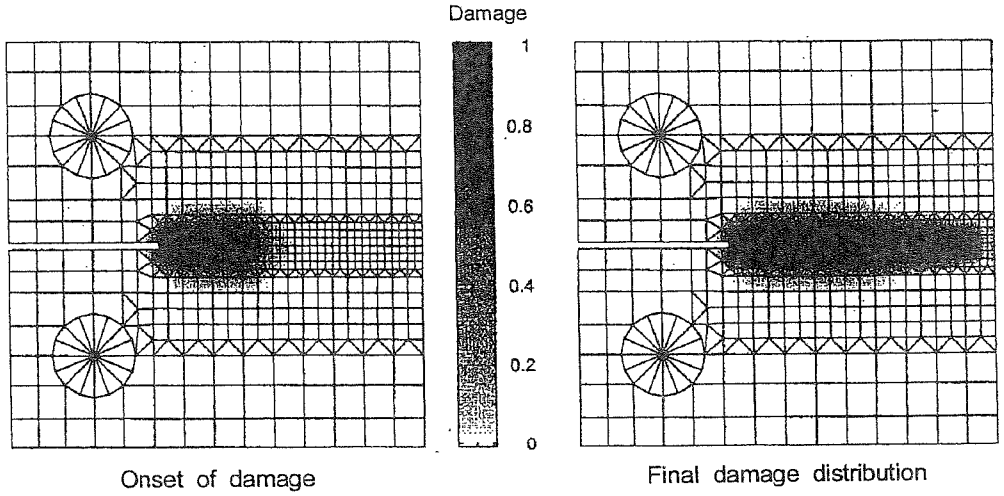

Figure 5-5 Damage distribution of a compact tension experiment on a short glass-fiber-reinforced polypropylene simulated by a strain-based transient-gradient damage model (from Geer's 1997).

In practice, damaged material should unload with the fracture propagation and a finite width of the damaged zone should be reached. This is correctly simulated with a modified formulation (Figures 5-5 and 5-6), where a new variable ζ denoted gradient activity is introduced. This parameter models the mobilized non-local coupling between particles at the micro-level. When it is equal to 0, one retrieves the local formulation. When it reaches its maximal value c, the constant gradient model is recovered. The transient behavior of ζ requires a supplementary evolution law. According to this reasoning, the non-local coupling

between the material particles is more and more mobilized as the local deformation increases and with an increasing value of ζ. The final finite element formulation satisfactorily handling this model is a three-field formulation (velocity field, non-local damage equivalent strain field and a C^0 version of variable ζ field). Details can be found in Geers 1997.

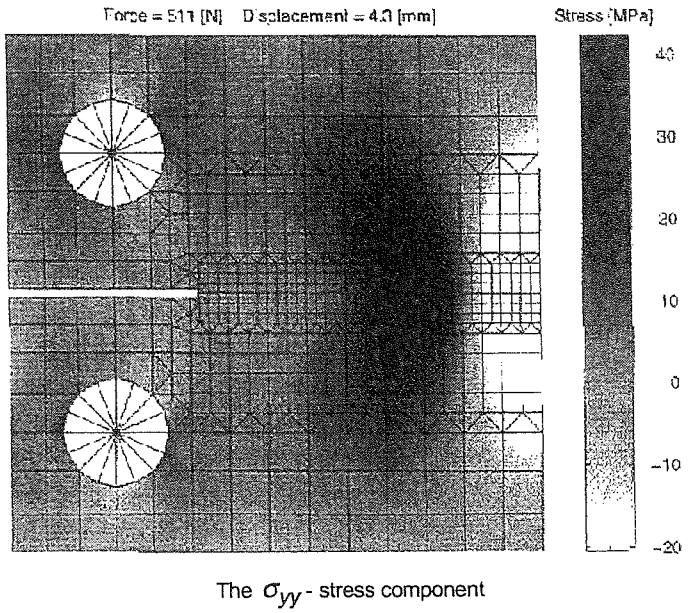

Figure 5-6 σ_{yy} stress component distribution of a compact tension experiment on a short glass-fiber-reinforced polypropylene simulated by a strain-based transient-gradient damage model (from Geer's 1997).

5.3.2. Gradient plasticity theory

The incorporation of the gradient dependence into large deformation macroscopic plasticity theory has microscopic roots, as underlined by Aifantis 1984 who considers dislocation motion and evolution. Numerous proposals have followed this research and a typical new formulation of the von Mises yield locus is:

$$F_p = \sigma_{eq} - \sigma_F(\varepsilon^p_{eq}, \nabla^2 \varepsilon^p_{eq}) = 0 \tag{5-12}$$

As the Laplacian of equivalent plastic strain is involved in the yield function, the increment of the plastic multiplier cannot be obtained at a local level (integration point). To solve this problem, the plastic multiplier is taken as an independent global variable, in contrast to the conventional approach in computational plasticity.

Pamin 1994 proposes an algorithm the fundamental feature of which is a weak (and not point-wise) satisfaction of the yield condition, which is coupled with a weak equilibrium condition. The dependence of the yield function on the Laplacian of the equivalent plastic strain induces the necessity of C^1-continuous interpolation of the plastic strain field in the finite element formulation. A new C^0-approach has been developed, in which the continuity requirement is relaxed by treating the first derivatives of the plastic multipliers as additional unknowns and connecting them to the plastic multiplier field using a penalty constraint. Pamin has examined several C^1- and C^0- continuous, rectangular and triangular elements. The behavior of these various gradient plasticity elements has been compared using a shear band test. The use of rectangular elements with reduced integration seems to give the best efficiency. This algorithm for gradient plasticity performs very well for relatively smooth strain, stress fields. However, the return mapping determined by the nodal plastic multiplier variables is not sufficiently accurate in case of stress concentrations and sudden changes of the plastic flow direction. This problem, which is a consequence of the weak fulfillment of the yield condition, causes convergence deterioration especially in the peak load regime.

Li & Cescotto 1996 propose another method. Even through the yield condition at each integration point is no longer local, it is satisfied in a point-wise fashion and at every iteration of a load step. The plastic multipliers are internal state variables locally defined at each integration point. The Laplacian of the equivalent plastic strain at an integration point is evaluated from the derivatives of the polynomial, which is interpolated by using the values of the plastic multipliers at neighboring integration points. As the plastic multipliers are not taken as independent global unknowns there is no requirement on C^1-continuous shape functions for the interpolation of the plastic multiplier.

5.4. Conclusion

Solutions exist to solve the mesh dependence and to follow crack propagation with finite element method. As underlined above, a characteristic length or internal length is necessary and is introduced in a non local computation or gradient computation. This new material data is not so easy to determine but is generally linked to microstructure information or measured by means of localization experiments. For instance, Bazant & Pijaudier-Cabot 1989 propose a characteristic length $l \approx 3\, d_a$, in which d_a is the size of the largest heterogeneity in the material. An idea from different characteristic lengths is given hereafter:

Geers 1997:	short glass-fibre-reinforced polypropylene: $l^2 = 1$ to 5 mm^2 (non local approach);
Peerlings 1999:	concrete : $l^2 = 1$ mm^2 (non local approach);
Gutierrez de la Merced 1999:	concrete : l =1.7 to 2 mm (non local approach);

Pamin 1994:	concrete : l =3 mm (non local approach);
Pardoen 1998:	copper : l =0.006 mm, inter distance between inclusions, internal length required in Thomason's rupture criterion;
Suresh 1991:	1015 steel : l =0.1 mm, a rough estimate of the maximum grain size, internal length used in non local damage model;
Wilsius 1999:	very large bibliographical review covering steels and aluminum alloys. It gives the Finite Element size required at the crack tip in order to model fracture propagation with the models of Rice & Tracey 1969, Rousselier 1987 and Gurson 1977. The range of values goes from 0.033 mm to 0.8 mm but values are generally smaller than 0.2 mm.

This quick review clearly shows that the characteristic length required in non local formulation is under the mm for metal materials. As quite a few finite elements must discretize this length scale, it leads to very refined meshes. So if real structures must be studied, very large number of elements appear and parallel computers are required. A possibility to prevent this drawback is to use remeshing techniques that refine the zones where possible cracks are detected.

If the goal is to study crack propagation, the refined meshes and non-local approach cannot be avoided with the finite element method. The crack opening appears thanks to elements without stiffness or thanks to node duplication and automatic injection of a mesh opening related to damage evolution. Specific new developments of finite elements allow no explicit meshing of the crack surfaces (Sukumar *et al.* 2000). The users of meshless method argue that one advantage of their approach is an easy study of crack propagation as no mesh adaptation is required.

In the present thesis, the main purpose is the prediction of crack appearance. Conforming to this idea of "no specific study of crack propagation", the local approach is avoided and "coarse" meshes, as compared to the internal length, are used. However, this choice already provides some difficulties of results mesh dependence.
One conclusion can be that non-local models are interesting but if real industrial parts are aimed, at this step must be coupled with parallel computer facilities.

References

Aifantis, E.C., (1984) On the microstructural origin of certain inelastic models, *Trans. ASME. J. Eng. Mater, Technol.*, **106**, 326 – 330.

Aifantis, E.C., (1988) The physics of plastic deformation, *Int. J. Plasticity*, **3**, 211-247.

Aifantis, E.C., (1992) On the role of gradients in the localization of deformation and fracture, *Int. J. Eng. Sci.*, vol. **30**, n°**10**, 1279-1299.

Bazant, Z.P. (1984) Imbricate continuum and its variational derivation, *J. Eng. Mech. ASCE*, **110**, 1693-1712.

Bazant, Z.P. ,Belytschko, T., Chang, T.P. (1984) Continuum theory for strain softening, *J. Eng. Mech. ASCE*, **110**, 1666-1692.

Bazant, Z.P. ,Chang, T.P. (1984) Instability of non-local continuum and strain averaging, ASCE, *Jnl. of Eng. Mech.*, **110-10**, 1441-1450.

Bazant, Z.P., Pijaudier-Cabot, G. (1989) Measurement of characteristic length of nonlocal continuum, *J. Engrg. Mech., ASCE*, **115(4)**, 755-767.

Belytschko, T., Fish, J. (1989) Spectral superposition on finite elements for shear banding problems, *Proc. 5th Int. Symp. On Num. Meth. In Eng.*, ed. Grüber R. *et al.*, **1**, 19-29.

Benallal, A., (2000), Continuous Damage and Fracture, Elsevier.

Brunet, M., Mguil-Touchal, S., Morestin, F. (1997) Numerical and experimental analysis of necking in 3D sheet forming processes using damage variable, *Advanced Methods in Materials Processing Defects*, Predeleanu M. & Gilormini P.,Elsevier, 205-214.

Borino, G., Fuschi, P., Plizzotto, C. (1999) A thermodynamic approach to nonlocal plasticity and related variational principles, *Journal of Applied Mechanics 1*, **66**, 952-963.

Carmeliet, J., Hens, H., Probabilistic nonlocal damage model for continua with random field properties, *J. of Engineering Mechanics*, **120 / 10**.

Castagne, S. (1998) Application d'un modèle isotrope élastoplastique couplé à l'endommagement à un aluminium. Travail de fin d'études, Université de Liège.

Comi, C., Perego, U. (2001 to appear) Numerical aspects of nonlocal damage analyses, Revue Européenne des Eléments Finis.

de Borst, R. (1991) Simulation of strain localization : a reappraisal of the Cosserat continuum, *Engineering Computations*, **8**, 317-332.

de Borst, R., Muhlhaus, H.B. (1992) Gradient-dependent plasticity : formulation and algorithmic aspect, *Int. J. Numer. Methods Eng.*, **35**, 521-539.

de Borst, R., Geers, M.G.D., Peerlings, R.H.J., Benallal, A. (1998) Some remarks on gradient and nonlocal damage theories, *Damage Mechanics in Engineering materials*, edited by Voyiadijs, G.Z., Ju, J.-W.W., Chaboche, J.-L., Elsevier.

de Borst, R. (1999) Recent issues and future prospectives in computational mechanics of materials, 5th U.S. National congress on computational

mechanics, University of Colorado, ed. Carosio, A., Smolarkiewicz, P., Willam, K., Yang, J.

de Vree, J.H.P., Brekelmans, W.A.M., van Gils, M.A.J. (1995) Comparison of nonlocal approaches in continuum damage mechanics, *Computers & Structures*, **55/4**, 581-588.

Desoyer, T., (1995), Contribution à la modélisation de l'endommagement diffus et localisé, Mémoire d'habilitation à diriger des recherches, Ecole Nat. Sup. de Mécanique et d'aérotechnique, Université de Poîtiers.

Doghri, I., Billardon, R. (1995) Investigation of localization due to damage in elasto-plastic materials, *Mechanics of Materials*, **19**, 129-149.

Doghri, I. (2000) Mechanics of Deformable Solids, Linear, Nonlinear, Analytical and Computational Aspects, Springer Ed.

Geers, M.G.D., (1997) Experimental Analysis and Computational Modelling of Damage and Fracture, Ph. D. thesis, Technische Universiteit Eindhoven.

Gurson, A.L. (1977) Continuum theory of ductile rupture by void nucleation and growth. *J. Engng. Materials Technology* **99**, 2-15.

Gutierrez de la Merced, M.A. (1999) Objective simulation of failure in heterogeneous softening solids : the use of stochastic imperfections in localization analysis, Ph. D. thesis, Technische Universiteit Eindhoven.

Hartley, P., Hall, F.R., Chiou, J.M., Pillinger, I. (1997) Elastic – plastic finite – element modelling of metal forming with damage evolution, *Advanced Methods in Materials Processing Defects*, Predeleanu, M., Gilormini, P, Elsevier.

Lazzarotto, L., Picart, P. Oudin, J. (1996) Benchmarks for finite element modeling of cold forging processes with elasto-plastic microvoided materials. *Computational Materials Science*, **5**, 167-176.

Li, X.K., Cescotto, S. (1996) Finite element method for gradient plasticity at large strains, *Int. J. Num. Meth. in Eng*, **39**, 619-633.

Lippmann, H., (1995) Cosserat plasticity and plastic spin, *Appl. Mech. Rev.*, **48**, **11 part I**, 753-762.

Loret, B., Prevost, J.H. (1990) Dynamic strain localization in elasto-visco-plastic solids, part 1. general formulation and one-dimensional examples, *Comp. Meth. Appl. Mech. Engng.*, **83**, 247-273.

Pamin, J., (1994) Gradient-dependent plasticity in numerical simulation of localization phenomena, Ph. D thesis, Technische Universiteit Delft, Delft University Press.

Pardoen, T. (1998) Ductile fracture of cold-drawn copper bars : experimental investigation and micromechanical modelling, Doctorat en sciences appliquées, Université de Louvain-La-Neuve.

Peerlings, R.H.J., de Borst, R., Brekelmans, W.A.M., de Vree, J.H.P. (1996) Gradient-enhanced damage for quasi-brittle materials. *International Journal for Numerical Methods in Engeneering*, **39**, 3391-3403.

Peerlings, R.H.J. (1999) Enhanced damage modelling for fracture and fatigue, Ph. D. Thesis, Technische Universiteit Eindhoven.

Picart, P., Piechel, G. & Oudin, J. (1997) Damage influence in the finite element computations for large strains elastoplastic mechanical structures, *Advanced*

Methods in Materials Processing Defects, Predeleanu, M. & Gilormini, P., Eds. Elsevier, 175-184.

Rice, J.R. (1976) The localization of plastic deformation. *Proc. 14th Int. congress of theoretical and applied mechanics*, 207-220, Koitier W.T. Eds.

Rice, J.R. & Tracey, D.M. (1969) On the ductile enlargement of voids in triaxial stress fields, *J. Mech. Phys. Solids*, **17**, 201-217.

Rousselier, G. (1987) Ductile fracture models and their potential in local approach of fracture, *Nuclear Engineering and Design*, **105**, 97-111.

Simo, J.C. (1989) Strain softening and dissipation : a unification of approach, *Crack and Damage*, Ed. Marzars, J., Bazant; Z.P., Elsevier, 440-461.

Sluys, L.J. , (1992) Wave propagation, localization and dispersion in softening models, Dissertation, Delft University of Technology.

Stainier, L. (1996) Modélisation numérique du comportement irréversible des métaux ductiles soumis à grandes déformations avec endommagement. Thèse de Docteur en sciences appliquées, Université de Liège.

Suresh, S. (1991) Fatigue of Materials. Cambridge University Press, Cambridge, U.K.

Sukumar, N., Moës, N., Moran, B., Belytschko, T. (2000) Extented finite element method for three-dimensional crack modelling, *Int. J. Numer. Meth. Engng*, **48**, 1549-1570.

Wang, X.C. (1993) Modélisation numérique des problèmes avec localisation de la déformation en bande de cisaillement, Thèse de Doctorat, Université de Liège.

Wilsius, I., (1999) Etude expérimentale et numérique de la déchirure ductile basée sur des approches locales en mécanique de la rupture, Ph. D. Thesis Université des Sciences et Technologie de Lille.

Zbib, H.M., Aifantis, E.C. (1988) On the localisation and postlocalization behavior of plastic deformation, I, II, III, *Res Mechanica*, **23**, 261-277, 279-292, 293-305.

Zhu, Y.Y. (1992) Contribution to the local approach of fracture in solid dynamics, Ph. D. Thesis, University of Liège, Department MSM.